Modeling the Decomposition of Sulfuric Acid for a Nuclear-Powered Integrated Energy System

A Thesis Presented for the

Master of Science

Degree

The University of Tennessee, Knoxville

CT Ragan Callaway

August 2023

Acknowledgements

The opportunity to pursue this work has been incredible and the author would like to thank Dr. Nicholas Brown for his guidance, trust, and patience throughout the process of this thesis. Additional thanks go to Dr. Jamie Coble and Dr. Ivis Chaple for their support at The University of Tennessee. Further acknowledgement goes to Dr. Ryan Anderson, Dr. Cecily Ryan, and Dr. Robert Walker for the support and guidance they provided at Montana State University.

Immeasurable thanks go to the numerous other people who provided friendship and support throughout this process. Firstly, the author's wife, who has been gracious and incredible. Secondly, Dr. Brown's lab has been incredible, and have not only been supportive as colleagues but have been a great network of friends. Thirdly, the author's family whose belief and support have been something that he could not have completed this work without. Finally, the amazing friends who have provided help and relief.

This work was funded by the NEUP under federal grant DE-NE0009214.

Abstract

Integrated Energy Systems (IES) serve as a method of cogeneration for both electrical and thermal energy. The cogeneration of both energies has served as a method of reducing waste heat and improving the efficiencies of the processes that operate within the IES grid. Thermal energy storage and distribution within an IES is a key point for an IES which uses a nuclear reactor as the main form of thermal energy provider. Desalination has been a common endothermic process used within an IES grid, mainly due to the low thermal demands required for such a process, and the wide variety of applications the produced water has, either as drinking water, industrial heating, or other such uses.

With the growing interest in the feasibility of nuclear reactors used in applications alternative to electrical generation, the history of previous work has left us with important lessons for the future. The Aktau Nuclear Power Plant (NPP), along with other nuclear desalination operations in Japan and other countries, has laid the groundwork for nuclear IES operations. The lessons learned from the low-temperature desalination process provide key framework for high-temperature IES operations like nuclear hydrogen production. The Aktau NPP was the only Molten Salt Reactor (MSR) operated within an IES, providing an additional demand for a review for future IES work with an advanced reactor.

Hydrogen production, especially nuclear hydrogen production, has also been experiencing an increase in interest. This is due to the ability of hydrogen energy to reduce carbon emissions in the wide range of applications that produce hydrogen. While electrolysis is currently the hydrogen production method that has the most interest, thermochemical cycles also show promise as production methods competitive with electrolysis. Sulfur-based thermochemical cycles like the Sulfur Iodine and Hybrid Sulfur (HyS) cycles are among the most promising, and previous work has established them as cycles that are the most favorable for nuclear hydrogen production, and as endothermic processes capable of integration within a nuclear IES.

Previous work has shown that the HyS cycle can be competitive with electrolysis from an efficiency standpoint. For future IES grid evaluations, a reduced and simplified model of the complex sulfuric acid decomposition reaction is necessary. This model can serve the purpose of providing a wide variety of outputs, including efficiency and energy demand as well as conversion, based on only a few inputs. Creating an agnostic model capable of use with a variety of different

types of nuclear reactors, heating fluids, and IES grid setups, while providing results comparable to previous work.

The reduced order model was able to generate results based on temperature, pressure, and weight fraction sulfuric acid that agreed with previous work. Generating an operational range for weight fraction between 0.63 and 0.89 weight fraction sulfuric acid that agreed with past work and met efficiency goals. High temperatures and high pressures saw the best efficiencies as well, with lower temperatures and high pressures becoming more inefficient than lower temperatures and lower pressures.

Outside of the operational parameters the model produces results that are overestimations when compared to previous work. However, these operational ranges are already outside of desirable conditions and therefore unlikely to be used in normal, steady-state conditions. The assumptions that play key roles in these overestimations have been identified for moving forwards with a more complex model for transient operations, and future work using the methodology outlined in this thesis is expected to provide key information for advanced nuclear reactors powering hydrogen production within an IES.

Keywords: Integrated Energy Systems, Hybrid Sulfur, Thermochemical, Nuclear Hydrogen

Table of Contents

List of Tables

List of Figures

Chapter 1. Introduction

1.0 Background and Motivation

With the push for clean energy sources and reducing carbon emissions nuclear hydrogen has emerged as a very promising way of both a source of clean energy and as a method of reducing carbon emissions. The increased interest in advanced reactors, such as Molten Salt Reactors (MSR), provides an avenue of interest for Integrated Energy Systems (IES) for thermal energy distribution and storage through the coupling of an advanced reactor to applications, like electrical generation, and endothermic processes, like desalination and hydrogen production. The high-concept view of an IES is shown in Figure 1, with thermal energy delivered to the energy conversion process and the chemical process through a thermal manifold.

The questions that this work addressed to determine nuclear hydrogen's role in IES moving forward were:

1. What lessons can be learned from previous experience with advanced reactors driving chemical plants?
2. What simplifying assumptions can be made in a reduced-order model of sulfuric acid that still produces good agreement with past experiments?
3. Can the reaction and thermodynamics be coupled into a simplified model of the overall integrated energy system?
4. Does the hydrogen production process meet efficiency goals to be competitive with electrolysis?

Question one addresses lessons that can be learned about IES safety features from the Aktau Nuclear Power Plant (NPP). Then in turn how they can be applied to hydrogen production within an IES. Additionally, the question serves to address the effects of the transition between the implementation of a low-demand process (desalination) to the implementation of a high-demand process (hydrogen production).

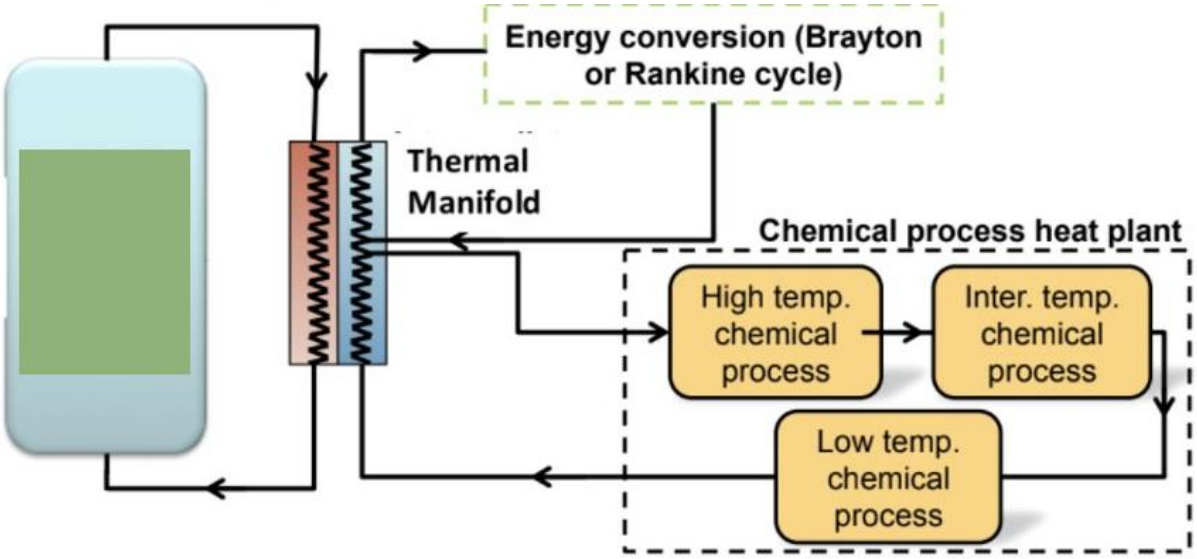

Figure 1: General concept design of an IES.

Question two asks if a reduced and simplified model of the complex sulfuric acid decomposition reaction can agree with previous, more complex models of sulfuric acid decomposition. Then if the model in turn can be implemented in an extended hybrid sulfur cycle model incorporating other processes seen in the hydrogen production method.

Question three addresses the importance of the effects of temperature and pressure on the conversion of sulfur trioxide must be included in a simplified sulfuric acid decomposition model. This is due to the effect that pressure and temperature have on the extent of the reaction. Additionally, the question asks if the resulting effects on process efficiency can be incorporated into the model.

Lastly, question four addresses the ability of the Hybrid Sulfur cycle to be competitive with electrolysis as a method of hydrogen production. For the Hybrid Sulfur cycle to be considered for hydrogen production it must be able to meet efficiency goals to be competitive with electrolysis. By answering these questions, the role of nuclear IES and nuclear hydrogen moving forward in accomplishing the goals of achieving clean energy and reducing carbon emissions can be addressed, and key points identified for further work moving forwards.

1.1 Integrated Energy Systems

IESs are power plants capable of cogenerating both electrical and thermal energy [1]. Capable of utilizing nuclear, renewable, and fossil fuels, they are appealing due to their overall plant efficiency which can utilize energy that would otherwise be lost as waste [2]. There has been a history of both fossil fuel and nuclear plants operating in IESs [3, 4]. The Aktau NPP serves as the only advanced reactor operational within an IES [3]. A review of the Aktau NPP's operational history can discover the lessons learned: IES safety features with an advanced reactor, specifically how to address the energy scale mismatch between a thermal power-driven operation, and how to set the scale of the process for the desired operation.

In addition to energy production, an IES can utilize the thermal energy produced for an industrial process [3]. The thermal energy from the power plant is transported to the process through a thermal couple. For a process with low thermal requirements, like desalination, the thermal couple can take heated water from a turbine to drive the process [5]. For a high thermal process, like hydrogen production, the thermal couple must be implemented closer to the nuclear reactor's thermal source.

For an IES with a thermally driven process and a nuclear reactor, the two processes must be matched for high thermal efficiency while keeping the same level and stability of operations expected [6]. Expected, and unexpected, shutdowns of the nuclear reactor and the chemical plant need to be accounted for within the other. For chemical processes with multiple stages within the process the effects of each process on the others, as well as the stability of the overall plant and the nuclear reactor must be considered as well [7]. Increasing the efficiency of the plant could harm the scale of the feedback between the plants while introducing stricter levels of control between each stage of the chemical process and the nuclear reactor could decrease the efficiency, the result would create an IES not worthwhile [8].

1.2 Hydrogen Production

With the challenges of the world's population increase, the ensuing increase in energy demands, and fossil fuel pollution and depletion, the demand for clean energy has only been growing over the last few decades. Renewable and nuclear energy sources have made great strides in combating these issues, and with current capabilities are the most favorable for large-scale applications [9]. However, there is a lack of practical technology in both of these sectors that limits the direct application of electrical energy generated by these sources [10]. A previous study estimated that hydrogen can supply nearly 18% of the world's energy demands [11]. Hydrogen also has great potential as the main energy source to replace fossil fuels [12]. To accomplish this, it is estimated that for transportation alone the thermal energy equivalent would be 450 GW per year, or 12 times the current U.S. hydrogen consumption [13, 14].

Hydrogen is readily available from water and can be separated using one of many simple processes [15]. Processes that use electrical or thermal energy are the most mature and readily implemented [16]. Furthermore, hydrogen production processes show great promise in their adaptability to any method of nuclear thermal energy generation, from the common BWR and PWR reactors to advanced fission reactors, and even fusion reactors [9-12, 15-17]. However, a large-scale hydrogen production process that is also cost-effective and non-pollutive is still a way off from implementation.

Contemporary methods of hydrogen production, such as steam methane reformation and coal gasification heavily rely on fossil fuels. This is due to the availability of these resources as well as their economic appeal [9]. This reliance has associated hydrogen energy with high carbon

emissions which has led to a lower appeal for hydrogen as a clean energy source [12]. Renewable energy processes, such as solar, wind, or photobiological, show great promise for hydrogen production but are unlikely to make a large economic impact in the next couple of decades [12]. The processes that show the greatest likelihood to make a large impact in the next decade are nuclear-powered water electrolysis or thermochemical cycle, CO_2 scrubbing of steam methane reforming plants, and thermal disassociation of hydrocarbons [12].

Hydrogen is readily available from water and many different compounds with carbon such as natural gas or crude oil. Furthermore, hydrogen's high chemical potential has made it ideal for energy processes, which can be used for further power or heat, and hydrogen is an important component in many other chemical processes such as in the petroleum and fertilizer fields as well as other high-value chemicals like deuterium [17, 18]. The largest consumers of hydrogen energy are ammonia and methanol production and oil refineries [19]. Unlike the electrical and thermal energy generated by power plants, hydrogen can be stored for later use in fuel cells [15, 20]. These fuel cells are considered to be the most efficient method of converting chemical energy to electrical [12]. However, the high thermal demands of water splitting have created a carbon-intensive process, with the contemporary fossil-fuel-driven methods producing large amounts of CO_2 for every kilogram of hydrogen. Thermochemical processes are one method of lowering the thermal energy and therefore the carbon emissions of hydrogen production.

Thermochemical processes implement chemical reactions into the water-splitting reaction that lower the overall thermal requirements, leading to their recognition as the likely candidate for the most economical method of hydrogen production [9]. Hydrogen production through this method shows the greatest promise for large-scale hydrogen production that is both cost-effective and non-pollutive. The Generation IV nuclear plant development has been focused heavily on thermochemical and electrolysis processes coupled with an advanced high-temperature reactor [21]. There are a few different thermochemical processes available for nuclear hydrogen production, the sulfur-based Hybrid Sulfur and Sulfur Iodine cycles, and the Copper Chlorine cycle are just a few options. The addition of thermochemical cycles into hydrogen production lowers the temperature requirements of water splitting into the range achievable by advanced reactors [8].

Chapter 2. Literature Review

2.0 Nuclear Process Heat and Integrated Energy Systems

Electrical energy generation within a nuclear power plant creates a large amount of heat waste that has the potential for integration into an integrated energy system, which not only reduces heat waste but also has the bonus of increasing overall efficiency [2]. Nuclear process heat for an industrial process can be directly utilized in one of two ways: a dedicated plant for direct heating, or parallel co-generation of heat and electricity [1]. These systems are called Integrated Energy Systems (IES) and are power plants capable of cogenerating both electrical and thermal energy. These systems are appealing due to the increase in overall efficiency they can have, and that they can further utilize thermal energy that would otherwise be lost as thermal waste [1]. There has been a history of both fossil fuel and nuclear plants operating with an IES [3, 4]. The IES could utilize the thermal energy produced for an industrial process transported to the process through a thermal couple. For a process with low thermal requirements, like desalination, the thermal couple can take heated water from a back-pressure turbine to drive the process [5].

For an IES with a thermally driven process and a nuclear reactor, the two processes must be matched for high thermal efficiency while keeping the same level and stability of operations expected [6]. Expected, and unexpected, shutdowns of the nuclear reactor and the chemical plant need to be accounted for within the other. For chemical processes with multiple stages within the process the effects of each process on the others, as well as the stability of the overall plant and the nuclear reactor must be considered as well [22]. Increasing the efficiency of the plant could increase the scale of the feedback between the plants, while introducing stricter levels of control between each stage of the chemical process and the nuclear reactor could decrease the efficiency, making an IES not worthwhile [8].

Almost 70% of primary energy produced worldwide is used for transportation, hot water, steam generation, and heat, leaving a substantially sized market available for non-electrical operations for nuclear plants [1]. Industrial processes like district heating, desalination, oil refinement, and hydrogen production stand to benefit from direct nuclear-supplied heat, and even higher temperature limit processes like steel production can utilize secondary energy carriers from a nuclear-driven process [1].

The operational outflow coolant temperature range for advanced nuclear reactors, such as a molten salt reactor, meets the temperature required to drive many chemical and industrial processes. Nuclear hydrogen can be produced by water decomposition through one of four different types of processes: electrolysis, direct thermal decomposition, chemical reaction, and thermochemical reaction [15]. Any of these methods show potential to be candidates for the utilization of process heat provided by an MSR or another nuclear reactor.

District heating in an integrated energy system has been an attractive option for nuclear co-generation due to the ease of application and preexisting systems already in place [1]. In Finland, the Loviisa nuclear power plant studied co-generation for district heating [23]. France studied the feasibility of transporting 1500 – 3000 MWth from Nogent-Sur-Seine over 110 km to Paris [24], and in Poland, an economic analysis was performed on the district heating of several different towns from planned nuclear power plants [25]. The size and scope of these projects require an expected budget of $1-$2 billion and a significant amount of technological and economic investigation [2].

2.1 Desalination with Nuclear Power Overview

Water scarcity is a significant challenge that humanity faces and the result of it is felt in both the agriculture and production industries [26]. With predicted population growths, especially in third world or other developing countries meeting this expectation will prove to be a challenge without the development of large-scale desalination plants to boost the availability of fresh water in regions like the middle east which already face a lack of available freshwater [27]. The increasing demand for freshwater for personal, industrial, and agricultural use provided by desalination will also be reflected in carbon and other environmentally harmful emissions produced by desalination [28]. The nuclear non-proliferation and safety issues that affect the majority of countries in the world that would benefit the most from nuclear desalination have been major roadblocks to nuclear desalination as well [29].

Almost 98% of all water readily available for use is salt water [30], and close to 40% of the world’s population lives in coastal areas [31]. and because of increasing populations and increasing scarcity of available freshwater even now the lack of fresh water is felt in areas around the earth [30]. With global consumption increasing, water stress is felt most strongly in areas such as Asia and the Middle East [26]. Agriculture and industry water consumption has increased with

population growth and the higher quality of life seen in many countries, from 1990 to 1995 the consumption of water increased over twice as quickly as population growth [30]. The increasing urbanization in the global population drives the demand for safe water supplies and clean drinking water [30].

The Middle East had almost 60% of the world's desalination capacity, with almost half of that in the Arabian Peninsula [29]. The considerable growth seen in both the desalination and nuclear industries means the technology is there to address the current and future demands for water and energy in areas like the Middle East and North Africa [29]. Both areas have experienced consumption demands exceeding production capabilities [31], and both have relatively low electric energy demands compared to freshwater demands [32]. Of the countries expected to suffer moderate to severe water crises in the coming decade, very few have the existing nuclear infrastructure, and none have adequately proceeded down the path of nuclear-powered desalination [29]. However, an IAEA assessment previously indicated that nuclear desalination would be technically feasible and economically competitive in these water-stressed areas [33].

Nuclear power plants have been proven to be large-scale, low-carbon emissive energy resources [27]. Furthermore, in addition to the environmental and economic aspects discussed, nuclear energy may also have a positive impact on water cost as well as availability [27]. For countries with a high water demand, but with few or no fossil energy resources, nuclear fuel is the cheapest form of imported energy [27]. Even though the interest in nuclear desalination is not as great as the interest in power or district heating [27], the operation of the Aktau power plant demonstrated the ability of a nuclear reactor to provide both electrical energy and fresh water. Namely by the coupling of the desalination plant to the nuclear reactor through a thermal manifold [34].

Co-locating a desalination plant within a power plant has many benefits aside from providing desalinated water [35]. Implementing a desalination plant in a grid can increase the unit sizes of the power plant, reduce the number of facilities and employees required by eliminating redundancy in both plants, and reduce harm to the ecosystem by mixing both plants' effluent before dispersal [35], additionally including a method of co-generation, like for district heating or desalination, can utilize the excess, or waste heat [24]. However, the drawbacks to such implementation have slowed the process. Flexibility in the plant can be lost due to the ratio of

produced water to electricity having little variation due to the plant's overall efficiency, and economic comparison is difficult due to the added product [35].

The promise of nuclear-driven desalination is great, but there still are many roadblocks to large-scale implementation. The main one is safety, but also the mismatch in the energy demand of the process to the energy provided by the reactor, and the unknown costs associated with such a process [27]. Furthermore, the cost of produced water must be considered, especially in areas with low water availability with a high likelihood of targeted subsidies to ensure water access to the poor [31]. Sufficient water production could harm economic growth and have uncontrollable consequences as a result of water provided at unacceptable costs [27]. In an IAEA study on the capacities of Northern Africa, it was determined that small to medium-sized reactors would be the most effective in desalination processes in the area considering the grid size and economic capacity in the region [36].

There are several examples of the potential use of nuclear energy to drive a desalination process, this is due to the maturity of the desalination process and the extent of our knowledge on the topic [28]. These examples are both real systems and paper studies exploring water-cooled, gas-cooled, and liquid metal reactors [27]. One specific example in the 1980s Israel and the United States cooperated to design a desalination plant for coupled operation with a Light Water Reactor (LWR) [37]. However, research has been done throughout the world in India, South Korea, America, Japan, and Russia [28]. The desalination process was designed to utilize exhaust heat from the turbines for desalination, which is a similar method to the process used by the Aktau plant. Since then the United States, Germany, and Japan have all conducted further research into the process focusing on Modular HTGR power plants and reverse osmosis desalination processes [37]. While previous and current experience and research operating nuclear and desalination processes in conjunction show promising results, the Aktau power plant is our only experience with operating a desalination process with a sodium-cooled reactor.

2.1.1 Previous Nuclear Desalination Processes:

A joint research operation in Israel was undertaken by US and Israel in the 1980s at the Ashdod plant in Israel, to simulate the coupling of a Multi-Effect Desalination (MED) to a nuclear reactor [38]. The desalination plant was a six-effect MED which was coupled to a steam turbine, like the Aktau NPP [38]. The main goal of the Ashdod plant was to demonstrate the feasibility of

a MED coupled to a nuclear reactor [38]. Like the Aktau NPP, the Ashdod plant had a make-up fossil-fueled power unit, however, the MED plant was operated at a much lower temperature than the Aktau plant [38]. The Ashdod desalination unit ran for two years, and the demonstration was promising enough to generate a positive attitude towards more nuclear desalination [38].

In a similar operational experiment, the Water and Electricity Company of Curaçao, in the Netherlands Antilles demonstrated the demands of MED compared to MSF in an IES [38]. In dual-purpose compounds, such as a compound that provides electricity for a city and thermal energy for desalination, MSF is usually the desalination process of choice [38]. However, the lower energy demands of MED meant that by using MED another turbine for energy generation can be added to the system [38]. A common question for such IESs is whether the first effect of the MED or the steam turbine should set the demand of the process. The operational experience showed that the turbine's operational conditions should be fixed, and the first effect's operational conditions and therefore the desalination plant's operational conditions should adjust to match the demands of the turbine [38].

Japan has had extensive experience with nuclear desalination utilizing MED, MSF, and Reverse Osmosis (RO). Table 1 shows the operational conditions of a few operations compared to the Aktau NPP desalination process. The country's nuclear reactors are built on the coastline and utilize seawater for steam generators and due to their design additionally include seawater as their heat sink [39]. These desalination plants have operated in conjunction with PWRs or BWRs [39], unlike the Aktau NPP. The types and capacities of the desalination plants varied by site, but were used for boiler feedwater supply and potable water in more remote areas [39]. These desalination plants were MED, MSF, and RO plants, and had a max capacity of 1000-3000 m^3/day [39]. During the operational lifetimes of the plants, the plants were successful with no significant problems seen, nor radioactive contamination of the water experienced [39].

The first nuclear desalination plant in Japan was the Ohi Nuclear Power Station, commissioned in 1978, and natural sources of freshwater were not sufficient to meet the plant's needs so desalination units were added to make up for the demand [40]. Initially, MSF and MED were used to supply potable water to the original two units, and with the addition of units III and IV RO was added to the desalination process [40]. In the case of both MSF and MED processes the designs were identical to fossil-fuel-powered desalination processes, with slight adjustments made to the RO plants [41]. The decision to use RO processes was due to the low corrosion and

ease of operation and maintenance for RO, as well as the fast advancement of RO technology in the years after the initial plant's establishment [39].

Each RO plant required seawater intake, pretreatment, two stages of RO, and discharge treatment [40]. Each plant had a capacity of 1300-1700 m^3/day, with about 200 m^3/day of the desalted water provided to a further drinking water facility and used for potable water [40]. MED and MSF plants were used at several locations as well, however, even though minor corrosion was observed in many of these plants they still had an exemplary record of performance [40].

India and Pakistan have been involved in desalination research as well. India successfully operated an experimental facility in Trombay, with plans to couple a hybrid RO-MSF plant in Tamil Nadu [42]. The Karachi Nuclear Power Plant (KANUPP) in Pakistan also required a seawater desalination plant to provide water for normal operations and emergency feedwater [41]. The KANUPP reactor was a type of horizontal heavy water reactor, and the Pakistan Atomic Energy Commission (PAEC) researched the implementation of MED, MSF, and RO desalination coupled to the reactor [43]. The KANUPP desalination plant had a good performance record, and the water provided met WHO standards for potable water [41].

2.2 Aktau NPP

The Aktau power plant operated off the coast of the Caspian Sea in what is now Kazakhstan from 1973 until 1999 [34]. A review of the discoveries made during its lifetime and in the years of research afterward is desirable due to an increase in the demand for high thermal demand industrial and chemical processes operated in conjunction with nuclear reactors. While the Aktau power plant's primary use was for electrical production, the experience gained from the low thermal desalination can be used to better inform future nuclear desalination processes [37] as well as models made today of high energy hydrogen production such as sulfur-based thermochemical water splitting, or high-temperature steam electrolysis.

In this literature review first, an overview of desalination with nuclear power is given, both in the context of the Aktau power plant, and other international efforts. Then a summary of the Aktau power plant: its location, history, and operational background. Next, the BN-350 reactor overview summarizes the reactor and its operational history with the desalination plant. The thermal manifold and water flow scheme are summarized, and finally, the Aktau desalination process is explored.

2.2.1 Aktau Power Plant Overview

The Aktau power plant was in an arid zone in the Mangyshlak peninsula on the Caspian Sea. The low rainfall on the peninsula coupled with the high salinity of the groundwater, ranging from 3.5-3.8 g/L, made a desalination plant a desirable addition to the city of Aktau [34]. The complex objectives were to minimize heat loss in the transmission of steam to industrial processes and to minimize water transport costs [3]. Originally the complex utilized 3-stage evaporation distillation, 2-stage flash, electrodialysis, and ion exchange units [5]. After a period of experimentation, multi-stage thermal evaporation distillation was decided to fit the Aktau complex, starting with a 4-stage in 1963, and increasing to three 5-stage commercial processes in 1967 [5], with each distillation process attached to a turbine [3].

Previous experience running desalination plants in the USSR under conditions similar to what the Aktau complex would undergo resulted in the decision to implement 10-stage MED evaporation units [5]. These units had previously established themselves as reliable, resistant to disturbances, and highly effective at removing salt [5]. For thermal energy, the complex had the BN-350 reactor and a natural gas energy source that provided energy to the desalination plant, as well as the turbines [44].

The complex was located 12 km from the city, with a potable water preparation station closer to the city with a 2 km channel for seawater intake and brine water outfall [3]. The Aktau power plant consisted of a BN-350 reactor, a gas-fueled preparation station, a potable water preparation station, ten MED units with production capacities of 8000-14500 m^3/day of water, and a feed water preparation unit for the steam generators [34]. Further treatment of the distillate was not required for the feed streams to electric generators [5].

For thermal energy application and distribution the exhaust steam from the back pressure turbines for the first stage evaporators, with surplus steam and heat sent to supply additional thermal energy to industrial processes within 7 km of the complex [34]. Steam boilers utilized thermal energy from the extraction of steam from the turbines as well, supplying heat to the district heating system, distillates were also fed into the heating system to keep normal pressure [34].

Table 1: Parameters of Previous Nuclear Desalination Operations

Name	*Kashiwazaki [40]*	*Ohi I, II [40]*	*Takahama [40]*	*Genkai IV [40]*	*Ikata III [40]*	*Ohi III, IV [40]*	*Genkai III [40]*	*Aktau [34]*
Type of Reactor	BWR	PWR	PWR	PWR	PWR	PWR	PWR	Sodium
Reactor Capacity (MWe)	1100	1175	870	1180	890	1175	1180	1000
Type of Desalination	MSF	MSF	MSF	MED	RO	RO	RO	MED
Desalination Capacity (m^3/day)	1000	1300 per line	1000	1000	2000	1300 per line	1000	14500
Number of Stages	18	18	18	8	36x2 lines	95x2 lines	54x1 line	5
Max Temperature (℃)	120	118	120	116	25	30	25	105

2.2.2 BN-350 Reactor Overview

The BN-350 reactor was a sodium-cooled fast breeder reactor [34]. With six primary coolant loops, five operational and one backup, and six secondary loops split into two rooms [34]. The primary and secondary heat exchange system can be seen in Figure 2. The BN-350's operation was largely satisfactory, with the majority of events initiated in the steam-generating system as a result of faulty manufacturing and welding [27].

The secondary coolant loops were sodium as well, connected to the primary sodium loop through an intermediate Na-Na heat exchanger [34], and it was this loop that was coupled to the tertiary water loop through an intermediate heat exchange system [34]. A flow diagram of the complex can be seen in Figure 3, and Table 2 shows the operational parameters of the reactor and the loops. The thermal section of the reactor was made up of six steam generators with natural circulation [34]. The low pressure of the sodium coolant and lack of noticeable corrosion ensured the leak tightness of the sodium piping and components [34].

There were four variants of probable failures considered in the design of the BN-350 reactor: primary loop sodium leaks, gas system failure, loss of sodium circulation, and core subassembly damage during refueling [34]. Safety features in place to prevent contamination of steam delivered to the consumers after probable failures which included low pressure in the reactor vessel and three circuits system of reactor cooling, from lowest to highest pressure [34]. These safety systems prevented contamination of the steam circuit in the case of any failure [34].

The nuclear power plant's designed operational power was estimated to produce up to 1000 MW with up to 150 MWe provided to the city of Aktau, with plans for plutonium production included in the original design [45]. The actual operational power of the plant was estimated to be 130 MWe to the city of Aktau and 150 MWth to the coupled desalination process, and Table 3 shows figures from the reactor's operation [34]. The Aktau nuclear reactor achieved criticality in 1973 with a 20-year planned lifespan and had a peak production of 120,000 m^3 of potable water per day [5] and a maximum output of 750 MWth occurring in 1984 [34]. After the fall of the Soviet Union the United States government worked cooperatively with Kazakhstan to extend the operational life of the power plant on a yearly basis, finally shutting the plant down in 1999 with a cumulative operation time of over 150000 hours [34], after the IAEA determined that major upgrades were necessary for further operation that were deemed to be too expensive to be worthwhile [45].

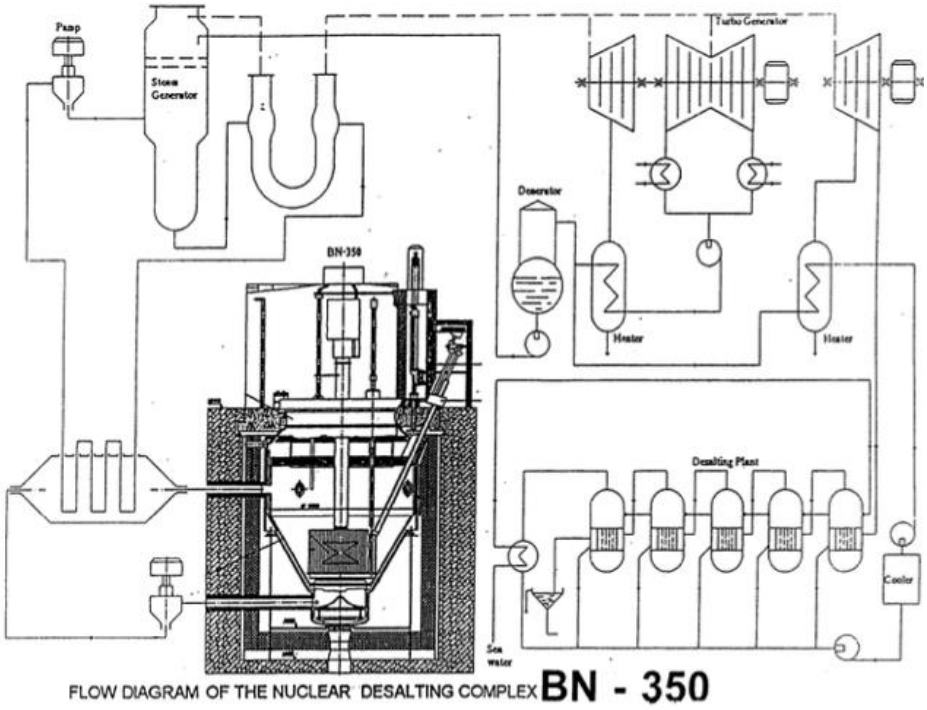

Figure 2: BN-350 complex flow diagram [45].

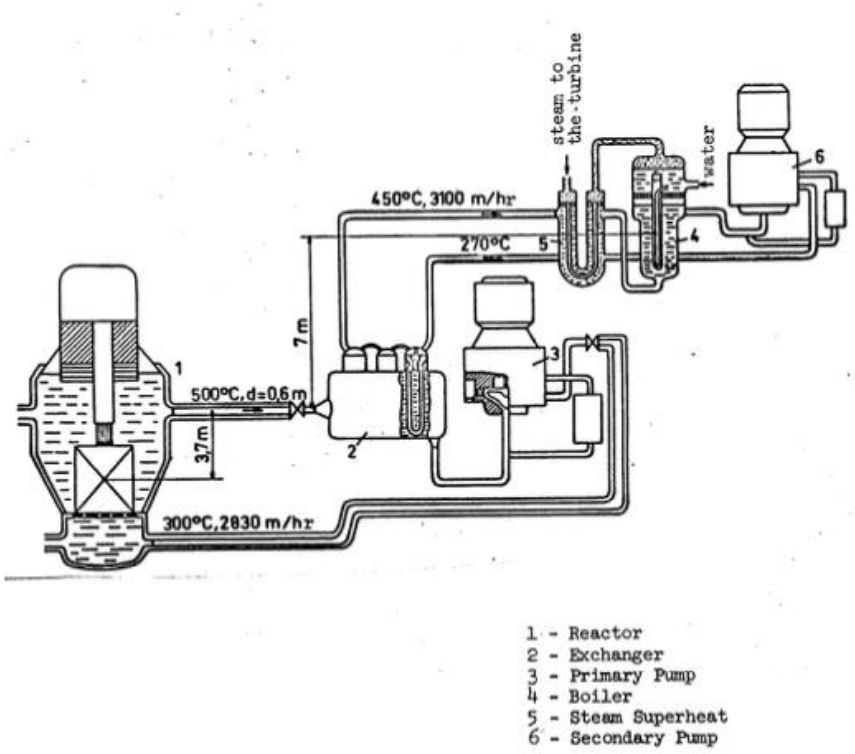

Figure 3: BN-350 primary and secondary heat exchange flow diagram [45].

Table 2: Main Technical Parameters of the BN-350 [34].

Reactor Thermal Power	750 MW (th)
Inlet/Outlet Sodium Temperature of the Primary Loops	288/437 °C
Inlet/Outlet Sodium Temperature of the Secondary Loops	260/420 °C
Steam Outlet Temperature	405 °C
Steam Pressure	4.5 MPa
Steam Flow	1070 t/h
Loop Number	5

Table 3: Principal results of the BN-350 reactor's operation from 1973-1995 [34].

Power Level Operation	159921 hr
Average Power	592 MW (th)
Average Load Factor	0.85
Refueling Number	56
Number of Unplanned Power Decrease	62
Fuel Burnup	11.8 %

In the early start-up tests of the reactor, leaks were found at weak points in several of the welds on the water side of the heat exchange system as well as along other manufacturing defects. One of the key safety points identified in the design and operation of the plant was the high reactivity of sodium in the presence of water, creating a need for high-integrity parts to avoid the consequences of such a reaction taking place in the heat exchange system [45]. In the first few years of the plant's operation, all but one loop experienced leaks leading to the decision to retube all loops except the one loop that had not failed, as well as replace one of the steam generators. The largest accident occurred in 1974 when steam generator pipes depressurized, and water reacted with the sodium coolant. A visiting US delegation in 1975 speculated that reaction products were carried into the shell of the heat exchanger and that their presence exacerbated the tube failure problem [34].

The design of the plant incorporated over 40 initiating events for abnormal operation. Over the plant's operational lifetime, 64 events required the decrease of the reactor by 10-12%. There were also 77 events that resulted in the high-speed shutdown of the reactor, however, none occurred in the last six years of plant operation [34]. The BN-350 reactor was shut down for 20 days to undergo refueling and maintenance twice per year, during these scheduled outages the thermal power station supplied heat for the desalination plant.

Later analysis by the NRC and other American delegations determined that the Soviet use of sodium coolant with water created several barriers to safe operation. Manufacturing techniques of steam generator components needed to be improved. Sodium and feedwater quality control needed a better design to avoid the buildup of scale from evaporation and other reaction products in the heat exchange system. Finally, provisions focusing on detection, containment, and remediation were crucial in the event of tube failure to mitigate extreme reactions between the coolant and water heat exchange systems [46].

When shutting down the BN-350 reactor the majority of the plant's shutdown safety concerns had to do with sodium. A heavy emphasis on fire safety and sodium containment was implemented, and the brunt of the draining and processing of the sodium had to be carried out in conjunction with the United States. Cesium traps were implemented to decontaminate the sodium before its draining and conversion into a form for safe storage [34].

2.2.3 Thermal Manifold, Water Loop Scheme, and Reliability

Figure 4 shows the water loop in the Aktau plant, including the desalination process and other uses such as district heating. For the desalination process, seawater from the Caspian Sea was brought into the Aktau plant MED units, where thermal energy from the reactor was used to drive the desalination process. After treatment, the desalinated water was then sent to other parts of the plant, either to the tertiary water coolant loop that powered the four steam turbines for electricity or for further water treatment to be used as potable water or in district heating. Fossil fuel-fired boilers were used in conjunction with the reactor in the tertiary loop to make up for pressure and heat loss and to continue providing water and electricity in the area in case of a planned or unplanned reactor shutdown [34]. The incorporation of the desalination process into the water loop offset the energy mismatch between the reactor output and the process requirement, sending the majority of the power to the turbines and having enough excess heat as a byproduct to power the desalination process, which would have otherwise been rejected through the condenser [27].

Scale build-up in preheaters was avoided by the addition of CO_2 and "seed" to the incoming seawater [5]. The introduced "seed" was similar to what is used in other desalination plants to prevent scale build-up [28]. This "seed" circulated in a closed loop within the evaporators, eliminating the need for additional scale-preventing reagents [5]. Seeding prevented scale buildup over 0.15 mm in the high-temperature evaporators, however, some plugging of preheaters by chalky plugs occurred [5]. To reduce the scale in the preheaters further steps were taken. These were washing the seed crystals, reduction of solids in incoming seawater, and partial acidification of incoming seawater by adding CO_2 taken from blow-away devices of the second evaporator [5].

Incorporating the CO_2 stabilization system complicated the water deaeration system in the evaporation units [5]. Two types of deaerators were then designed to try and meet the early demands of the system [5]. In the 1980s these were upgraded to jet ejection blocks working in conjunction with a vacuum pump [5].

Over the accumulated operational time the entire plant experienced no significant sodium leaks. All major and minor accidents were the result of depressurization within the steam generators. Furthermore, there was no abnormal sodium pump operation or significant cavitation in the pumps [34]. While sodium and water reactions did occur, none caused catastrophic failure.

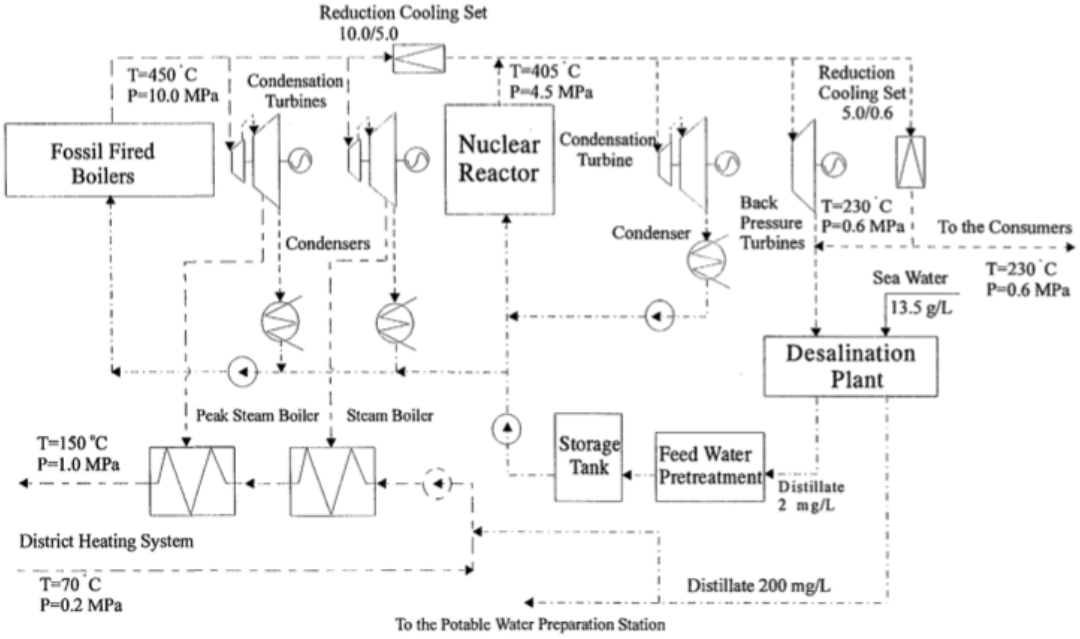

Figure 4: Water flow diagram for the Aktau plant [33].

Later in the operation of the plant, a reserve loop was maintained in the heat exchange system, this was able to prevent a loss of power in the reactor in the event of a heat exchange failure [34].

Three independent water sources were connected to the water circuit comprising the feed water storage for the steam generators, thermal power station water tanks, and distillate storage of the desalination plant [34]. These water sources were also available as an additional heat sink in the case of emergency, providing high reliability and safety [34]. In the case of a high-speed reactor shut down only one steam generator would remain to provide reactor cooling, and steam production would rapidly decrease to zero necessitating steam supply from the fossil fuel boilers to keep the desalination process operating [34].

The desalination plant provided both potable water for drinking and personal use, 200 mg/L, and high-quality water for industrial uses such as for the turbines, 2-10 mg/L. Both met WHO guidelines for safe water, which are shown in Table 4. However, the feedwater was initially contaminated by corrosion leading to the necessity of additional purifying and filtration methods [37]. The main concern in the plant design was contamination by tritium migration, however, monitoring of the water established that any contamination by tritium was well below background levels of radiation [34].

2.2.4 Desalination Plant

The MED process is one of the oldest large-scale evaporation processes used for producing desalinated water [28]. The two most utilized MED processes are with either vertically aligned heat transfer tubes, or horizontally aligned heat transfer tubes, both of which are easy to operate and maintain and show the largest potential for low-cost production of water [27]. While batch desalination processes were commonly used on ships as early as the 18th century, the MED process only saw use in large-scale industrial desalination processes in the 20th century [28]. The essential features of MED are the heating of steam or hot water that is used to evaporate brine, the heat of the initial vaporization is then reused in the subsequent vaporizations and condensations in the following effects [28]. Additionally, MED systems are in series from highest to lowest temperatures, with the option to feed seawater backward or forward with the effect temperature [28].

Before the incorporation of the nuclear reactor as the thermal energy source, desalination plants were developed for experimentation in which a total of five MED effects were settled based

on technical and economic calculations of a desalination plant coupled to a fast reactor [47]. The 5-effect MED proved to be the best option over a 10-effect MED, and a 34-stage MSF desalination process [27]. Previous experimentation on the seawater from the Caspian Sea showed that the maximum sea water temperature for evaporation effects was 115 °C, with a maximum concentration coefficient of 4-4.5 [47]. Under these conditions, calcium carbonate and magnesium hydroxide were separated from the seawater [47].

Figure 5 shows the original 5-effect MED industrial evaporation plant flow sheet described in Novikov, Chernozubov et al. 1969. Incoming seawater was first heated in condenser 6 by steam from the last effect, then the small percentage of water that was not rejected back to the sea was filtered through filter 7, then heated in heater 8 to 38 °C, and then next heated to 48 °C in heat exchanger 9 by condensing vapor from the 4^{th} effect. After heating the seed pulp was added and the mixture was de-aerated in deaerator 10 and heated to 70-75 °C by steam from the third effect. Then in heat exchangers 11 and 12 steam from the first effect heated the mixture to its boiling point 100-105 °C. The first effect concentrates the seawater to brine at 18-22 g/L, which flows through all five effects, concentrating to 45-50 g/L in the fifth and final effect, corresponding to a concentration factor of 3.5-4.

The deaerator was a vertical cylindrical reservoir with a 1.8 m diameter and a conical bottom. Steam was introduced from below through a conical diffuser, and at the upper part, conical nozzles sprayed out the de-aerated water stream [47].

Boiling the brine was prevented in the heating tubes by lowering the heat exchange surfaces below the level of the evaporating brine, creating an elevated boiling area [47]. A 6 m tall pipe was placed in the separator above the lattice of the heating chamber, providing hydrostatic pressure to the heated brine to avoid flash [47]. An umbrella-shaped petalled deflector was installed above the pipe to ensure uniform vapor stream distribution across the separator surface and to subdue the energy of the vapor-liquid jet [47].

Operating on a once-through, forward-flow system [47], incoming seawater from the Caspian Sea was at a particulate level of 13.5 g/L where it was heated to 98 °C before it entered the first evaporator by passing through a condenser, deaerator, and preheaters [5]. There were five evaporation chambers in the process, and the outcoming brine exited at a particulate level of 45 g/L [5], which is the maximum salt concentration. Only the first evaporation chamber was heated by steam provided by the reactor system, with heating for the following chambers, as well as the

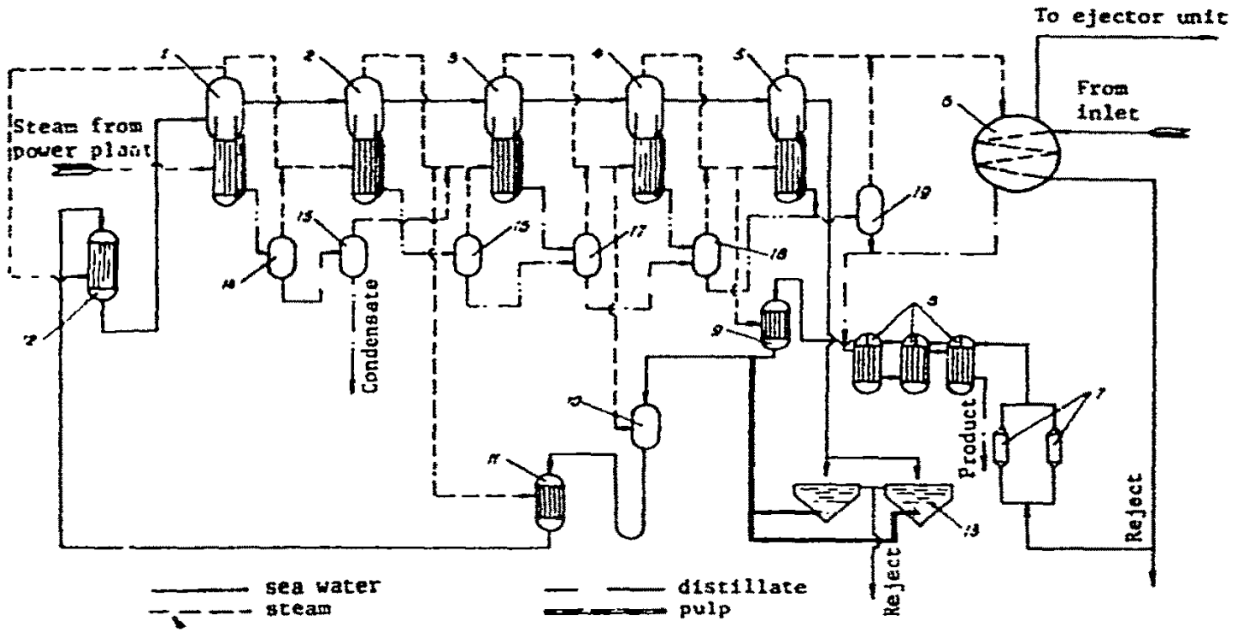

Figure 5: Desalination Plant flowsheet [47].

Table 4: Water product characteristics [34].

Characteristics	WHO Guideline values	Distillate G	Distillate A
Total Dissolved Solids (mg/L)	<1000	1.96	198.6
Temperature (°C)	NG	45	28
Color (TCU)	15	-	-
Turbidity (FTU)	5	-	-
Conductivity (μS/cm)	NG	4.05	326.7
pH	6.5 – 8.5	8.46	8.07
Total Hardness $CaCO_3$ (mg/L)	500	0.78	66.0
Chloride (mg/L)	250	0.48	55.6
Sulfate (mg/L)	400	0.31	33.2
Calcium (mg/L)	NG	0.08	7.6
Magnesium (mg/L)	NG	0.09	8.2
Sodium (mg/L)	200	0.18	48.5
Aluminum (mg/L)	0.3	-	-
Copper (mg/L)	1.0	0.013	0.06
Iron (mg/L)	0.3	0.033	0.09
Zinc (mg/L)	5.0	-	-
Fluoride (mg/L)	1.5	-	-
Nitrate (mg/L)	10.0	-	0.27
α-activity (Bq/L)	0.1	-	-
β-activity (Bq/L)	1.0	-	-

NG – No guideline value set

pre-heating system, heated by secondary steam, and the vacuum in the system provided by steam jet ejectors [5]. Distillate was collected from condensate produced in all evaporation chambers but the first and supplied for potable water production and other forms of consumption [5].

Distillate that was used for potable water was first saturated with CO_2 and enriched with calcium by filtration through carbonate sand, this was done to reduce the number of chemical reagents required for potable water preparation [5]. The seeding caused the scale build-up to occur on the seeds themselves instead of the heating surfaces [47].

Desalination units were equipped with long-tube vertical evaporators with a boiling zone after the heating tubes and naturally circulating brine [5] and were composed of a separator, heating chamber, and circulation tubes [47]. The effect heating chamber had a 3.0 m diameter and was 7 m tall, containing 2922 38 x 2 mm brass tubes with a heat transfer area of 2700 m^2 [47].

Connected to the lower part of the heating chamber by circulation pipes, the separators were 6.4 m in diameter in the first three effects, and 8 m in diameter in the last two effects to ensure acceptable steam velocities, with baffle traps in the upper part, and in only the first effect were Raschig rings used for further steam cleaning [47]. The circulation ratio, or the ratio between the circulating brine to the production capacity of the plant varied between 100-200 [47]. The brine velocity in the tubes was 1-2 m/s, this created a turbulent flow regime that maximized the heat transfer coefficient as well as separated any solid phase particulates and seeding crystals [47].

Drawbacks to the Aktau desalination plant design were increased heat consumption per unit of desalinated water produced, limited evaporation stages due to temperature drop between units, large heat recuperation and makeup required to ensure heat drop between stages did not exceed 12 °C, and a long start-up period required for the evaporators to reach equilibrium [5]. Using the 10-stage MED satisfies the specific needs of a desalination plant operated in conjunction with a nuclear reactor. Able to increase and reduce heat consumption rapidly as well as provide distillate to make-up steam generators for energy production [5].

2.2.5 Lessons from The Aktau NPP

The Aktau NPP is the only historical example of an advanced reactor within an IES. The review of the work that has come out of its extensive and successful operational history, as well as the experience gained from other IES both nuclear and non-nuclear, as well as experimental and

operational, has distilled down to basic lessons to be learned. From a review of the Aktau NPP, the questions that were desired to be answered were:

1. The safety features important to an IES.
2. How the energy mismatch in large-scale operations was addressed.
3. What drives the process?

For low-temperature processes like the desalination plant at Aktau, the design of the IES addressed these issues by:

1. Adding redundancy in thermal supply & dimensions of feedback between the processes and reactor to reduce radiation contamination, as well as providing layers of safety in the case of outages.
2. Implementing the process into a grid so that the excess heat supplied by the nuclear reactor was not wasted and had many routes to utilization.
3. Setting the scale for the process with the nuclear reactor and its heat availability.

The Aktau NPP was an IES with a low-temperature process. Hydrogen production requires significantly more thermal energy to operate efficiently, and integrating such a high-temperature process into an IES raises more key questions:

1. What about direct feedback between high-temperature processes and nuclear reactors?
2. How can hydrogen production fit into an energy grid?
3. What if thermal demand for the process is higher than provided?

To answer these questions, a further review for a better understanding of hydrogen production was necessary.

2.3 Nuclear Hydrogen Production

Nuclear hydrogen can be produced through water decomposition through one of four different types of processes: electrolysis, direct thermal decomposition, chemical reaction, and

thermochemical reaction [15]. Hydrogen production now heavily relies on the more mature available processes such as steam methane reforming or coal gasification; nearly 95% of the commercial hydrogen produced in the United States is produced using steam methane reforming [12]. Whereas only 0.3% of the produced hydrogen is from renewable resources [48] which produce high carbon emissions, an estimated output of 13.7 kg of CO_2 per kg of hydrogen produced [19]. Close to 1.5 million tons of saleable hydrogen is produced in the United States per year [49]. Figure 6 shows a variety of different thermal applications and the temperature requirements required to drive them.

Electrolysis is the closest to implementation within a large-scale nuclear hydrogen production process and is largely considered the most effective process, but there is still much work to be done to minimize costs associated with electricity generation [9]. Process heat is a less expensive and more direct method of energy transfer making thermochemical cycles more attractive long-term for nuclear hydrogen [8]. Current generation nuclear reactors, such as PWRs or BWRs, can demonstrate 21-23% LHV efficiency, and Gen IV reactors, such as HTGRs, show the potential to have a LHV efficiency as high as 33% [8].

Carbon scrubbing, or sequestration, has been a major focus in the last few years in the reduction of carbon emissions from hydrogen production [12]. This is accomplished through the capture and storage of CO_2 in sinks to prevent emissions from reaching the atmosphere [12]. Even though the method has been shown to be viable with current technology [50], and has seen implementation in current oil recovery processes [51]. This method of carbon emission reduction is estimated to increase the cost of hydrogen production by as much as 30% [52], and the long-term ecological effects of CO_2 storage are unknown [12].

2.3.1 Electrolysis

Electrolysis is a simple method for hydrogen generation and uses the water splitting reaction to convert electrical energy to chemical energy stored in the hydrogen product. Two reactions take place, one at the anode and one at the cathode. Low-temperature electrolysis takes place at 70-90°C and high-temperature electrolysis takes place at 700-1000°C [53]. The high-temperature steam electrolysis takes place at much higher temperatures but utilizes less electrical energy [53]. High-temperature electrolysis has the added benefit of achieving almost no emissions

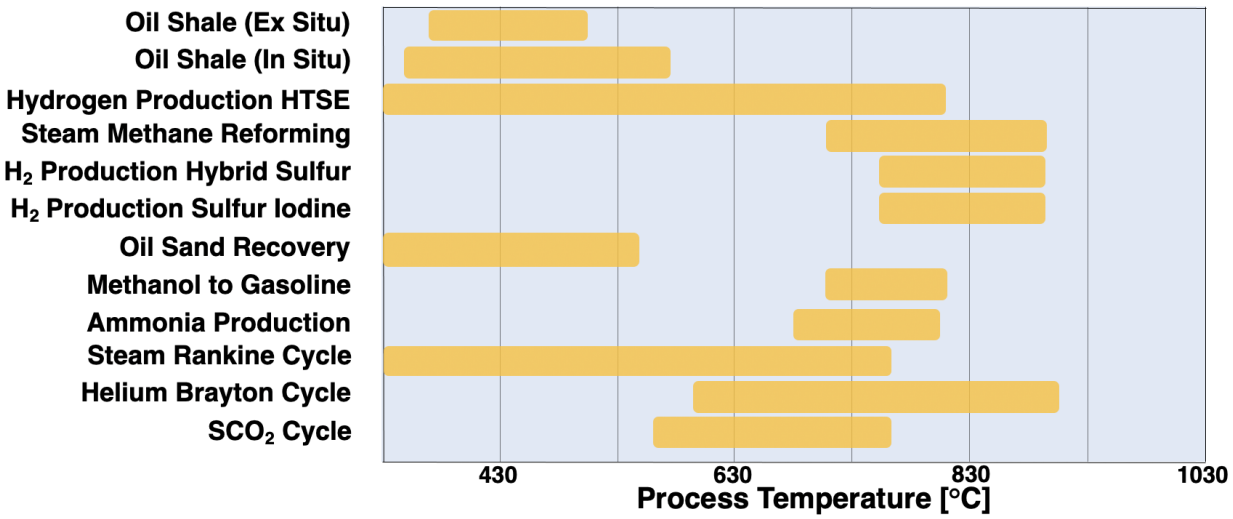

Figure 6: Process temperature requirements for different industrial operations.

if coupled with a clean heat source [20]. It is estimated that the cost of hydrogen produced by electrolysis is now competitive with gasoline [54].

When evaluating methods of electrolysis for hydrogen production the primary consideration is the cost of electrical energy [10]. Generally, high-temperature electrolysis sees thermal efficiency increase with the temperature of the electrolysis reaction [9, 10]. High-temperature electrolysis driven by nuclear power is expected to generate hydrogen with 50-70 percent efficiency, depending on the overall design of the electrolyzer [10, 55, 56]. Conventional electrolysis achieves only 30-35 percent efficiency, thus nuclear-powered electrolysis is much more effective than conventional electrolysis powered through the normal power grid [10].

The design of the electrolyzers varies on the method of electrolysis. Water electrolyzers operate between -1.7 to -2.0 V at economically reasonable electric current densities [8]. For high-temperature steam electrolysis, the electrolyzer must minimize the thermal stresses that occur due to the heating and cooling temperature cycle during operation, with internal temperatures fluctuating as much as 1400°C [10]. However, the challenges of implementing electrolysis are due to the lower efficiencies of electrical generation and electrolysis in general [9].

The main reaction, equation 2.1 that takes place in the electrolyzer is endothermic water splitting, which can be accomplished with liquid or vapor water, and is the reverse of hydrogen combustion:

$$H_2O \rightarrow H_2(g) + \frac{1}{2}O_2(g) \quad \Delta H = 285.8\ kJ/mol \tag{2.1}$$

Two of the most promising forms of electrolysis are the Alkaline and Proton Exchange Membranes (PEM). The Alkaline electrolyzer reactions, equations 2.2 and 2.3, at the anode and cathode are:

$$Anode: 2OH^-(aq) \rightarrow \frac{1}{2}O_2 + H_2O(l) + 2e^- \quad E^0 = -0.4\ V \tag{2.2}$$

$$Cathode: 2H_2O(l) + 2e^- \rightarrow H_2(g) + 2OH^-(aq) \quad E^0 = -0.8277\ V \tag{2.3}$$

PEM electrolysis has the following reactions, equations 2.4 and 2.5, which take place at the anode and cathode:

$$Anode: H_2O(l) \rightarrow 2H^+(g) + \frac{1}{2}O_2(g) + 2e^- \quad E^0 = -1.23\,V \tag{2.4}$$

$$Cathode: 2H^+(g) + 2e^- \rightarrow H_2(g) \quad E^0 = 0\,V \tag{2.5}$$

2.3.2 Direct Thermal Decomposition

The most common method that utilizes chemical reactions for hydrogen production is fuel processing, where a hydrogen-containing material such as ammonia or methane is reacted to form a hydrogen-rich product [17]. Figure 7 shows the net greenhouse gas emissions from the operation of a methane reforming plant. The study indicated that for every MJ of fossil fuel used by the operation, only 0.66 MJ of hydrogen energy was produced [19]. Utilizing a renewable or nuclear resource would not only substantially lower the impact of emissions but have a positive effect on overall process efficiency as well [19].

Thermal decomposition, or methane cracking, of methane, is a CO_2-free reaction that has been explored as an alternative method of hydrogen production [57]. The process itself is not CO_2 emission-free, as it requires thermal energy to drive the reaction. The endothermic reaction, equation 2.6 that takes place in methane cracking is:

$$CH_4 \rightarrow C + 2H_2 \quad \Delta H^0 = 75.6\,kJ/mol \tag{2.6}$$

Methane cracking has a lower energy requirement and lower CO_2 emissions than steam methane reforming: 37.8 kJ/mol H_2 compared to 63 kJ/mol H_2, and 0.05 mol CO_2 per mol H_2 compared to 0.43 mol CO_2 per mol H_2, respectively [12, 57].

2.3.3 Thermochemical Reactions

Thermochemical cycles introduce additional series of intermediate chemical reactions into the water-splitting reaction, with the benefit of decreasing the overall energy required for the process. These water-splitting cycles are favorites for large-scale nuclear hydrogen generation over electrolysis because of better efficiencies and their ability for scaling up [8]. All introduced reactants are recycled which makes the overall process equivalent to water splitting since the only consumed reactant is water and the only products are oxygen and hydrogen gas [58]. Thermochemical cycles utilize thermal energy for their processes, some only use thermal energy

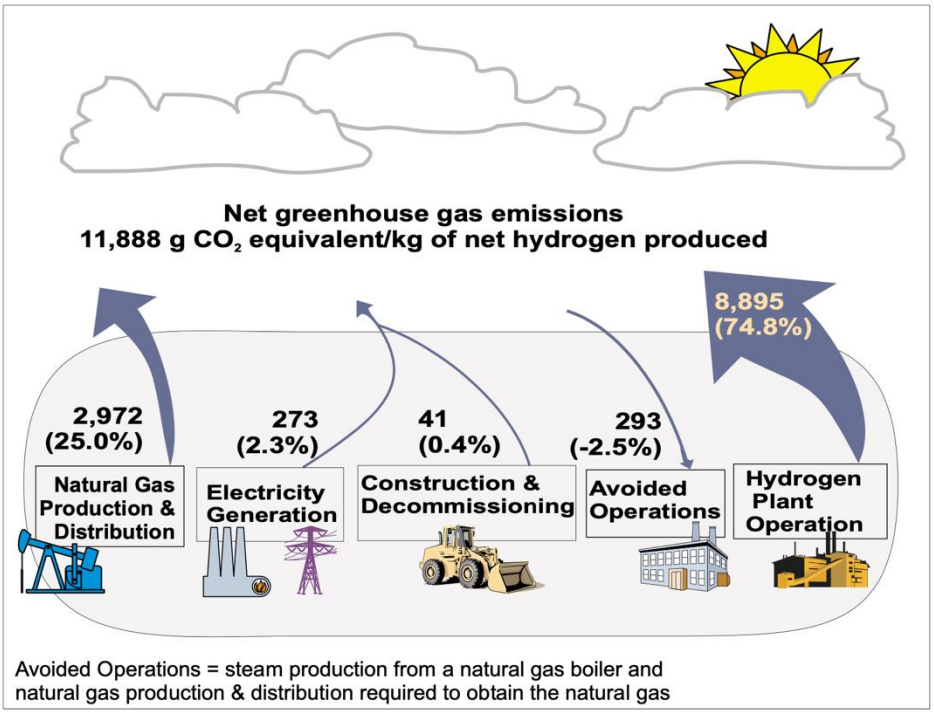

Figure 7: Net greenhouse gas emissions of a steam methane reformation plant [19].

while other hybrid thermochemical cycles utilize other forms of energy in conjunction with thermal energy.

There are over 200 available thermochemical cycles, however, only a few have been identified as likely candidates for large-scale nuclear hydrogen production [59]. Challenges facing the large-scale implementation of these processes with a nuclear thermal energy source vary depending on the process. This can depend on the complexity of the process, with some containing two chemical steps and others containing more than four. The ability of the nuclear reactor to supply enough thermal energy, the complexity of the intra-process feedback within the chemical process, and the feasibility of large-scale operations for the hybrid processes are a few of the other challenges that face thermochemical cycle implementation.

The Hybrid Sulfur (HyS) and the Sulfur Iodine (SI) cycles are two such processes that could utilize thermal energy from a nuclear reactor. These processes have been identified as potential cycles to be used as intermediate reactions of water splitting that decrease the thermal energy required for hydrogen production [60]. Both processes utilize the endothermic decomposition of sulfuric acid which, under standard conditions, sees the full extent of the reaction take place at or above 850ºC (1123 K) [61].

The decomposition of sulfuric acid takes place in two steps, the rapid decomposition into sulfur trioxide and water, and then the much more temperature-dependent and slower decomposition of sulfur trioxide into sulfur dioxide and oxygen gas which are the desired products [62]. This temperature is at the maximum of the temperature range identified as ideal for thermochemical processes: 750-850°C. This temperature range is also desirable for nuclear-powered thermochemical processes because lower temperatures lead to lower process efficiencies and higher temperatures require exotic construction materials [63].

The electrolysis of water coupled to conventional nuclear power generation has served as the benchmark against which thermochemical cycles have been compared [8, 64]. Water electrolysis has been the hydrogen production technology closest to deployment, utilizes simpler technology, and requires a smaller capital investment [64]. Therefore, thermochemical cycles such as the hybrid sulfur cycle will require better thermal efficiencies than electrolysis [8, 64].

Compared to water electrolysis, thermochemical cycles have a greater likelihood of higher energy efficiency [8, 12, 64, 65]. Both the hybrid sulfur and sulfur iodine cycles demonstrate this potential, and both have had real-world demonstrations at a small scale [8]. The implementation

of thermochemical cycles with nuclear or renewable energies has the long-term potential of reducing total emissions to near zero [66]. However, the implementation of a thermochemical cycle would require significant technological advancements before coupling it to a nuclear reactor [12]. Thermochemical cycles that require temperatures above 1600 °C are impossible to implement with nuclear reactors, and thermochemical cycles that have a max temperature of 350 °C would be inefficient to couple to a nuclear reactor [63].

2.3.3.1 Sulfur Iodine Cycle

Developed by General Electric in the 1970s, the Sulfur Iodine Cycle is one of the more well-known and mature thermochemical cycles available [67]. When integrated with a nuclear reactor with high-temperature capabilities it has demonstrated an efficiency as high as 47% [9] to 52% [68] for a stand-alone plant which can increase as much as 10% for an IES plant [63]. The three chemical reactions, equations 2.7-2.9, that make up the sulfur iodine cycle are:

$$2H_2O + SO_2 + I_2 \rightarrow H_2SO_4 + 2HI \quad (2.7)$$

$$H_2SO_4 \rightarrow H_2O + SO_2 + \frac{1}{2}O_2 \quad (2.8)$$

$$2HI \rightarrow H_2 + I_2 \quad (2.9)$$

Issues that face the sulfur iodine cycle include the exothermic Bunsen reaction, the high-temperature requirement for the endothermic sulfuric acid decomposition, the need for excess iodine, and corrosive reactants [69]. The sulfur iodine cycle faced early rejection due to the difficulty of separating sulfuric acid and hydrogen iodide which is an exothermic reaction [63]. However, the sulfur iodine cycle is the cycle that is the most attractive for nuclear coupled thermochemical hydrogen production alongside the UT-3 Br-Ca-Fe-based cycle, followed by the hybrid sulfur cycle [63].

2.3.3.2 Hybrid Sulfur Cycle

Hybrid thermochemical cycles utilize a process with an other-than-thermal energy source, in addition to the thermal energy, usually electrochemical as this results in a lower energy consumption than regular water electrolysis. This secondary process has the additional benefit of

the ability to utilize waste heat from the nuclear reactor to at least partially meet the electrical energy requirements of this step [8, 53].

The two-step hybrid sulfur cycle developed by Westinghouse in the 1970s is a combined thermochemical and electrochemical process [70]. It consists of the two-step thermal decomposition of sulfuric acid into SO_2, H_2O, and O_2, and the electrochemical oxidation of SO_2 into hydrogen gas and sulfuric acid [8]. Only having two reactions makes the hybrid sulfur cycle one of the simplest available cycles [8].

The main challenges facing the large-scale implementation of the hybrid sulfur cycle are the decomposition of SO_3 within the sulfuric acid decomposition stage and the corrosivity of the sulfur-based compounds. The incorporation of a silicon carbide (SiC) bayonet reactor has the potential to address these issues [8, 64, 65]. Figure 8 shows a design concept of a bayonet reactor. SiC has been shown to be able to withstand the high temperatures and pressures that sulfuric acid decomposition requires, however, the challenges that face the implementation of the reactor have made the evaluation of the hybrid sulfur cycle with a bayonet reactor highly desirable [64].

Sulfuric Acid Decomposition

Many of the difficulties that come with implementing the Hybrid Sulfur cycle are due to the challenges that come with the high temperature and pressure requirements of sulfuric acid decomposition. Thermochemical cycles are very attractive options for hydrogen production, but to make these processes viable options for nuclear hydrogen production they must be able to match thermodynamic efficiency benchmarks set by current methods of water splitting. Sulfur-based cycles show the greatest likelihood of meeting these demands [60], as well as being promising candidates for coupling to a nuclear reactor [60].

The decomposition of sulfuric acid is a two-step reaction where sulfuric acid first decomposes into sulfur trioxide and water, and then the sulfur trioxide breaks down into sulfur dioxide and oxygen [8]. Shown in equations 2.10 and 2.11. The much slower breakdown of sulfur trioxide takes place at higher temperatures than the first step, requires a catalyst, and is the limiting step for the production of sulfur dioxide, and therefore hydrogen production [8]. This decomposition is a common feature in sulfur-based thermochemical cycles.

$$H_2SO_4 \rightarrow SO_3 + H_2O \quad \Delta H^o = 97.54\ kJ/mol \tag{2.10}$$

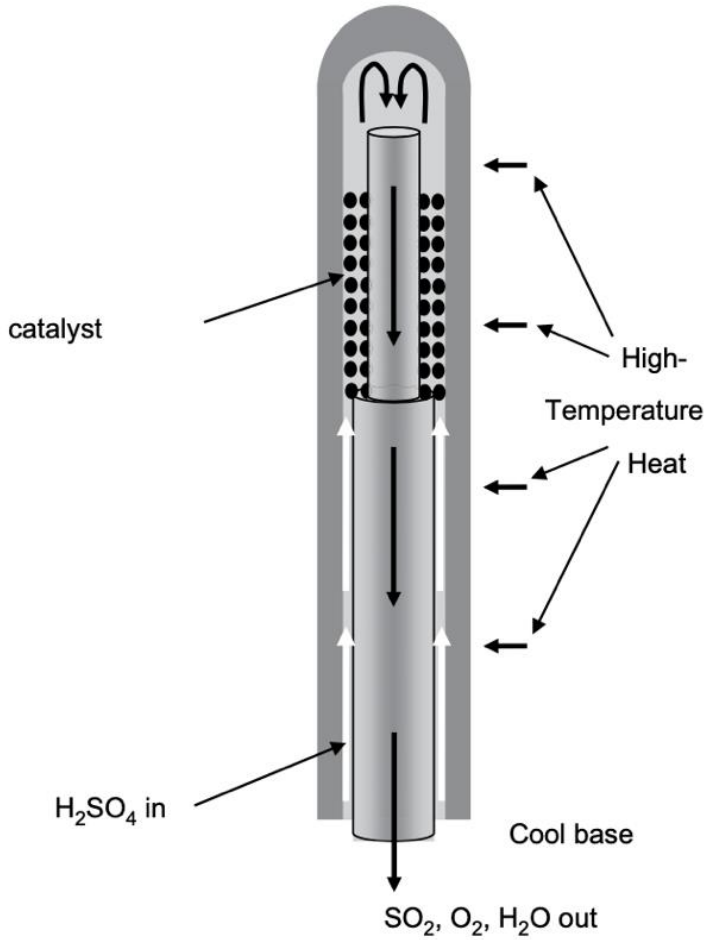

Figure 8: High-temperature bayonet reactor concept [8].

$$SO_3 \rightarrow SO_2 + \frac{1}{2}O_2 \quad \Delta H^o = 98.92\ kJ/mol \tag{2.11}$$

The bayonet reactor was designed by Sandia National Laboratory and is expected to aid in the upscale of the hybrid sulfur cycle [8]. Using a silicon carbide-based material that could withstand the high temperatures and pressures required for the decomposition reaction, which is resistant to corrosion as well, and using a readily available shape that encourages internal heat recuperation [8, 71, 72]. The reaction takes place within the catalyst bed, and the vapor product is condensed by heat recuperation transferring the thermal energy to the incoming reactants with negligible pressure drop [8]. Heat transfer limitations may limit the capacity of one bayonet reactor, however, the reactors could be arranged in parallel for commercial operations [8].

Electrolysis in the Hybrid Sulfur Cycle

For the viability of future hybrid sulfur cycle implementation, the electrolysis section is important because it needs to be competitive with water electrolysis. The electrical energy target for the SO_2 electrolysis is 116 kJ/mol H_2, this is based on an assumed -0.6 V cell potential, and keeping the energy efficiency higher than water electrolysis [8]. Using this benchmark gives a thermal energy equivalent of 352 kJ/mol H_2 for conventional reactors, and 258 kJ/mol H_2 for a HTGR type plant [8].

In the electrolysis section of the hybrid sulfur cycle make up H_2O and recycled H_2SO_4 are mixed with the H_2O and SO_2 from the decomposition reaction to form H_2 at the cathode and H_2SO_4 at the anode [8], shown in equations 2.12-2.14.

$$SO_2(aq) + 2H_2O(l) \rightarrow H_2SO_4(l) + H_2(g) \tag{2.12}$$

$$Anode: SO_2(aq) + 2H_2O(l) \rightarrow H_2SO_4(l) + 2H^+ + 2e^- \tag{2.13}$$

$$Cathode: 2H^+ + 2e^- \rightarrow H_2(g) \tag{2.14}$$

The standard cell potential for SO_2 electrolysis is -0.158 V at STP, which is lower than that of water and can be further lowered to -0.243 V if the reaction takes place in the presence of H_2SO_4 significantly lowering the electrical energy requirements for hydrogen electrolysis when compared to water electrolysis [8]. These are ideal operating conditions, however, which makes higher cell potentials likely under current electrolyzer designs [8]. Current research indicates that a proton

exchange membrane at temperatures above 100 °C and pressures above 10 bar could give a cell potential of -0.6 V, putting the cell potential well below that of conventional electrolysis [8]. This cell potential gives the decomposition process a benchmark of 450 kJ/mol H_2 for the hybrid sulfur cycle to be competitive with water electrolysis [8].

Thermodynamics of the Hybrid Sulfur Cycle

A key aspect of integrating the hybrid sulfur cycle, and other hydrogen production methods, into a nuclear-powered IES, is the energy efficiency of the cycle. A hybrid sulfur plant with a higher efficiency would result in a lower thermal energy requirement from a nuclear source [8]. Assuming a LHV from a contemporary BWR or PWR would leave about 728 kJ/mol H_2 of thermal energy for the remaining processes [8]. Whereas the LHV from a HTGR would leave 533 kJ/mol H_2 of thermal energy [8]. Assuming the demands of the auxiliary processes and a cell potential of -0.6 V in the electrolysis section, a benchmark of 450 kJ/mol H_2 has been set for the thermal decomposition of sulfuric acid, making the hybrid sulfur plant 25% more efficient than water electrolysis with BWR/PWR plants, and 10% more efficient than water electrolysis with a HTGR [8].

In previous evaluations of the bayonet reactor the kJs per mole of sulfur dioxide produced, or efficiency of the reactor, was shown to be dependent on the temperature and pressure in the reactor, and additionally on the composition of the incoming sulfuric acid and water mixture [8, 64, 65]. The temperature and pressure dependence is shown in Figure 9, where lower pressures had lower heating targets below 800 °C, or 1073 K [64, 65]. However, the most efficient processes were high-temperature and high-pressure processes, and at high temperatures, the lower-pressure processes saw higher heating targets [64, 65].

The weight fraction of the incoming sulfuric acid-water mixture played a significant part in the efficiency of the bayonet reactor [8]. The 80 wt% sulfuric acid saw the highest efficiency at 90 bar and 900 °C, 1173 K [64], and in additional flowsheet models the 80 wt% sulfuric acid saw the highest efficiency at various pressures and a constant maximum process temperature of 870 °C, 1143 K [8]. Figure 10 shows the dependence of the heat requirement for sulfuric acid decomposition as a function of the weight fraction of sulfuric acid. The resulting flowsheet evaluations determined the most efficient operations for the bayonet reactor were at high pressures

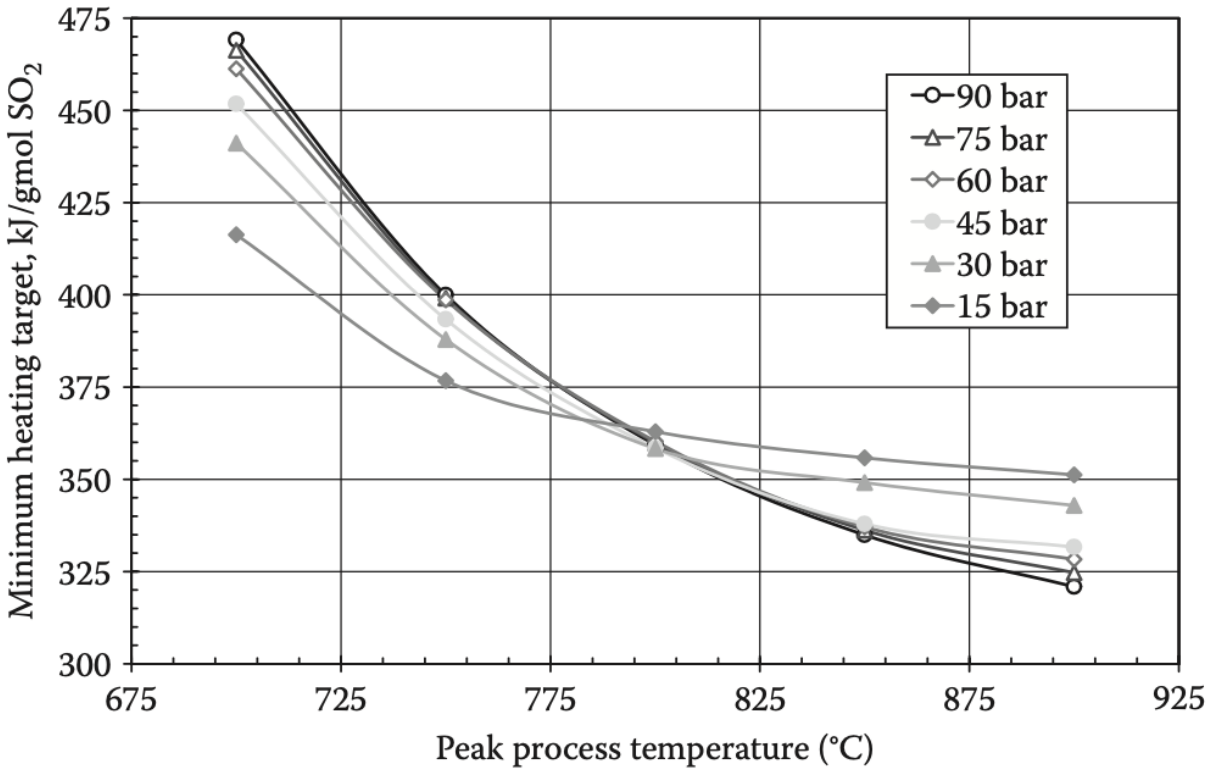

Figure 9: 80.1 wt% sulfuric acid and water mixture feed concentration [64, 65].

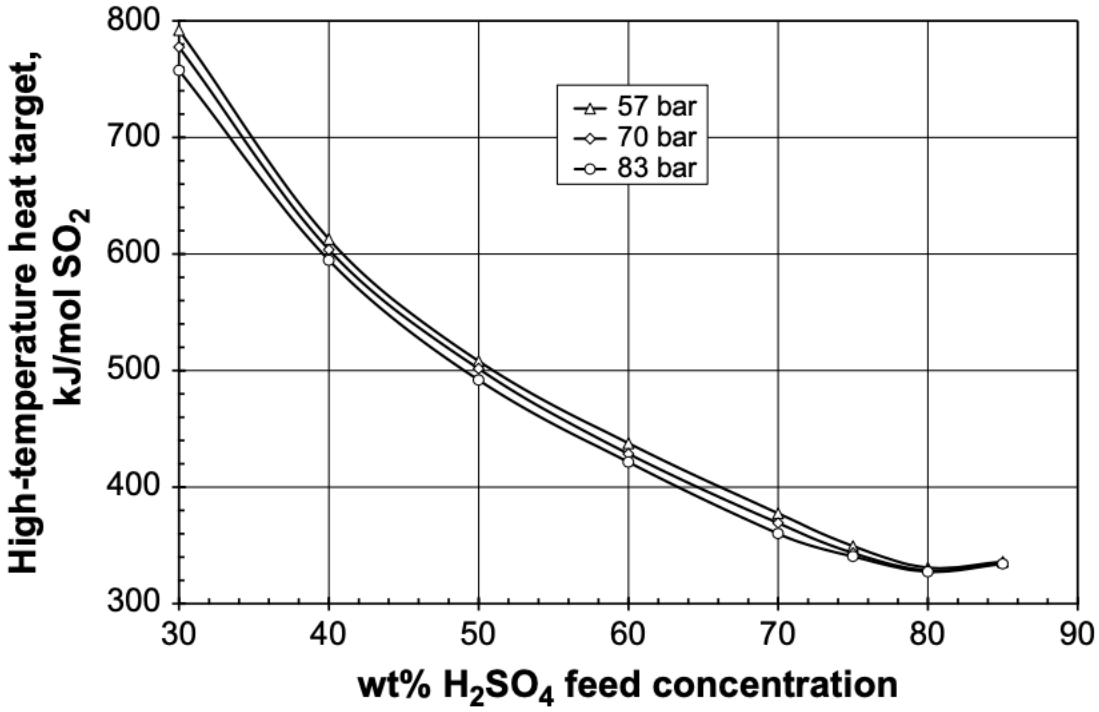

Figure 10: Bayonet heat requirement as a function of sulfuric acid concentration and pressure [8].

and temperatures, and above 60 wt% sulfuric acid concentration in the incoming mixture [8, 64, 65].

2.3.4 Applications of the Lessons from the Aktau NPP to a High-Temperature Process

For a high-temperature process like thermochemical hydrogen production, the questions to be addressed for implementation into a nuclear IES were:

1. What about direct feedback between high-temperature processes and nuclear reactors?
2. How can hydrogen production fit into an energy grid?
3. What if thermal demand for the process is higher or lower than what is provided?

A review of hydrogen production, specifically thermochemical hydrogen production provided new evaluation criteria for high-temperature processes:

1. A high-temperature process requires a direct supply of thermal energy, creating the need for evaluation of direct feedback and cascading effects between the high-temperature process and the nuclear reactor and their effects on the overall grid.
2. The ability to fit a high-temperature process, such as thermochemical hydrogen production, into a grid largely depends on the efficiency and thermal demand of the process.
3. The nature of the feedback between the high-temperature process and the nuclear reactor in the case of thermal energy supply and demand mismatch greatly depends on the chemical equilibria within the various processes.

To evaluate a nuclear IES with a high-temperature thermochemical cycle based on these criteria, a model of the endothermic sulfuric acid decomposition was required. As can be noted throughout the review of hydrogen production, many complex models of sulfuric acid decomposition have been developed. However, for IES grid evaluation, a more simplistic model was required for ease of implementation and flexibility. Agnostic in the sense that it could be operated in conjunction with a wide variety of IES designs and heating fluids. And holistic in that it could provide a wide range of results for the energy demand, chemical information, and cascade feedback based on a minimum of inputs.

The requirements of the desired model based on the needs of a high-temperature chemical process as found in the review were:

1. Robust enough to provide accurate outputs of chemical and thermodynamic data useful for grid evaluation.
2. Efficiency and thermal demand are consistent with previous work.
3. Chemical equilibrium data based on desired operational conditions, as well as capturing resulting equilibria based on possible transients.

Chapter 3. Methodology

3.0 Assumptions

To meet the goal of a simplistic model that could be used in a variety of different applications, there were a few assumptions made.

1. No pressure drop in the reactor. This made it possible to use C_p heat capacity instead of C_v for the thermal energy demand in the reactor, in addition to simplifying the energy balance equations and the conversion for the chemical reaction.
2. For the purposes of heat transfer the bayonet reactor energy demand models could use plug flow reactor equations for heat transfer.
3. The first step of sulfuric acid decomposition was fast, irreversible, and proceeded to full extent at the temperatures required for the second step of the reaction to take place. Additionally, the effluent temperatures would be low enough for the unreacted SO_3 to fully recombine with water back to H_2SO_4.
4. The reactants had enough time in the reactor bed to proceed to the full extent of reaction possible at the given temperature and pressure.

All simplifying assumptions were used in previous work modeling sulfuric acid decomposition found in the review. Assumption 3 was additionally used as a result-based assumption from the work performed modeling the reaction itself.

3.1 Sulfuric Acid Decomposition

It was decided that the model of the decomposition of sulfuric acid through a bayonet reactor required a stepwise series of functions that could represent each part of the reactor. These simulated the heating, vaporization, reaction, cooling, and then condensing of the chemical components. The fundamental requirement for this was an accurate model of the sulfur trioxide decomposition, as it was the real rate-limiting step, that could give both pressure and temperature-based chemical reaction equilibrium.

Given the unknown nature of the physical design and specifications of the bayonet reactor, a holistic approach to the model was necessary. Dimensions of the reactor were used where possible, and taken from previous literature, but the holistic nature of the model meant that the energy demand and chemical reaction models could provide a wide variety of outputs with a minimum of inputs. While this sacrificed some accuracy, the methods outlined provided results that agreed with previous work and gave a robust model that had the potential for a wide variety of grid analyses.

To track the energy required for the decomposition reaction, and for determining overall efficiencies, the enthalpy change in both the input and output must be included in the model. Previous research established 80 wt% H_2SO_4 in the incoming mixture as an efficiency benchmark [4]. The 80 wt% incoming H_2SO_4 can be easily maintained with a vacuum column, and the extent of the reaction can be assumed to be full due to the ease at which a chemical reaction can be maintained at 850 °C. These assumptions, however, do not give the plant model the flexibility required for accurate modeling of minor or major fluctuations in both plants' operational conditions, and the following work provides a method of modeling the process to accommodate these needs.

The decomposition of sulfuric acid is an endothermic two-step reaction. The sulfuric acid decomposes into water and sulfur trioxide, equation 3.1, which further decomposes into sulfur dioxide and oxygen, equation 3.2. Both reactions require thermal energy in the form of heat delivered to progress forward, however, high temperatures are required for an acceptable extent of reaction for the sulfur trioxide decomposition.

$$H_2SO_4 \rightarrow SO_3 + H_2O \quad (3.1)$$

$$2SO_3 \rightarrow 2SO_2 + O_2 \quad (3.2)$$

To model the reactions based on temperature-based reaction kinetics Arrhenius relations were used for the reaction constants, k, and equilibrium constants, K_C. Constants A, E_a, $k_c(T_R)$, and ΔH_{Rx} were identified from the literature and used to compare to existing models and data. The forms of the equations are shown in equations 3.3 and 3.4.

$$k = A * e^{\frac{E_a}{RT}} \quad (3.3)$$

$$K_c = k_c(T_R) * exp\left[\frac{\Delta H^o_{Rx}(T)}{R}\left(\frac{1}{T_R} - \frac{1}{T}\right)\right] \quad 3.4$$

The model of the reaction was based on the assumption that both reactions were first-order reactions with respect to the sulfur trioxide, an assumption taken from the literature, and a simple reaction model was created based on the time derivative using the form seen in equation 3.5. This

$$\frac{dC_i}{dt} = r_{f,i} - r_{r,i} = k_f f\left(C_{R,i}\right) - k_r f\left(C_{P,i}\right) \quad 3.5$$

model did not consider the pressure dependence of the reaction and assumed equation 3.6 applied to the reverse reaction constant.

$$K_c = \frac{k_f}{k_r} \quad 3.6$$

The extent of reaction over a range of temperatures is shown in Figure 11, which compares the model outputs to experimental data obtained for sulfuric acid decomposition. The results of the modeled extent of reaction were helpful to establish two different assumptions for following, more complex, process models.

1. At temperatures required for acceptable sulfur trioxide decomposition, the sulfuric acid decomposition into water and sulfur dioxide was fast, complete, and irreversible, and would proceed to its full extent.
2. Due to assumption 1, only the equilibrium constants and conversion of sulfur trioxide would be the limiting reaction within the decomposition section.
3. The only components in the heating sections would be sulfuric acid and water.

The effluent species composition and enthalpy are of high importance to bayonet reactor efficiency. The extent of reaction can have a significant impact on the thermodynamic efficiency of the process, and the process operations in other sections of the plant and overall plant efficiency

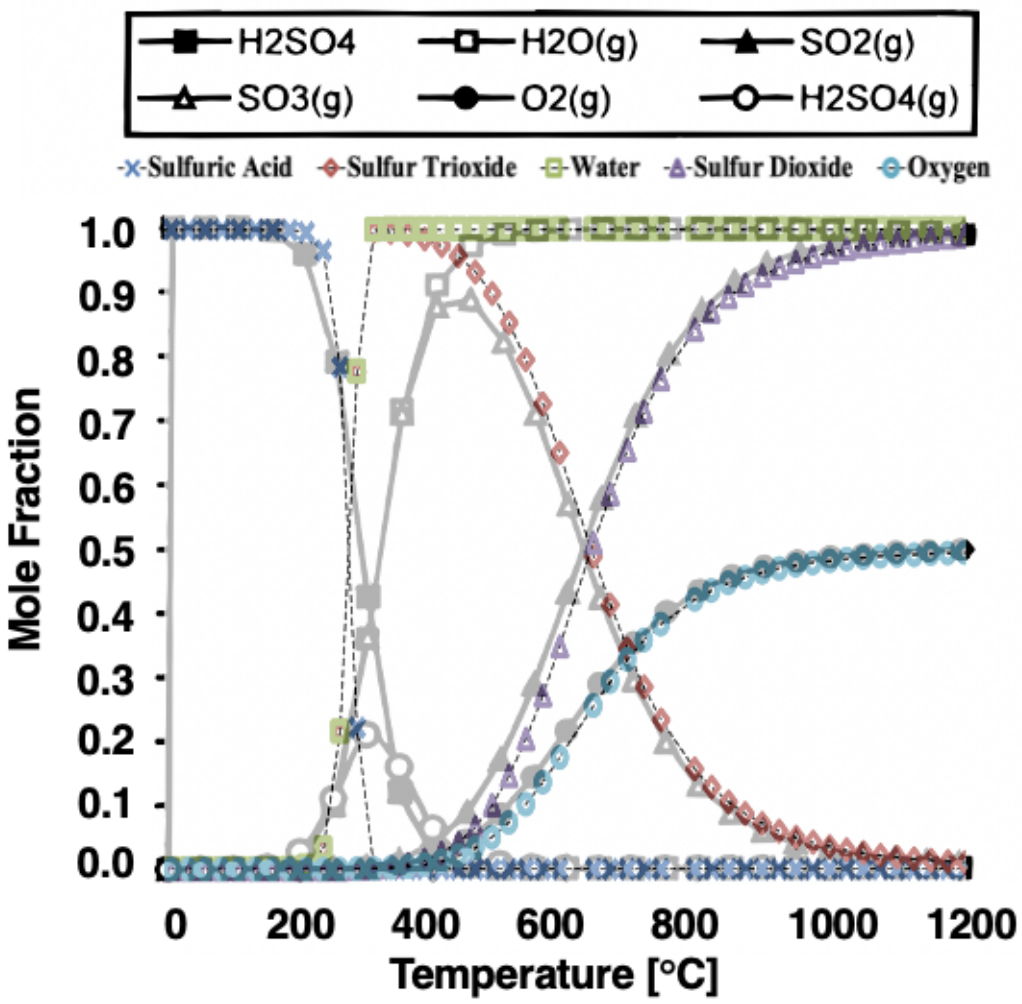

Figure 11: Comparison of modeled extent of reaction (colored) to experimental [73] (black and white).

To provide an accurate extent of reaction outputs, the reaction model then had to incorporate complex behavior.

3.1.2 Equilibrium Constant Verification

Determining the accuracy of the equilibrium constant for sulfur trioxide decomposition is very important for conversion and many other factors of the chemical reactor design. Previous models of sulfur trioxide conversion were compared to previous calculations done using the Gibbs energy method in equation 3.7, comparisons are shown in Table 5.

$$-\ln(K) = \frac{\Delta G^{\circ}}{RT} \tag{3.7}$$

The equation used for the equilibrium constant was equation 3.4, where the reference K_c was 0.041 at 973 K, and the heat of reaction was 98.93 kJ/mol at 298 K. Additionally the heat of reaction above the reference temperature was calculated using equations 3.8 and 3.9.

$$\Delta H_{Rx}(T) = \Delta H_{Rx}^{\circ}(T_R) + \Delta C_P(T) * (T - T_R) \tag{3.8}$$

Where:

$$\Delta C_P(T) = C_{P,SO_2}(T) + 0.5 * C_{P,O_2}(T) - C_{P,SO_3}(T) \tag{3.9}$$

The ideal heat capacities of each species were calculated using equations 3.10-3.12:

$$C_{P,SO_3}(T) = R * \left(8.06 + 1.056x10^{-3} * T - \frac{2.028x10^5}{T^2}\right) \tag{3.10}$$

$$C_{P,SO_2}(T) = R * \left(5.699 + 8.01x10^{-4} * T - \frac{1.015x10^5}{T^2}\right) \tag{3.11}$$

$$C_{P,O_2}(T) = R * \left(3.693 + 5.06x10^{-4} * T - \frac{1.21x10^4}{T^2}\right) \tag{3.12}$$

Comparisons of the modeled heat capacities to the Shomate polynomial, equation 3.13, heat capacities can be seen in figures 12-14.

$$C_P(T) = A + BT + CT^2 + DT^3 + \frac{E}{T^2} \qquad 3.13$$

Figure 15 shows the calculation using the NIST heat capacity values of the sulfuric acid-water mixture at 298.15 K. The red line is the ideal heat capacity of the mixture compared to the black line which was from DIPPR equations, and the experimental values which were the circles. The derivation seen at higher concentrations was a result of NIST values not existing for liquid sulfuric acid. However, the results were agreeable enough for the use of NIST heat capacities for the model of sulfuric acid decomposition.

3.1.3 Sulfur Trioxide Conversion

The conversion of the sulfuric acid decomposition is a crucial aspect of the entire hybrid sulfur cycle. The extent of the reaction could determine overall process efficiency, and low conversion could lead to detrimental effects throughout the process. Additionally, the conversion of sulfuric trioxide has been found to be inversely proportional to reactor pressure, see Figure 16.

To determine the relationship of conversion in the sulfur trioxide decomposition with pressure, the pressure and concentration equilibrium constants were set equal to each other. The concentration equilibrium was found by using equation 3.4 and set equal to equation 3.14 which was the method for relating pressure equilibrium and conversion.

$$K_c(P,T) = \frac{\left[4.86x10^{-5} * P\left(\frac{X}{1+\varepsilon X}\right) * \frac{1173}{T}\right]\left[4.86x10^{-5} * P\left(\frac{0.5 * X}{1+\varepsilon X}\right) * \frac{1173}{T}\right]^{0.5}}{\left[4.86x10^{-5} * P\left(\frac{1-X}{1+\varepsilon X}\right) * \frac{1173}{T}\right]} \qquad 3.14$$

Where epsilon was the ratio of the change of total moles to see complete conversion to the total number of moles fed to the reactor and was calculated with equation 3.15.

$$\varepsilon = y_{SO_3,0}(1 + 0.5 - 1) \qquad 3.15$$

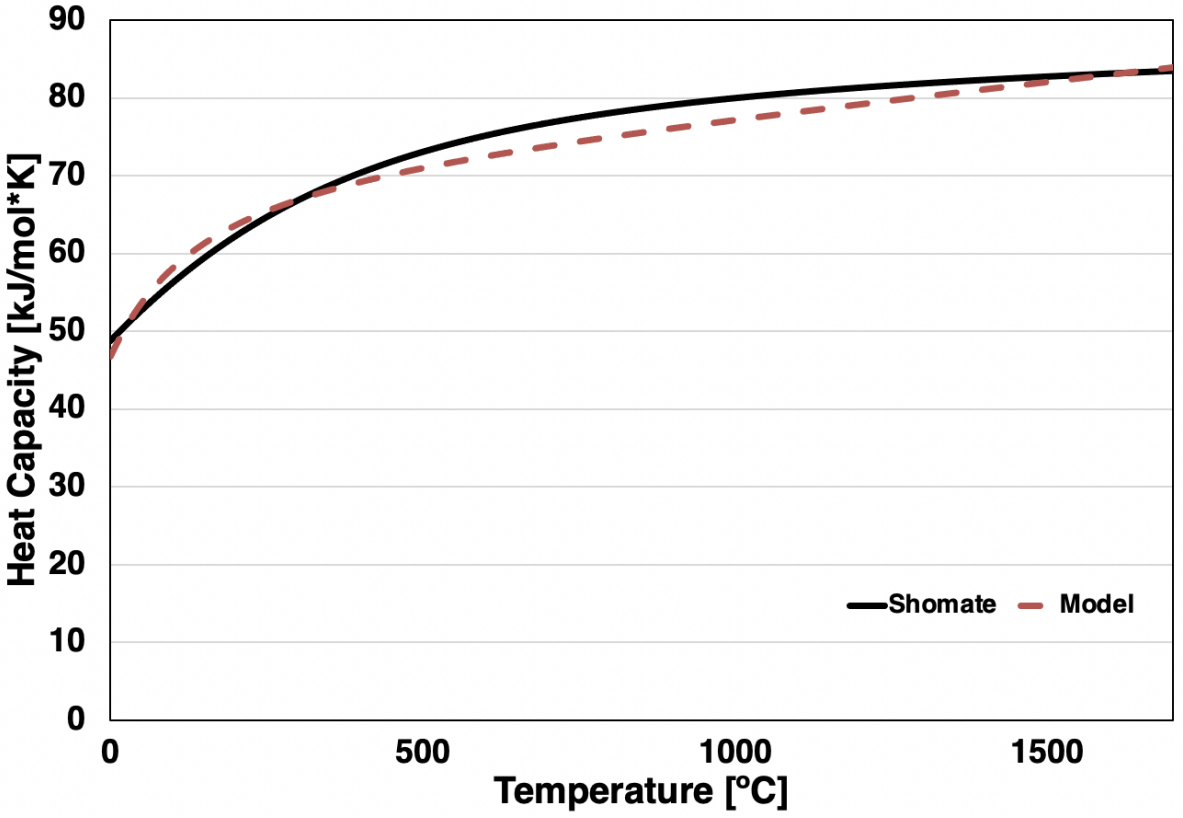

Figure 12: Comparison of heat capacities for sulfur trioxide.

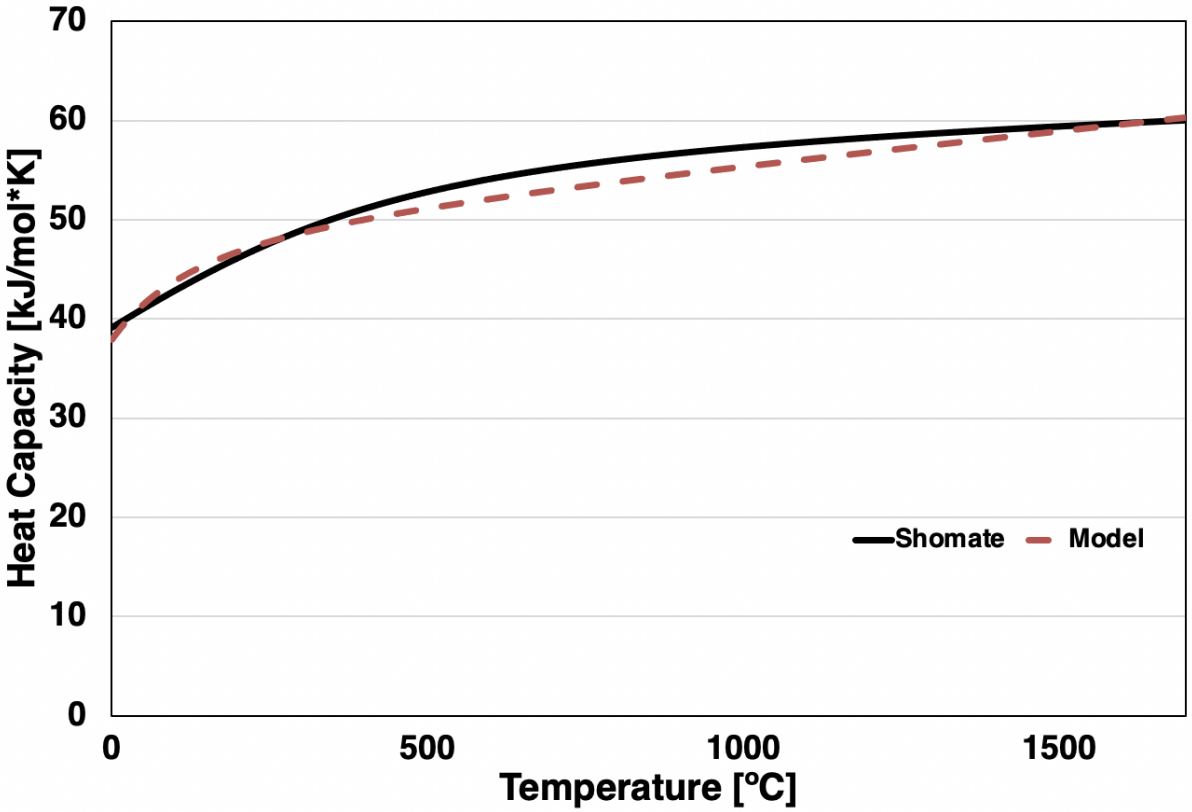

Figure 13: Comparison of heat capacities for sulfur dioxide.

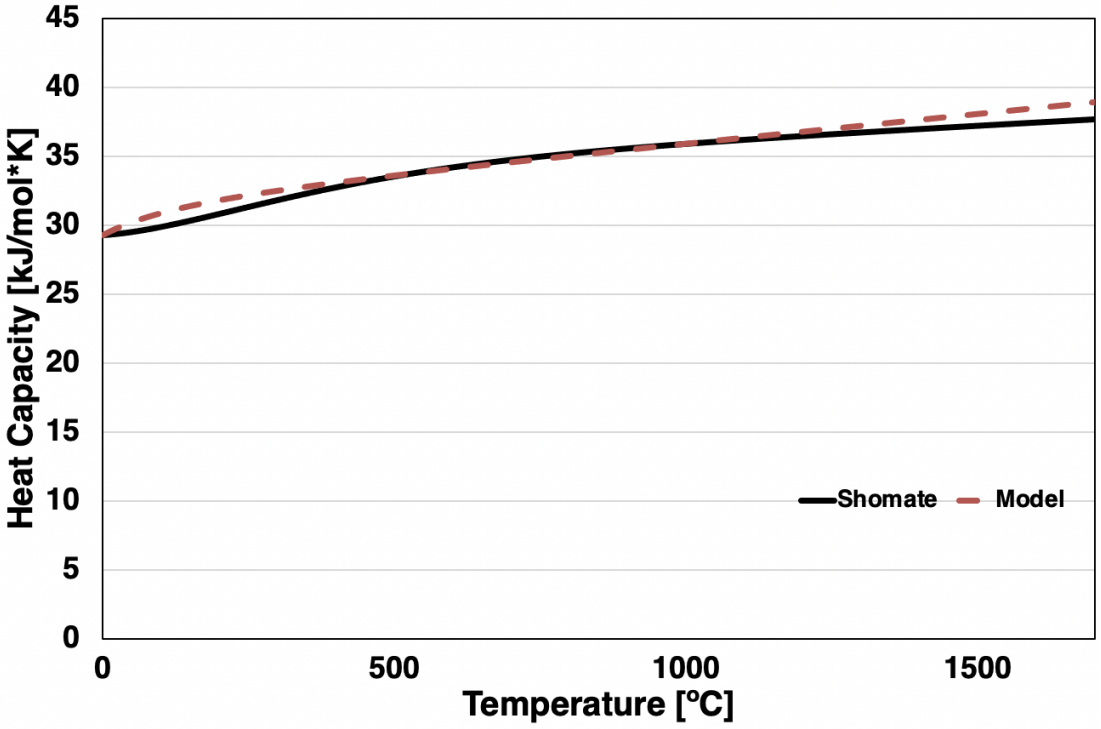

Figure 14: Comparison of heat capacities for oxygen.

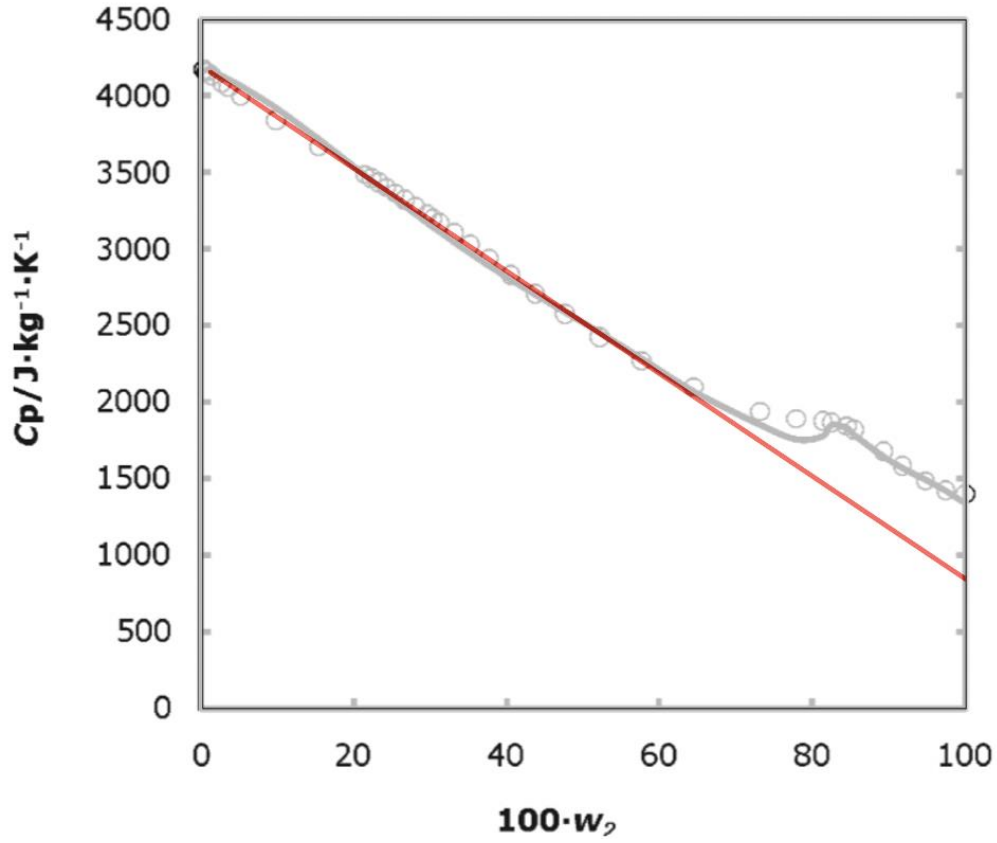

Figure 15: Specific heat capacity of aqueous sulfuric acid-water mixture (red, black, dots) at 298.15 K.

For an ideal model, the initial concentration of gaseous sulfur trioxide was initially assumed to be 1, causing epsilon to be 0.5, but can vary depending on the incoming fraction of water into the decomposer. This would result in an epsilon value in the range of 0.25-0.23. However, the results of the inclusion of heat capacities of the chemical species, and using an epsilon value of 0.5, did not result in large differences in conversion values when compared to a model with no heat capacities which used an epsilon value of 0.237. The largest differences can be seen in the high temperature and pressure conversions. The conversion values comparison can be seen in Table 6, and the percent error of the conversion methods in Table 7. The graphical representation of the modeled conversion based on pressure and temperature can be seen in Figure 17.

The conversion was an important component of reactor design and could be used to find the effluent composition and the overall energy required for the reaction. Chemical reactor design can incorporate various methods to improve poor conversion. However, specific design aspects of the physical bayonet reactor are yet to be determined, so to incorporate conversion improvement methods into the reactor model it could be important to design a recycling module that could recycle unreacted sulfur trioxide back into the reactor.

3.1.4 Vapor-Liquid Equilibrium

3.1.4.1 Sulfuric Acid-Water VLE and Boiling

The phase change from liquid to vapor phase was an important key to understand the thermal demands of the hybrid sulfur cycle. Due to the boiling point of sulfuric acid being so much higher than the boiling points of the other species in the system, and due to the assumption that the sulfuric acid decomposition step was fast and irreversible, the vaporization of the water-sulfuric acid mixture, and the water-sulfuric acid-sulfur trioxide mixture to a lesser extent, was the most important consideration for system thermodynamics. The boiling points of the chemical species in the reactor were an important consideration as well, see Table 8. Due to the higher boiling points of both sulfuric acid and water, it was a reasonable assumption that those two species would have the largest impact on vapor-liquid equilibrium, and therefore the energy requirements for phase change within the vaporization section.

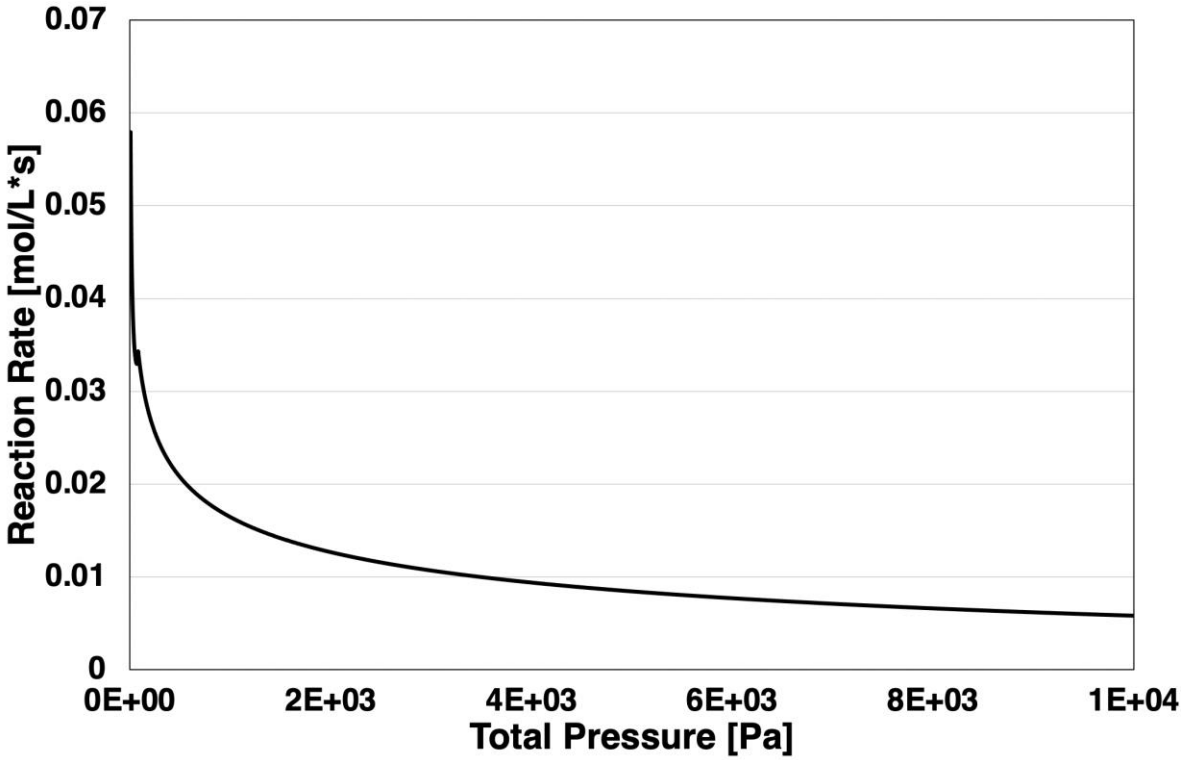

Figure 16: Sulfur trioxide decomposition rate as a function of total pressure.

Table 5: Comparison of equilibrium constants.

Temperature (K)	K_C [74] $(mol/dm^3)^{0.5}$	K_C $(mol/dm^3)^{0.5}$
300	$4.85x10^{-13}$	$4.66x10^{-13}$
400	$9.83x10^{-09}$	$8.10x10^{-09}$
500	$3.85x10^{-06}$	$2.98x10^{-06}$
600	$2.06x10^{-04}$	$1.56x10^{-04}$
700	$3.50x10^{-03}$	$2.66x10^{-03}$
800	0.0289	0.0353
900	0.1500	0.170
1000	0.5577	0.601
1100	1.6117	1.70
1200	3.8693	4.07
1300	8.2015	8.54
1400	15.4550	16.2
1500	26.6038	28.1

Table 6: Comparison of conversion values.

	Pressure (kPa)			
Temperature (°C)	100	300	3000	9000
427	**0.0305**	**0.0218**	**0.0100**	**0.0069**
427	0.0315	0.0220	0.0102	0.00713
527	**0.124**	**0.088**	**0.0422**	**0.0295**
527	0.127	0.090	0.0431	0.0301
627	**0.330**	**0.246**	**0.126**	**0.089**
627	0.332	0.248	0.126	0.089
727	**0.598**	**0.485**	**0.279**	**0.205**
727	0.595	0.482	0.276	0.203
827	**0.803**	**0.711**	**0.481**	**0.375**
827	0.795	0.702	0.471	0.365
927	**0.909**	**0.854**	**0.673**	**0.563**
927	0.901	0.844	0.656	0.544
1027	**0.956**	**0.927**	**0.810**	**0.721**
1027	0.950	0.918	0.790	0.696

Bolded values from [74]

Table 7: Percent error of model results and previous data.

	Pressure (kPa)			
Temperature (°C)	100	300	3000	9000
427	3.3%	0.61%	2.7%	3.4%
527	2.2%	2.3%	2.0%	2.0%
627	0.61%	0.71%	0.22%	0.49%
727	-0.55%	-0.64%	-1.2%	-1.2%
827	-0.95%	-1.3%	-2.2%	-2.6%
927	-0.87%	-1.2%	-2.6%	-3.4%
1027	-0.59%	-0.96%	-2.4%	-3.4%

Comparison values from [74]

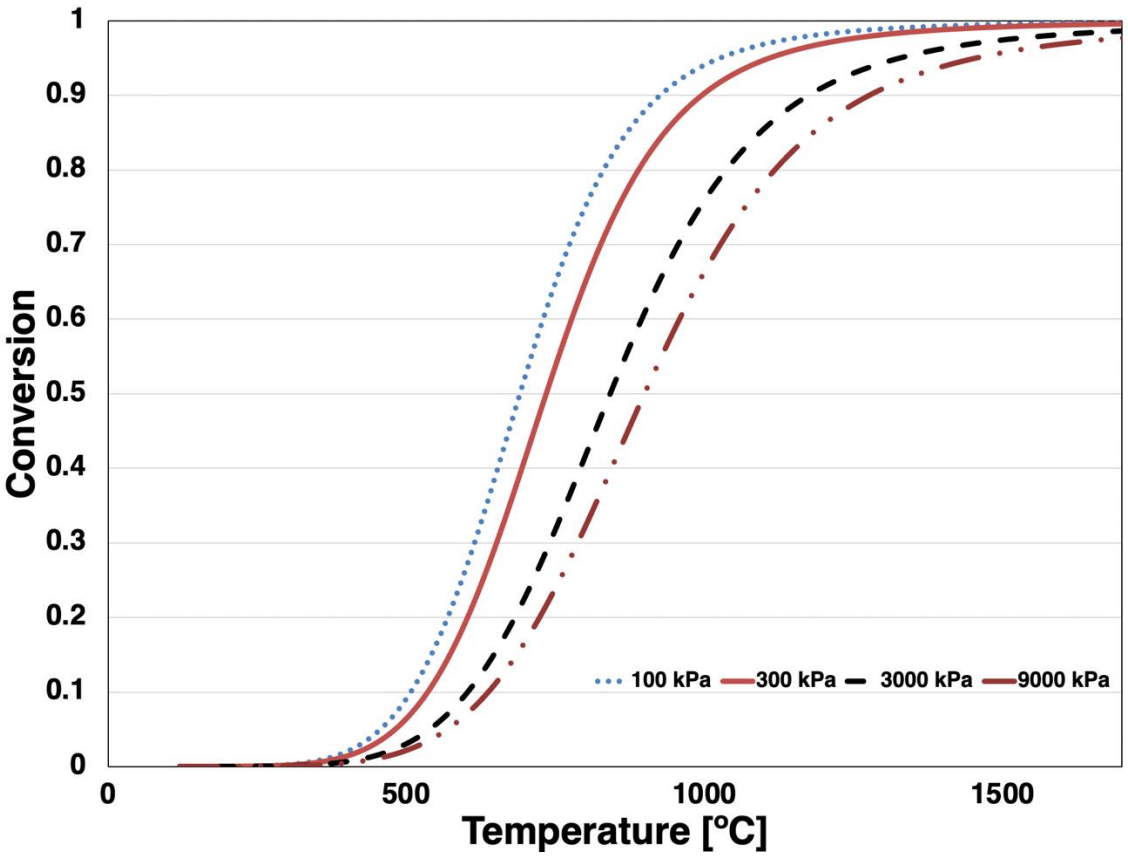

Figure 17: Sulfur trioxide conversion as a function of pressure and temperature.

Assuming ideal conditions for vapor-liquid equilibrium provided Raoult's law. Raoult's law is a method of calculating an ideal vapor pressure with the form in equation 3.16, neglecting the activities of the species. Where P_i^* is the equilibrium vapor pressure of species i, x_i is the mole fraction of species i in the liquid, and P_i is the partial pressure of the species exerted by the vapor phase. For a mixture, this became equation 3.17.

$$x_i P_i^* = P_i \tag{3.16}$$

$$P = \sum P_i = \sum x_i P_i^* \tag{3.17}$$

Raoult's law was used to model sulfuric acid-water mixture vaporization at 86 bar and 65 wt% sulfuric acid, shown in Figure 18. This mixture model had a boiling point at around 380 °C and only the vapor phase was present at temperatures above 635 °C. This temperature range agrees with previous models from Savannah River National Labs [8].

Figure 19 demonstrates the comparison of Raoult's law to the Rachford Rice method of determining vapor-liquid equilibrium and the Soave-Redlich-Kwong (SRK) equation of state. Rachford Rice incorporates a method of determining the activities of the species in equilibrium using their critical points and boiling temperatures, shown in equation 3.18. Previous models of sulfuric acid bayonet decomposition used the Redlich-Kwong or Soave-Redlich-Kwong (SRK) equations of state to model mixture boiling in the bayonet reactor. When compared to the other methods full vapor phase was achieved at lower temperatures, shown in Figure 19. Due to the non-ideal mixture quality of sulfuric acid and water, and because of its use in previously published work on the hybrid sulfur cycle, the SRK equation of state was used for boiling models in the hybrid sulfur model for this work using thermodynamic methodology from MIT's Chemical Engineering Design Library [75, 76].

$$K_i = \frac{P_{c,i}^{\frac{\frac{1}{T}-\frac{1}{T_{b,i}}}{\frac{1}{T_{c,i}}-\frac{1}{T_{b,i}}}}}{P} \tag{3.18}$$

At high wt% sulfuric acid, the vapor pressure models agreed with existing models and data. Figure 20 shows the comparison of the modeled vapor pressure to experimental data, and Figure 21 shows the comparison of experimental, calculated, and modeled vapor pressure of three different wt% sulfuric acid-water mixtures. However, as Figure 21 demonstrates, Raoult's law began to deviate from expected behavior not accounting for the activity. This was seen in Figure 21 where the deviations between the vapor pressures at small differences in wt%, shown by the experimental and calculated points, were not shown using Raoult's law.

The vapor pressure was calculated using the Antoine or extended Antoine equations, equations 3.19 and 3.20 respectively. Figure 22 shows the further deviation of this method has not accounted for species activities in the mixture when compared to previous work. Although, modeled sulfuric acid-sulfur trioxide mixture vapor pressures agree more with previous work at the temperatures and compositions likely to be seen in the decomposition stage of the hybrid sulfur cycle.

$$\ln(p) = A + \frac{B}{C + T} \tag{3.19}$$

$$\ln(p) = A + \frac{B}{T} + C * \ln(T) + D * T^{E} \tag{3.20}$$

Sulfuric Acid-Sulfur Trioxide VLE

Figures 23 and 24 show the same Raoult's method of mixture vapor pressures but for a sulfuric acid-sulfur trioxide mixture. It was important to note that the mixture of sulfuric acid and sulfur trioxide is unlikely to make an impact due to the assumption that the first step of the sulfuric acid decomposition is both fast and irreversible, as well as that sulfur trioxide is unlikely to be present in significant quantities below the temperatures required for the vaporization. But at the high temperatures and low wt% sulfur trioxide mixtures most likely to be seen in the vaporization module, the models show good agreement.

While accuracy in non-ideal vapor-liquid equilibrium models is important for complex system models, the simpler methods used to model the reactions and phase equilibria can show good agreement with previous work, both experimental and other models, to be considered for incorporation into a full hybrid sulfur model. This model can in turn be used to deliver more ideal results for overall process energy demand and hydrogen produced.

Table 8: Boiling and critical points of chemical species.

	Boiling Point (°C)	Critical Temperature (°C)	Critical Pressure (kPa)
Sulfuric Acid	337	650	6400
Sulfur Trioxide	45	218	8200
Sulfur Dioxide	-10	157	7880
Water	100	374	2205
Oxygen	-183	-119	5043

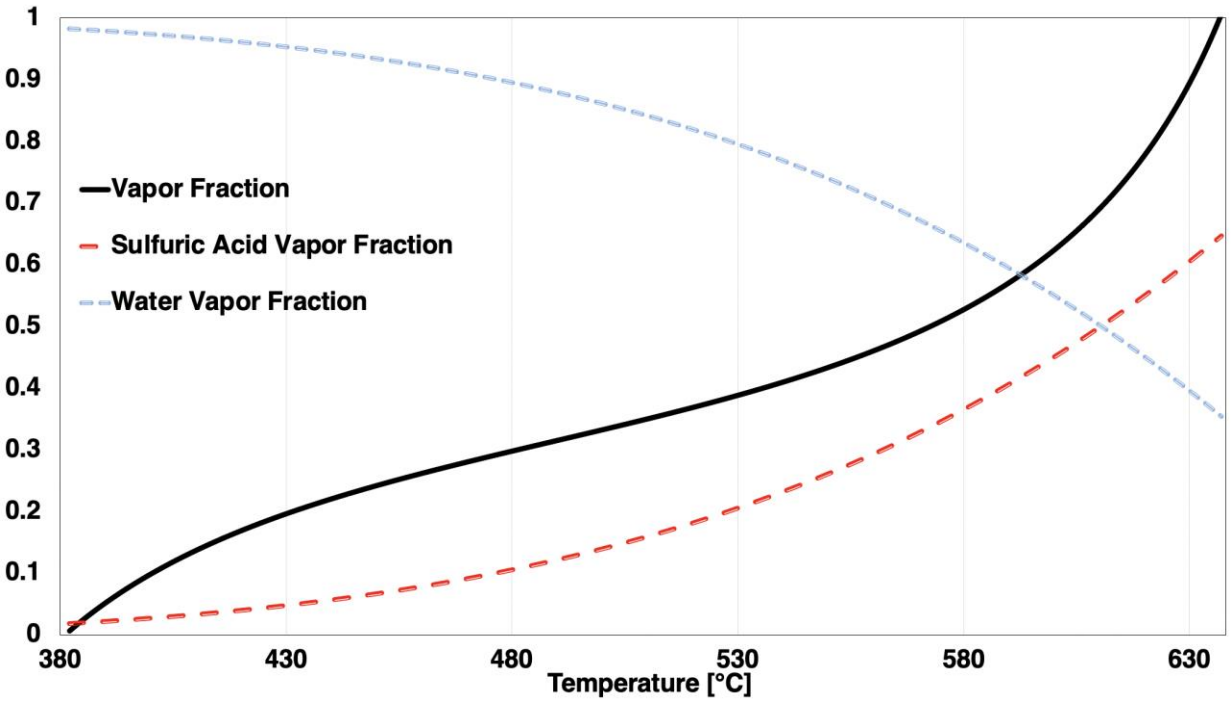

Figure 18: Sulfuric acid-water mixture vaporization

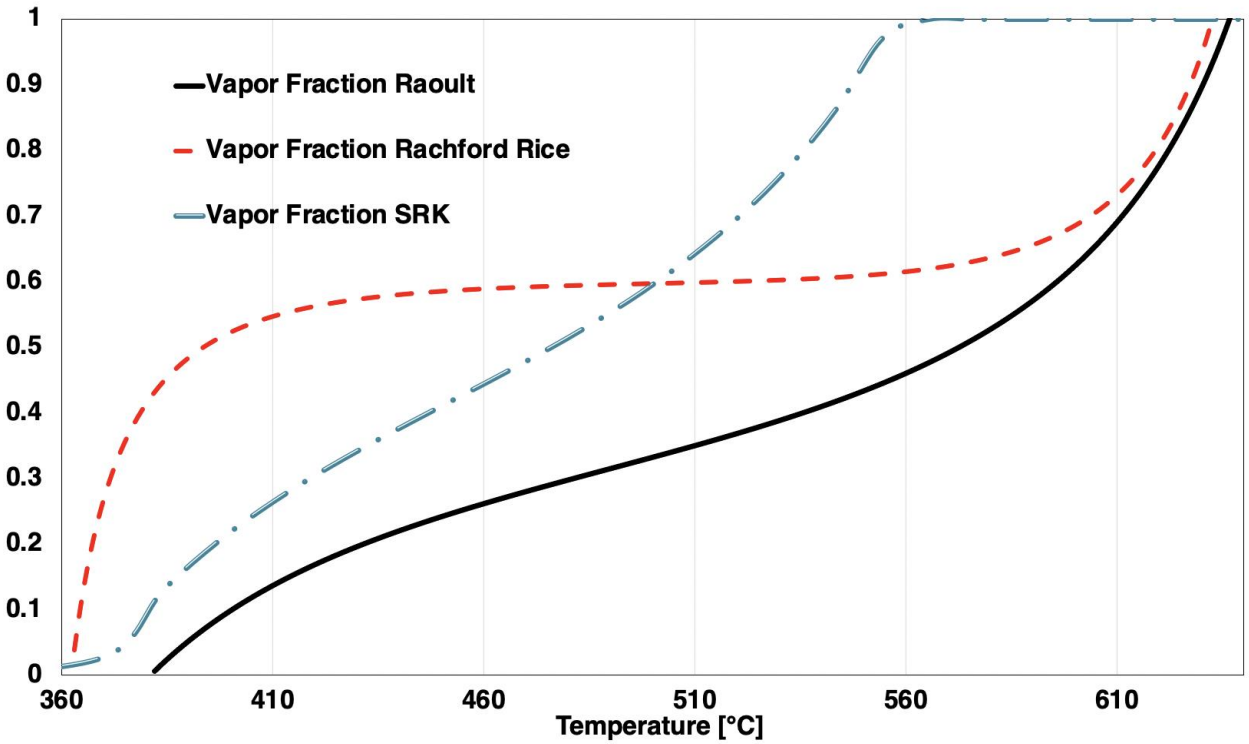

Figure 19: Comparison of Raoult's law to Rachford Rice and SRK equation of state.

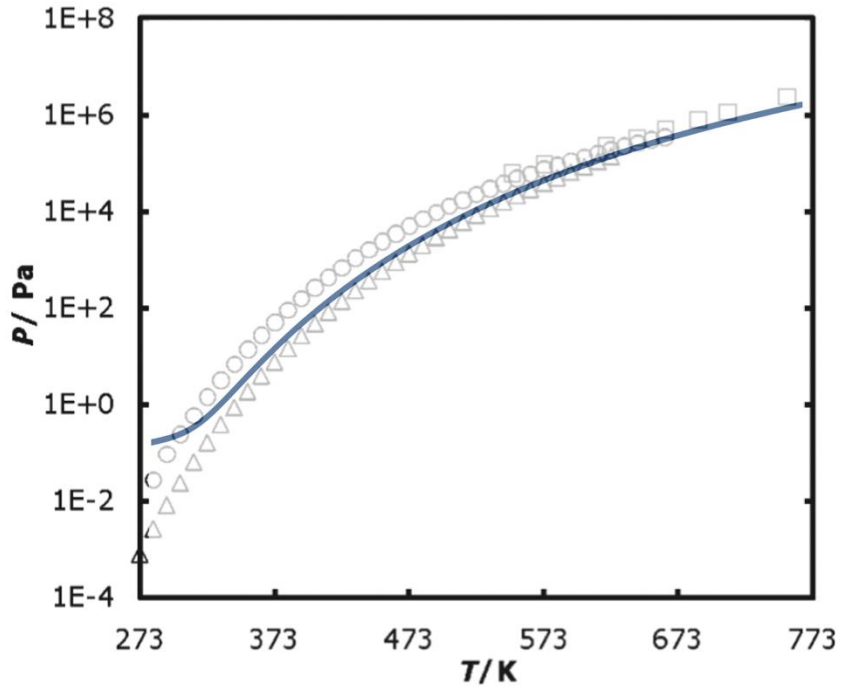

Figure 20: Modeled vs experimental [77] vapor pressure of a 0.985 wt% sulfuric acid-water mixture.

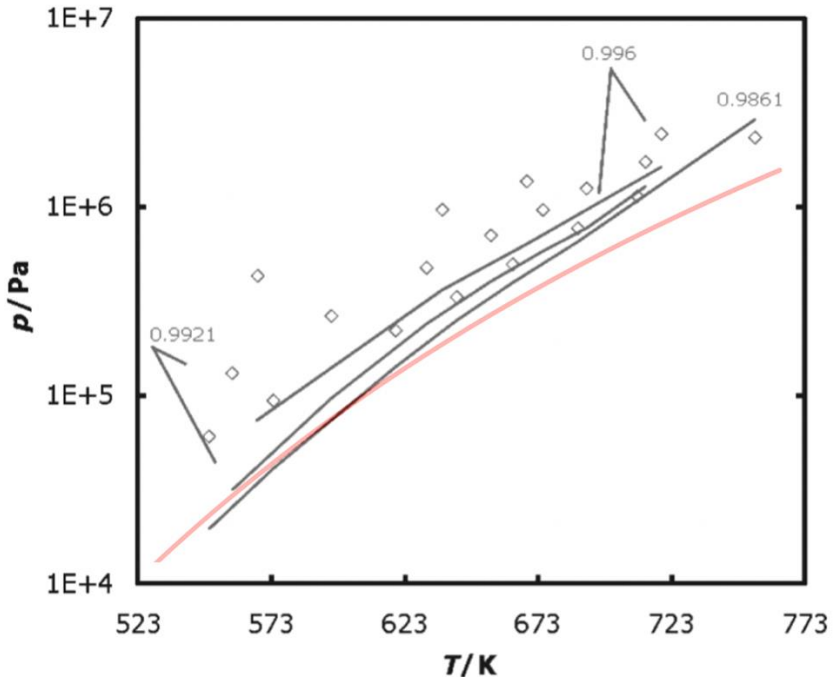

Figure 21: Model (red) compared to calculated [77] (black) and experimental [77] (points) sulfuric acid-water mixture vapor pressures.

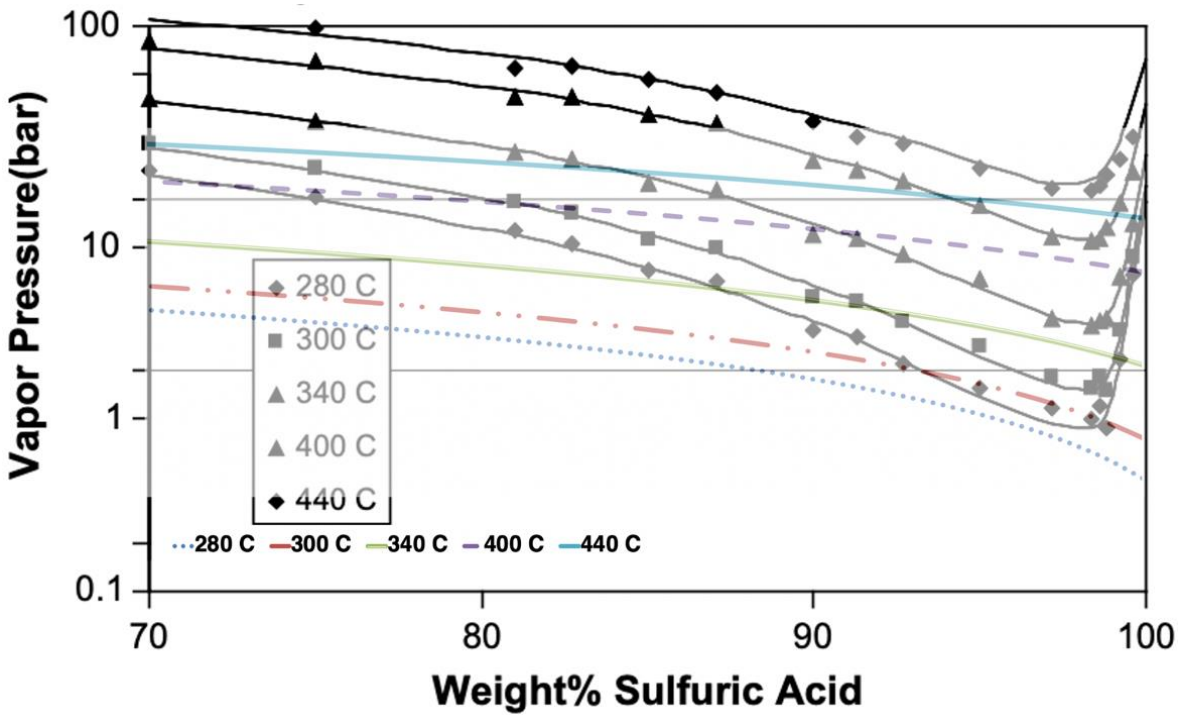

Figure 22: Comparison of modeled mixture vapor pressure as a function of sulfuric acid wt% to previous work [8].

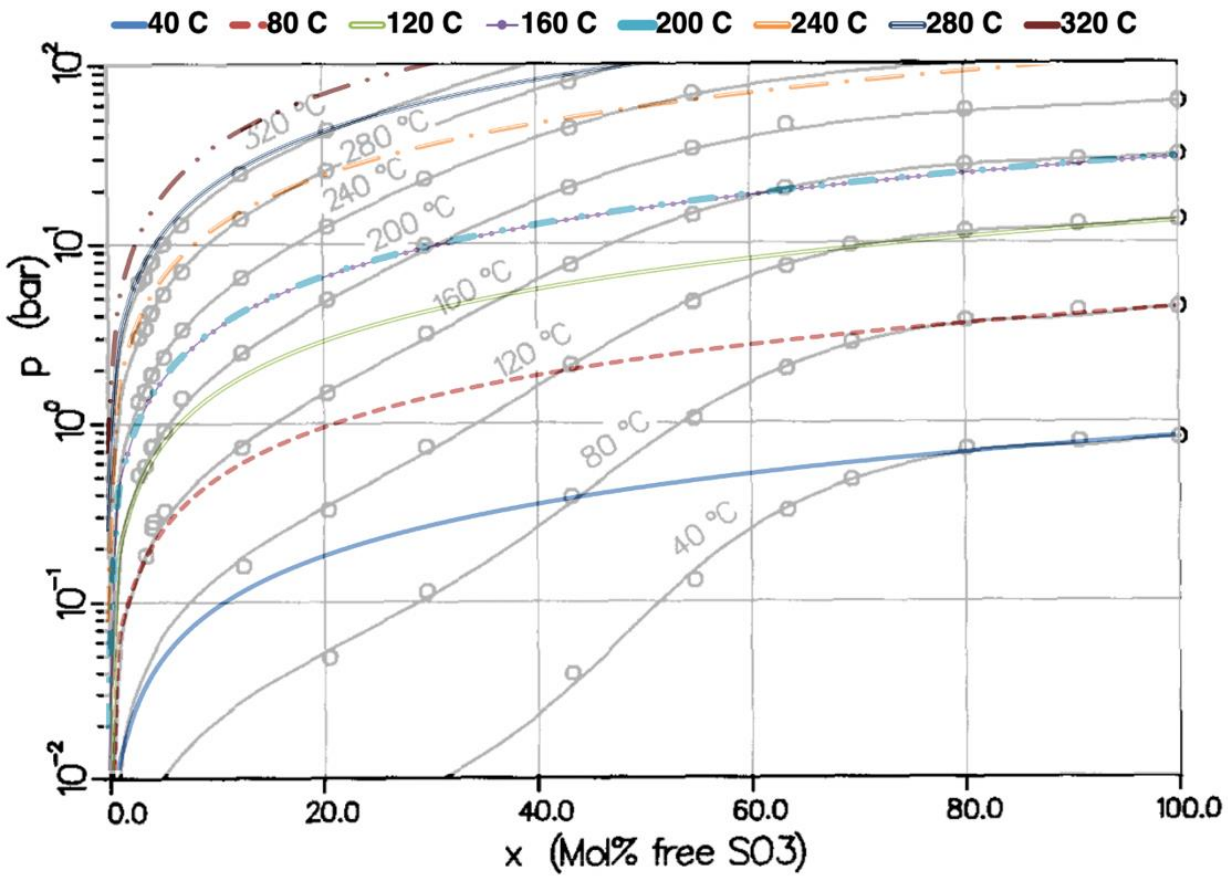

Figure 23: Comparison of modeled to previous [78] sulfur trioxide vapor pressure over a sulfur trioxide-sulfuric acid mixture.

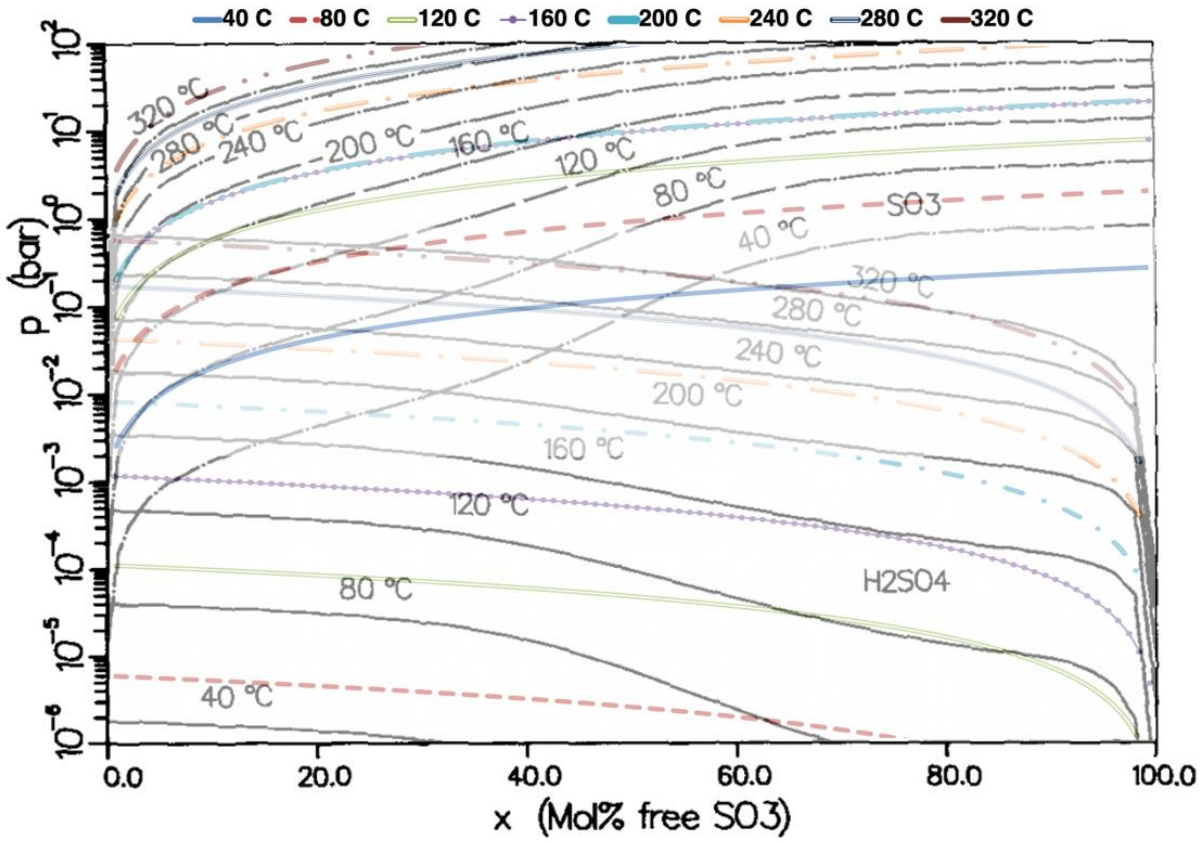

Figure 24:Comparison of modeled to previous [78] sulfur trioxide and sulfuric acid vapor pressure over a sulfur trioxide-sulfuric acid mixture.

3.2 Electrolysis

The nature of the modeled electrolysis section for this work was ideal. This was due to the high desirability of a complex model of a bayonet reactor, because it is the section that will utilize the most direct power from a nuclear reactor, and therefore have the largest direct impact on overall plant operation. The other large part of the electrolysis section was determining the amount of makeup water required for a full extent of reaction, and additionally to bring the flow of the sulfuric acid-water mixture to the bayonet reactor back to the desired wt% of sulfuric acid.

3.2.1 Electrolysis Power

The nominal power required for the operation of the electrolysis was found by first finding the standard free Gibbs energy change with equation 3.21:

$$dG_0 = zFE^0_{cell} \tag{3.21}$$

Where z is the number of electrons exchanged in the reaction, F is Faraday's constant, and E^0_{cell} is the change in potential across the cell and was 0.6 V [8] as the desired drop in potential across the cell.

Then the entropy change of the reaction was found using values taken from NIST. Where the change in entropy was represented by equations 3.22 and 3.23:

$$S = A\log(t) + Bt + \frac{Ct^2}{2} + \frac{Dt^3}{3} + \frac{E}{2t^2} + F \tag{3.22}$$

$$t = \frac{T}{1000} \tag{3.23}$$

Where the values for A, B, C, D, E, and G were taken from NIST and shown in Table 9. The entropies calculated were then used in equation 3.24 to find the reaction change in entropy for the reaction's enthalpy change.

$$dH_0 = dG_0 + TdS = dG_0 + T\left(\left(S_{H_2SO_4} + S_{H_2}\right) - \left(S_{SO_2} + 2 * S_{H_2O}\right)\right) \tag{3.24}$$

The reaction change in enthalpy was used to find the nominal energy for the reaction with equation 3.25:

$$E_{nom} = \frac{dH_0}{z * F} \quad 3.25$$

This was then input into equation 3.26, which used equation 3.27 to calculate current, to find the nominal power required for the overall process in MWe.

$$P_{nom} = I * E_{nom} * 10^{-6} \quad 3.26$$

$$I = nzF \quad 3.27$$

3.2.2 Hydrogen Produced

Faraday's second law was used to determine the mass of the hydrogen produced. Faraday's second law provides a relationship between the current and the mass of output. Using equation 3.27 to find the current, and equation 3.28 was used to find the mass of hydrogen produced.

$$m_{H_2} = \frac{M_{H_2} * I}{z * F} \quad 3.28$$

Where M_{H2} was the molar mass of hydrogen gas and was 2.016 x 10^{-3} kg/mol, the density of the hydrogen gas which was assumed constant at 0.06953 kg/m^3 could be used to determine the volumetric output of hydrogen gas as well.

3.2.3 Supplementary Water

Supplementary water was required for two reasons in the electrolysis model. The first was to ensure that there was enough water for the chemical reaction to fully progress. The second was to bring the effluent sulfuric acid-water mixture to the desired wt% of sulfuric acid. While the first method only adds water if the molar ratio of water and sulfur dioxide was not high enough, the second method calculated the amount of makeup water to bring the wt% down, or the amount of water that would need to be boiled off to bring the wt% up.

3.3 Energy Requirements for the Bayonet Decomposition

The model of the bayonet reactor had three different sections for energy balance calculations. Single-phase heat transfer for liquid and vapor, boiling heat transfer, and reaction energy for both steps of the sulfuric acid decomposition. To include heat recuperation in the model it was assumed that the incoming temperature profile was even at every point dx in the incoming section of the bayonet reactor.

3.3.1 Temperature Profile of the Incoming Mixture

The temperature profile of the surface of the bayonet reactor was a result of previous work and was calculated using equations 3.29 and 3.30 as shown in figure 25. Both steps of the sulfuric acid decomposition reaction were highly endothermic, resulting in a significant temperature drop with conversion. The temperature profile reflected this, as the fluid mixture decreased in overall temperature as it flowed into the return side. With this built into the temperature profile, this simplified the energy balance modeling for each section, especially the reaction models.

$$T = -854.17\left(\frac{x}{100}\right)^2 + 165.11\left(\frac{x}{100}\right) + 1173.14 \; for \; x < 90 \; cm \qquad 3.29$$

$$T = 321.43\left(\frac{x}{100}\right)^2 - 1012.14\left(\frac{x}{100}\right) + 1259.00 \; for \; x > 90 \; cm \qquad 3.30$$

It was assumed that the incoming mixture followed the same temperature profile due to the energy recuperation effects of the effluent mixture. The peak temperature was seen at 1.3 m, and the return side drop in temperature of the effluent is also seen in this temperature profile. This temperature profile was used for generating energy demand in the reactor models, as well as the other chemical models.

3.3.2 Single-Phase Energy Balance

Modeling single-phase heat transfer was accomplished by finding the first point of boiling and then the first point where the composition was all vapor phase. These were used as bounds for the single-phase energy demand models. With the other bounds being the incoming temperature for the liquid phase, and the max temperature for the vapor phase. Seen in equation 3.31.

Table 9: NIST Values for calculating entropy.

	A	B	C	D	E	F
H_2SO_4	47.28924	190.3314	-148.1299	43.86631	0.740016	301.2961
H_2O	-203.6060	1523.290	-3196.413	2474.455	-3.855326	-488.7163
SO_2	21.43049	74.35094	-57.75217	16.35534	0.086731	245.8872
H_2	33.066178	-11.363417	11.432816	-2.772874	0.158558	172.707974

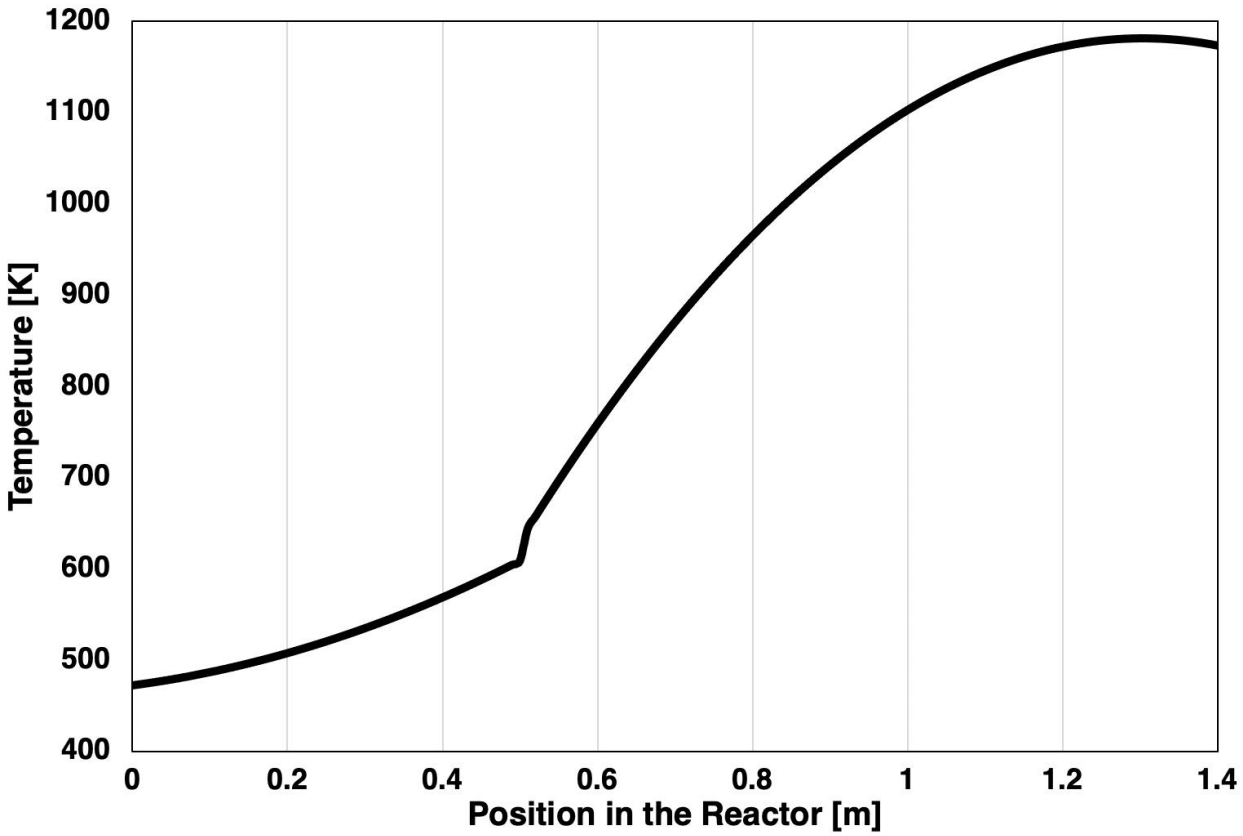

Figure 25: Temperature profile of the surface and incoming fluid of the bayonet reactor.

$$E_{single\ phase} = \dot{m}\left(\left(x_{H_2SO_4} * \Delta C_{p,H_2SO_4}\right) + \left(x_{H_2O} * \Delta C_{p,H_2O}\right)\right)\Delta T \quad 3.31$$

3.3.3 Boiling Energy Balance

The calculation of the energy required for boiling was done using the enthalpies of vaporization for sulfuric acid and water. The chemicals library was used for $H_{vap}(T)$ and then the resulting enthalpies of vaporization were used in equation 3.32.

$$E_{vap} = \dot{m}_{H_2SO_4} H_{vap,H_2SO_4} + \dot{m}_{H_2O} H_{vap,H_2O} \quad 3.32$$

The enthalpy of vaporization was temperature dependent, shown in Figure 26, with the total energy required to vaporize the mixture being inversely dependent on the temperature that vaporization began. This meant that the increase in the total pressure of the reactor lowered the energy required to boil the mixture by raising the mixture closer to the critical point. This resulted in better efficiencies with higher temperatures, however, the balance between pressure and temperature and the effect on the extent of reaction was another important factor to consider.

The effect that pressure had on the boiling point of the mixture can be seen in Figure 27. This showed the increase in the boiling point with an increase in overall system pressure. However, as the mixture approached the critical point, figure 26 showed that the energy required for vaporization decreased. Additionally, figure 28 shows that increasing pressure and weight fraction, and raising the boiling point of the mixture, the smaller the temperature change was from boiling to full vapor phase, which led to a more efficient process overall. The sharp drop in the ΔT at and above 0.90 wt fraction sulfuric acid, especially at high pressures, could explain the efficiency results seen at that weight fraction. This will be addressed further in the results and discussion chapter.

3.3.4 Heat of Reaction

The model of the two-step sulfuric acid decomposition reaction incorporated heats of reaction for both steps. These were used to find the energy demand of the bayonet reactor, examples of which were shown in figure 29 which used conversion as a function as both temperature and pressure.

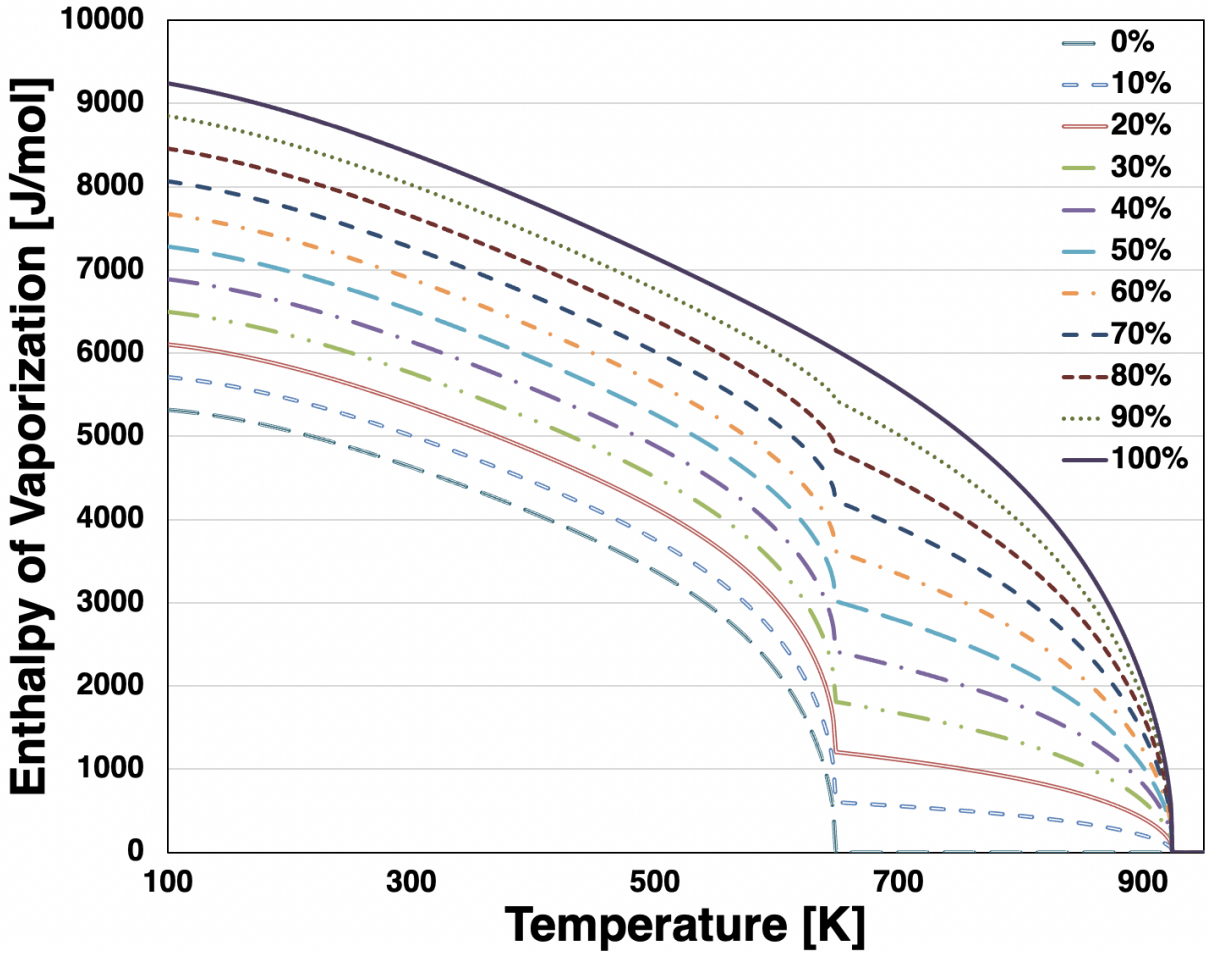

Figure 26: Enthalpy of vaporization for different wt% of sulfuric acid and water.

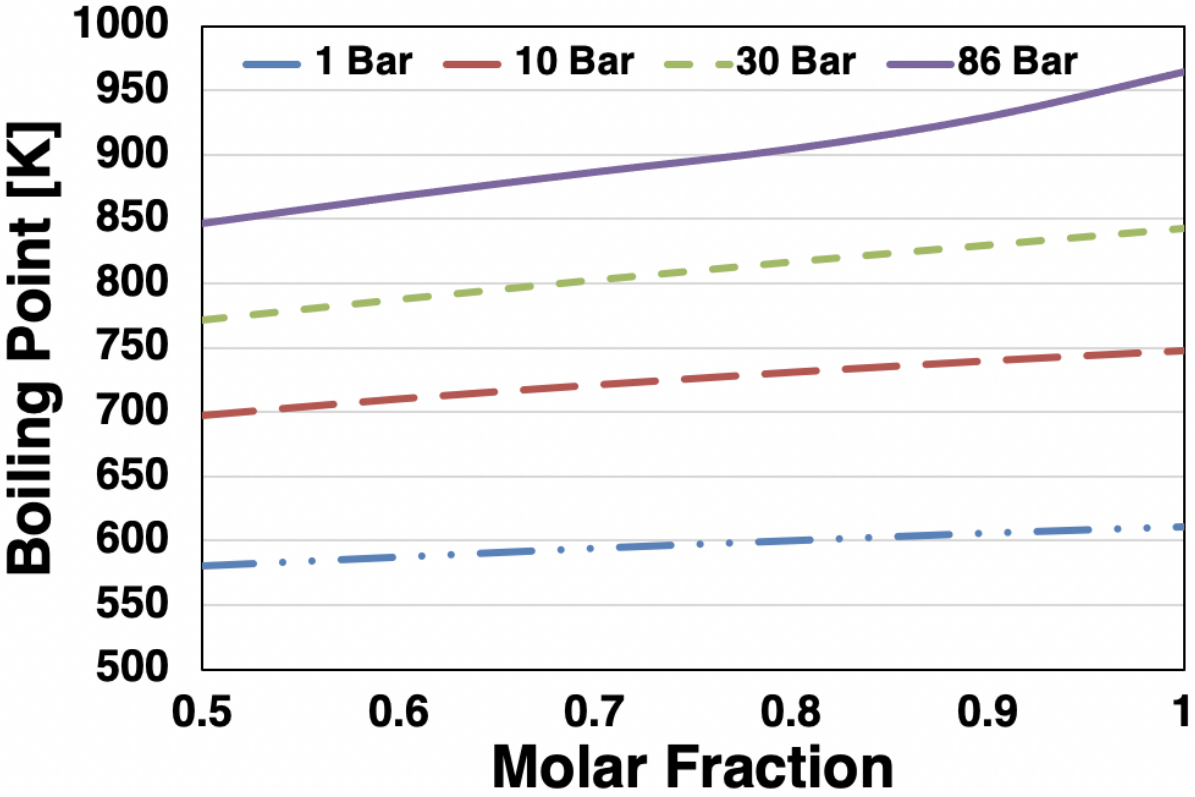

Figure 27: Boiling point of sulfuric acid-water mixture as a function of pressure and concentration of sulfuric acid.

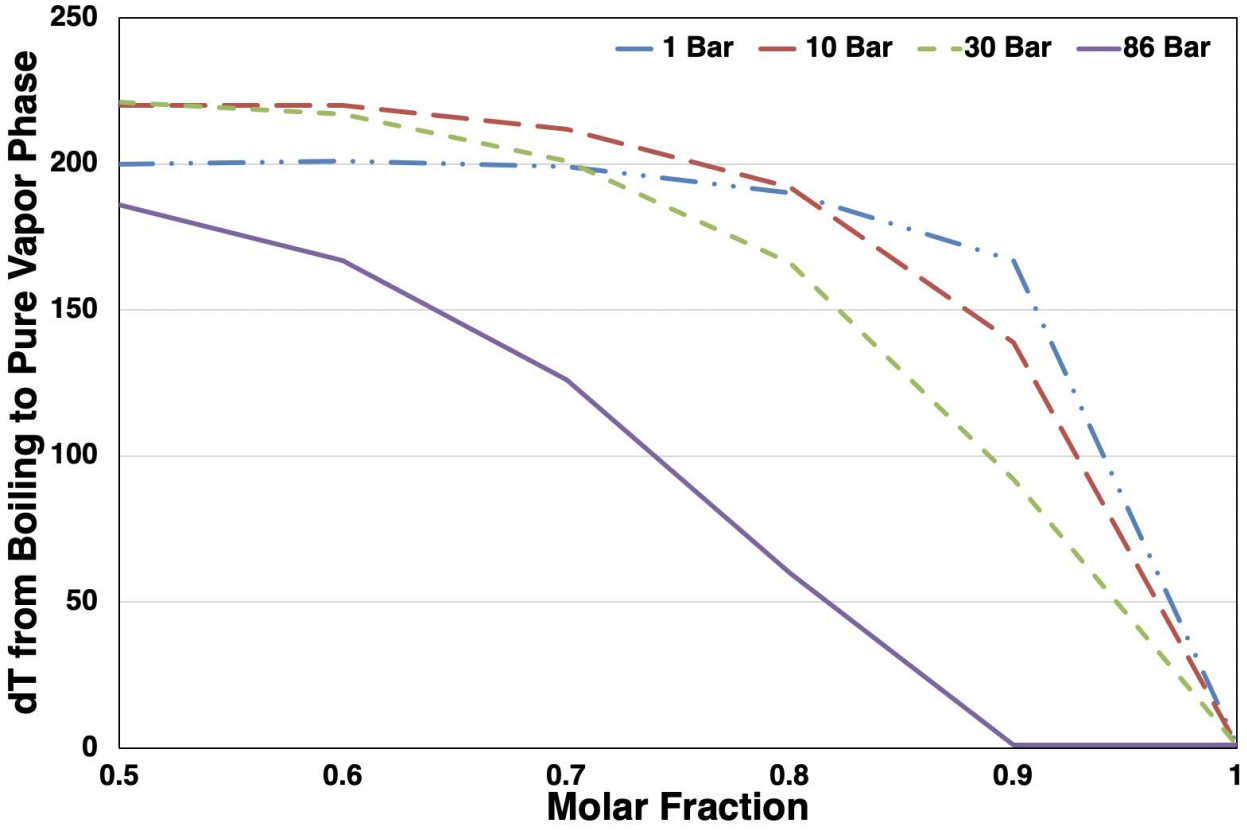

Figure 28: The change in temperature from the boiling point to full vaporization for various concentrations of sulfuric acid in water, as a function of pressure.

3.3.4.1 Sulfuric Acid Decomposition

The first step of the two-step reaction was assumed to proceed to the full extent, or conversion of 100%. This, in addition to the other assumptions from the conversion models, made the energy balance of the reaction modeled by equation 3.33, or just the change in enthalpy of the reaction itself. The change in heat capacity was represented by equation 3.34. To account for unreacted SO_3 it was assumed that it recombined with the excess water for effluent sulfuric acid, which is an exothermic reaction. Therefore, to incorporate the recombination exothermic heat of the reaction into the bayonet model, the conversion of sulfur trioxide was used to determine the proportion of energy required for the first-step reaction.

$$dH_{rxn1} = H_{Rx}^{0} + \left(\Delta C_p(T)\right) \tag{3.33}$$

$$\Delta C_p(T) = C_{p,H_2O}(T) + C_{p,SO_3}(T) - C_{p,H_2SO_4}(T) \tag{3.34}$$

3.3.4.2 Sulfur Trioxide Decomposition

In normal operational conditions, the highly endothermic nature of sulfuric acid decomposition results in a temperature drop, which was reflected in the temperature profile. The conversion calculations established for the second-step energy balance calculation are the more complex of the two reactions for bayonet modeling, equation 3.35. The heat of reaction was calculated in the same way as the conversion of sulfuric acid, shown in equation 3.36. Finally, the energy required by the reaction as a function of conversion was found using equation 3.37.

$$Q - W_s - F_{A0}\sum \theta_i C_{p,i}(T - T_0) - F_{A0} X \Delta H_{rxn2} \tag{3.35}$$

$$\Delta H_{rxn2} = H_{Rx}^{0} + \left(C_{p,SO_2}(T) + \frac{1}{2}C_{p,O_2}(T) - C_{p,SO_3}(T)\right) \tag{3.36}$$

$$Q_{rxn2} = F_{0,SO_3} * \left(y_{SO_3} C_{p,SO_3} \Delta T + X \Delta H\right) \tag{3.37}$$

The effect of both pressure and temperature on the efficiency of the decomposition of sulfur trioxide can be seen in Figure 29. These demonstrated the effect that increasing pressure can have on the overall efficiency of the process by showing the total energy required by the sulfuric acid decomposition reaction to produce one mole of sulfur dioxide. This metric was important because

the produced sulfur dioxide has a one-to-one molar ratio with produced hydrogen gas in the electrolysis reaction. Therefore, creating an efficiency threshold for the overall process. These show that at high enough temperatures the tradeoff for low-pressure reaction conversion was made up by the efficiency of vaporizing the mixture close to the critical point of the mixture.

The figures also demonstrate the absolute dependence of the process on temperature. A high enough temperature could make the reactor reach target efficiency at any pressure. The operational temperature output of the nuclear reactor providing the thermal energy may not be capable of providing high enough temperatures, which is where the weight fraction and pressure efficiency of the reaction is the most important.

3.3.5 Heat of Mixing

For liquids, the act of mixing can have a result on the total enthalpy of the mixture. For ideal mixtures this term could be ignored, however, the interactions within liquid sulfuric acid and water mixtures are not ideal and experimentally have been shown to have an exothermic enthalpy of mixing. To account for the heat of mixing within the bayonet reactor equation 3.38 was used.

$$\Delta H_{mix} = H^0_{mix} - \left(x_{H_2SO_4} * C_{p,H_2SO_4} + x_{H_2O} * C_{p,H_2O}\right) \quad 3.38$$

3.4 Reactor Bed Pressure Drop

While not directly used in the steady state model of the bayonet reactor, there were additional chemical models included whose outputs can be included with the regular outputs for more complex heat transfer models as well as improving the complexity and results of the overall bayonet model. One example of the uses of the additional chemical models was the calculation of pressure drop across the reactor bed. While the bayonet reactor model assumed no pressure drop, the inclusion of pressure drop in future versions of the model would be beneficial for tracking the effects of pressure drop on the operation. The following section provides a sample of the additional chemical work and its effect on the bayonet reactor model.

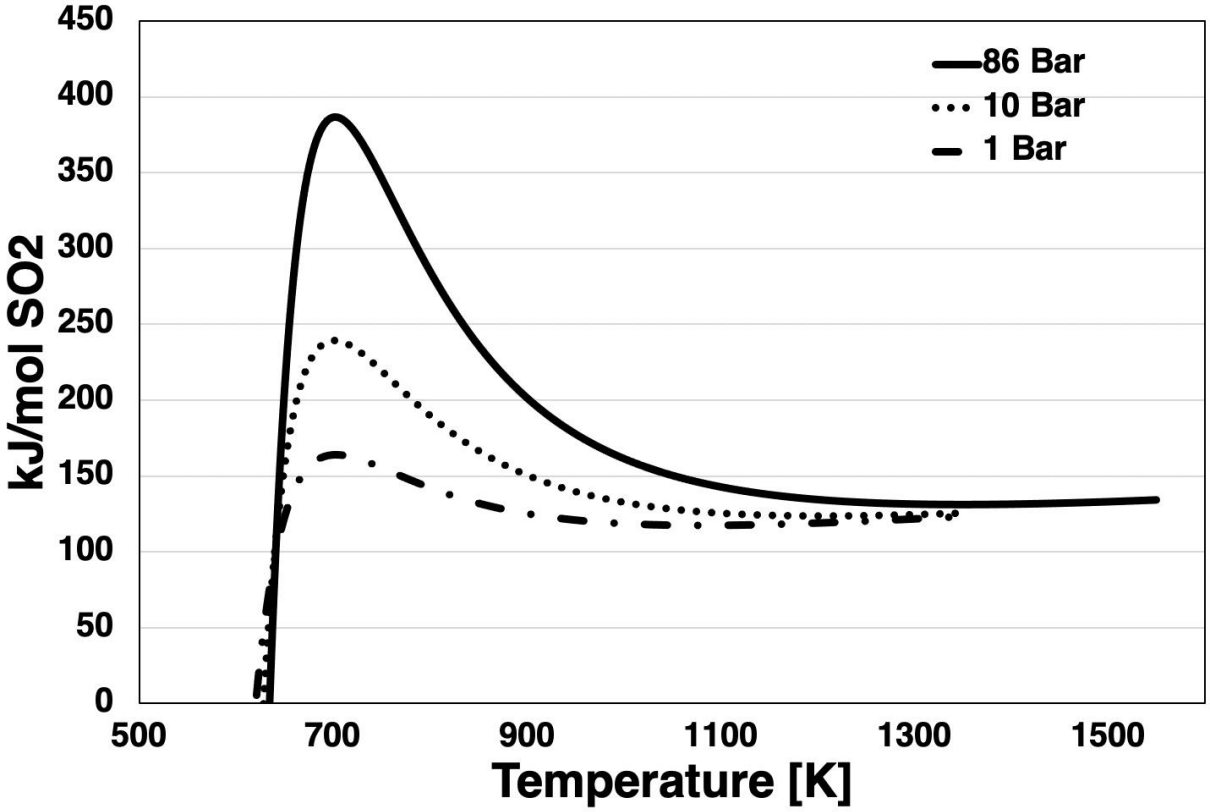

Figure 29: kJ per mol SO_2 produced by sulfuric acid decomposition as a function of temperature at 1, 10, and 86 bar pressure.

3.4.1 Ideal Gas Molar Volume

The calculation of the ideal gas molar volume of the sulfuric acid mixture was accomplished using the ideal gas law, equation 3.39. The SRK equation of state provides a method

$$PV = nRT \tag{3.39}$$

of calculating this as well, but the ideal gas molar volume provided an output of molar volume that could be used as a reference state for the SRK equation of state, as well as a basis for further chemical work noted in this section. The ideal gas law became equation 3.40, which used Raoult's law for total mixture vapor pressure for P_{sat}.

$$V_{molar} = \frac{RT}{P_{sat}} \tag{3.40}$$

3.4.2 Mixture Density

The density of a mixture can be calculated using a method that considers the liquid ideal for Raoult's law, assuming no volume change. Shown in equation 3.41. Where m was the mass and w was the weight percent. This was useful for the liquid mixture density, where calculations exist for single species densities, however, the density of the mixture gas is needed for further work such as pressure drop in the reactor bed. For this, the ideal gas molar volume could be used.

$$\rho_{mix} = \frac{m_1\rho_1 + m_2\rho_2}{m_{tot}} = w_1\rho_1 + w_2\rho_2 \tag{3.41}$$

Molar volume was defined by equation 3.42, where M is the molar mass. For a mixture, this equation became equation 3.43, which could be rearranged to solve for the density of the mixture vapor that used the previously calculated molar volume.

$$V_{molar} = \frac{M}{\rho} \tag{3.42}$$

$$V_{molar} = \frac{\sum x_i M_i}{\rho_{mixture}} \tag{3.43}$$

3.4.3 Ergun Equation

Because of the assumed one-dimensional nature of the mixture flow through the bayonet reactor, the Ergun equation was used to calculate the pressure drop through the catalyst bed in the bayonet reactor. The Ergun Equation calculates the pressure drop of a fluid through a packed bed, and the resulting pressure drop would be beneficial to know due to the effect that pressure drop has on energy balances, reaction rate, conversion, and numerous other important factors within a chemical reactor.

The Ergun Equation usually takes the form of equation 3.44. The first term represents the effect on the pressure drop by the laminar flow of the fluid through the packed bed, where μ is the viscosity of the fluid, D_p is the diameter of the packed bed particles, and ε is the fraction void or space in the packed bed not occupied by the particles. The second term is the portion of the equation that is dominated by turbulent flow, where ρ is the density of the fluid. For laminar flow, the equation can be assumed to be simpler with the negation of the turbulent flow in the packed bed.

$$-\frac{\Delta P}{\Delta L} = 150\left(\frac{\mu q}{D_p^2}\right)\frac{(1-\varepsilon)^2}{\varepsilon^3} + 1.75\left(\frac{\rho q^2}{D_p}\right)\frac{(1-\varepsilon)}{\varepsilon^3} \tag{3.44}$$

For gaseous flow through a packed bed, the Ergun equation can be modeled as equation 3.45. Where g was the gravity constant, and G was the superficial mass velocity, or ρ*u. Where both the density and the viscosity of the mixture were temperature dependent. To incorporate this into the bayonet reactor model to find the pressure drop as a function of length, the equation became equation 3.46.

$$\frac{dP}{dz} = -\frac{G}{\rho g D_p}\left(\frac{1-\varepsilon}{\varepsilon}\right)\left[\frac{150(1-\varepsilon)\mu}{D_p} + 1.75G\right] \tag{3.45}$$

$$p = \frac{P}{P_0} = \left(1 - \frac{2\beta_0 z}{P_0}\right)^{\frac{1}{2}} \tag{3.46}$$

Where:

$$\beta_0 = \frac{G(1-\varepsilon)}{\rho_0 g D_p \varepsilon^3}\left[\frac{150(1-\varepsilon)\mu}{D_p} + 1.75G\right] \tag{3.47}$$

While the resulting pressure drop was not included in the energy balance or conversion of the reaction itself, the calculated pressure drop could be useful in future work evaluating the effects of transients on an IES grid.

Chapter 4. Results & Discussion

4.0 Bayonet Reactor Efficiency

To establish the accuracy of the bayonet reactor model, the efficiency outputs of the reactor were compared to previous work done. The previous work outlined in the literature review established both the efficiency target of 450 kJ/mol SO_2 but also outlined the efficiency of the bayonet reactor for pressure, temperature, and composition of the inflowing sulfuric acid-water mixture.

4.1.1 As a Function of Pressure and Temperature

The first comparison was done with a constant incoming wt% of 80.1 sulfuric acid. Like the previous work, the bayonet reactor model had worse efficiency for low temperature and high pressure, and 90 bar at 900 °C was the most efficient of all, demonstrated in Figure 32. While the general shape and distribution of the efficiency results from the model were similar to the results of previous work, the lower temperature outputs of the reactor model were significantly less efficient when compared to the efficiency of the previous work.

This inefficiency could be the result of a few different things. First, the conversion of sulfur trioxide could have been a likely candidate for the drastic decrease in efficiency at lower temperatures if the conversion method used in this model had lower conversion results than what was used in the previous work. The other likely culprit could be the method of calculating the energy balance. By using ideal heat capacities, heats of vaporization, and PFR design equations the likelihood of an overestimation of the energy required increased.

As both current and previous models demonstrate, however, the temperature and pressure dependence of the bayonet reactor make high-temperature and pressure systems the most efficient. Current molten salt reactors may not be able to reach the high temperatures that result in ideal efficiency at high pressures. This could be addressed with additional heat supply from fossil fuels, but the alternative of operating the system at lower pressures, 15 bar or below, could address the efficiency issue of lower temperatures.

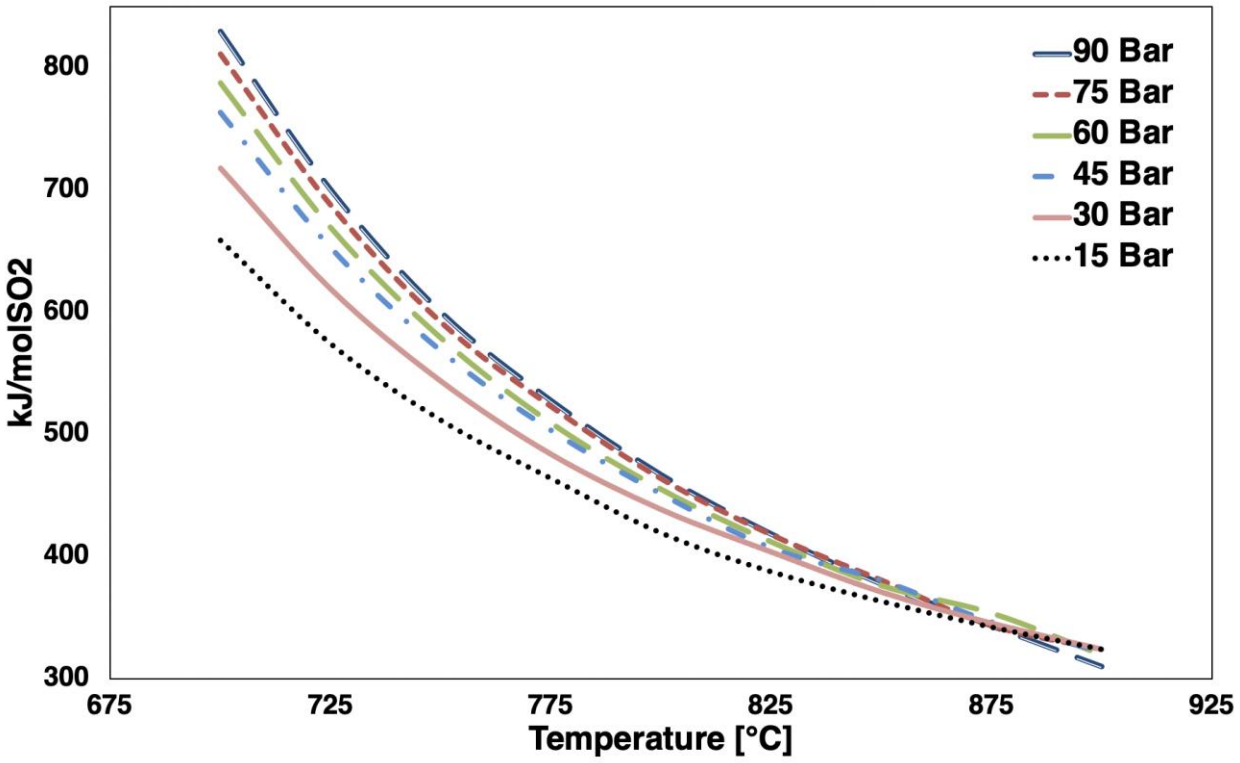

Figure 30: kJ per mol SO_2 produced as a function of pressure and temperature.

4.1.2. As a Function of Incoming Weight Fraction Sulfuric Acid

The other important efficiency comparison was the pressure and weight fraction efficiency. Previous work established a weight fraction of 0.8 sulfuric acid as the most efficient, at any pressure. This model demonstrated a similar trend when compared to the previous work at a constant temperature of 1143 K, 870 °C, shown in Figure 33, with the results in Table 10. The current model overestimated the kJ/mol sulfur dioxide when compared to previous work below 0.89 weight fraction sulfuric acid and did not demonstrate the same decrease of efficiency that the previous work did. However, the previous flowsheet work demonstrated a ~7% better conversion than the current model with a 0.8 weight fraction of sulfuric acid incoming, and the efficiency result for the current model was ~8% higher than the flowsheet's efficiency.

Table 10 shows the efficiency results for the current model. Using the target efficiency of 450 kJ/mol SO_2 as outlined by previous work, the previous work found that the desired efficiency was attained above 0.60 weight fraction with the best efficiency at 0.80 weight fraction sulfuric acid and 86 bar with 329 kJ/mol SO_2. The current model reached the target efficiency by 0.63 weight fraction sulfuric acid.

The current model's results mostly agree with the previous work for the incoming weight fraction of sulfuric acid. The target operational range based on the results would be above 0.63 weight fraction sulfuric acid. Based on the results of the current model and their comparison to the previous flowsheet work the resulting power required for efficient bayonet reactor operation would present conservative results between 0.63 and 0.89 weight fraction sulfuric acid. Above that range, the trend of the efficiency results may result in inaccurate power requirements due to the dissimilarity between the current model and the previous work.

The trend of the model efficiency estimations could have been a result of the method of estimating the enthalpy of vaporization in the reactor. Figure 28 demonstrated a sharp drop in the ΔT between the boiling point and full vaporization at 0.9 weight fraction sulfuric acid and above, which was even greater at high pressures. This could explain the derivation in efficiency calculations by weight fraction at 0.9 sulfuric acid.

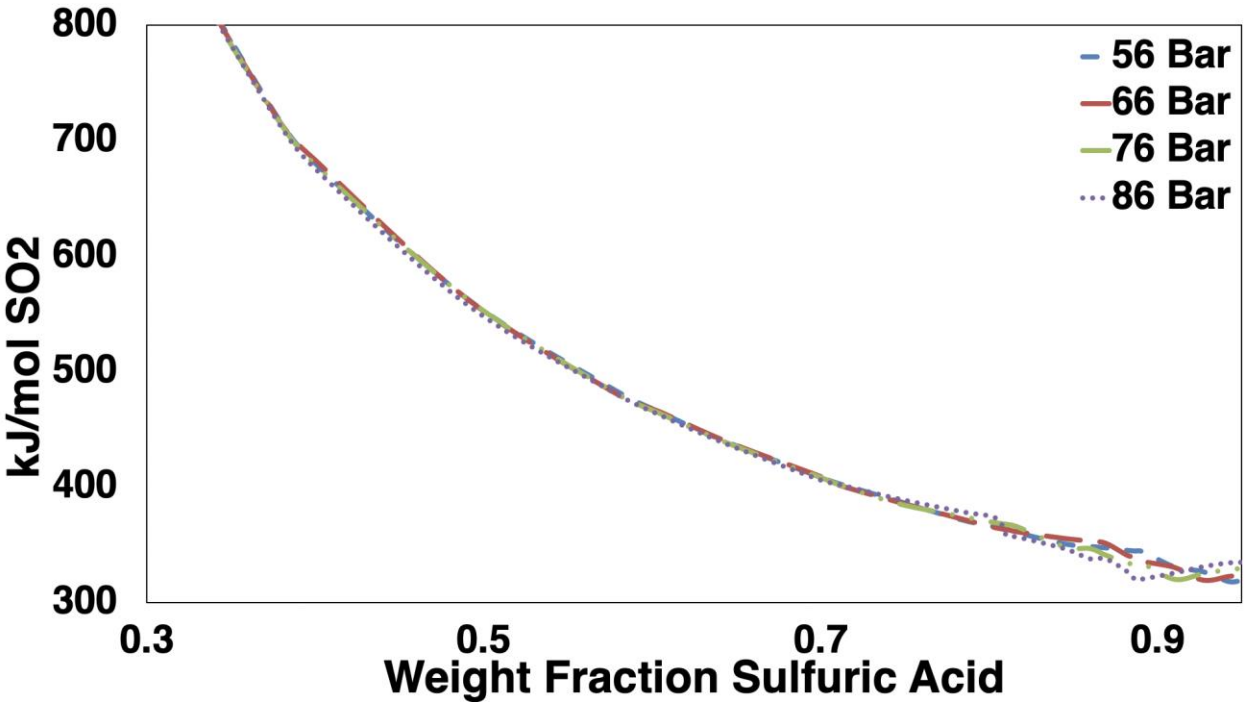

Figure 31: kJ per mol SO_2 produced as a function of weight fraction sulfuric acid.

Table 10: kJ/mol SO2 at different pressures for wt% H2SO4 at 1143 K.

	Pressure (Bar)			
wt% H_2SO_4	**56**	**66**	**76**	**86**
30%	933.15	931.86	925.17	928.06
40%	677.12	680.26	676.30	672.66
50%	563.17	563.18	563.21	558.09
60%	464.01	464.45	463.01	461.58
65%	438.54	439.09	437.96	436.76
70%	408.33	408.98	408.14	405.86
75%	387.77	387.03	385.60	389.76
80%	365.05	364.49	368.86	372.80
89%	344.39	340.06	333.80	319.40
90%	343.98	335.65	333.87	320.07
91%	330.63	330.25	319.90	325.33
95%	319.36	323.61	329.23	334.59

4.1 Test Cases of the Bayonet Reactor

Test cases were run on the bayonet reactor alone to gauge the performance of the model and its ability to handle various inputs. The reactor's ability to track the energy requirements for the various pressures, mixtures, and temperatures were the most important to the operation of the bayonet reactor within an IES. The outputs of sulfur trioxide conversion, power, and energy per mol sulfur dioxide were also important for a sense of the operational success of the bayonet model.

The bayonet model required inputs of pressure for the reactor pressure, a maximum temperature, and incoming flow rates for sulfuric acid and water. The maximum temperature was used to create a temperature profile based on the same temperature profile used for the efficiency tests but using the difference between the desired max temperature and the maximum temperature based on the profile using the previous work.

Figure 34 shows the first test case for the bayonet reactor model. The operational inputs were 5 bar of pressure, 1181 K or 908 °C, 100 mol/s inflow with 80% molar or 95.6% weight sulfuric acid. With these operational conditions, the bayonet reactor had a power demand of 18.7 MWth, or 298 kJ/mol SO_2. The SO_3 decomposition had a conversion of 0.787, which led to an effluent of 63 mol/s of SO_2 from the reactor. The reactor bed had a nominal pressure drop of 0.14 bar.

The favorable efficiency results are a result of the extremely good conversion results at the high temperature and low pressure of the reactor. The highest energy demand in the process was the boiling and reaction. The boiling required 6.4 MWth, and the entire decomposition reaction required 14 MWth, which gave the process a maximum heat recuperation of over 2 MWth. Even with the highly favorable conversion for the low-pressure system, the models likely returned more favorable results than would be seen in reality. This was due to the better efficiency seen at higher sulfuric acid concentrations when compared to previous work, and the possibility of overestimation of the heat recuperation giving the operation more favorable results. If the pressure drop was included in the model the overall efficiency would likely decrease.

The next test case was at 15 bar and a maximum temperature of 1123 K, 850 °C, 100 mol/s incoming with the sulfuric acid at 89.1 wt%. The temperature profile with the ranges of heat transfer can be seen in Figure 35. With these inputs, the total thermal power demand for bayonet operation was 12.2 MWth, or 345 kJ/mol SO_2. The conversion in the reactor under the conditions

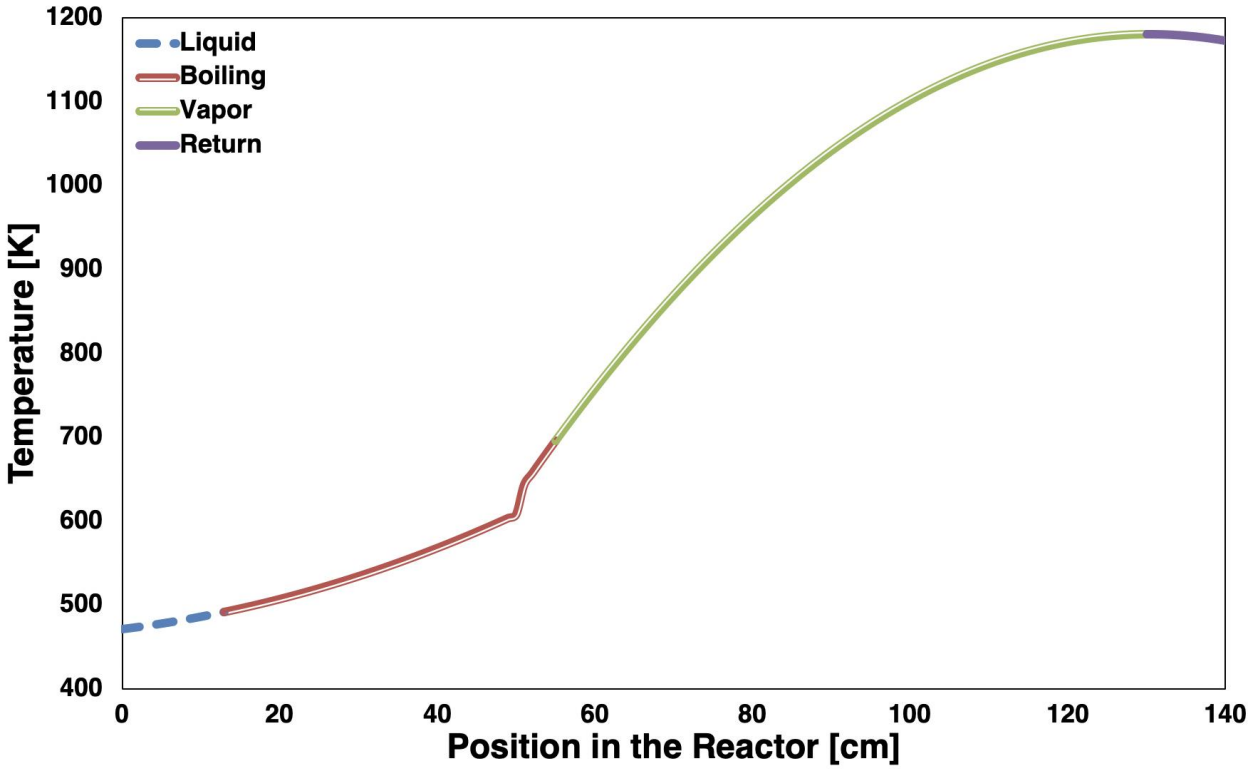

Figure 32: Temperature profile of the bayonet decomposition model at 5 bar, max temperature of 1181 K, 100 mol/s, 95.6 wt% sulfuric acid.

was 0.588 with the effluent of SO_2 at 35.3 mol/s. The nominal pressure drop in the reactor bed under these conditions was 0.11 bar.

Under these operational conditions, the reactor still was under the target efficiency of 450 kJ/mol sulfur dioxide, with a decrease in overall thermal demand even if the process was less efficient than when operating under lower pressure and higher temperature. The boiling of the mixture required 5.92 MWth, and the decomposition reaction required 9.32 MWth, with a maximum heat recuperation of 2.5 MWth.

The next test case was at 86 bar and had a maximum temperature of 1103 K, 830 °C. The incoming was 200 mol/s with a concentration of sulfuric acid at 81.7 wt%. Figure 36 shows the temperature profile of the incoming mixture. The total power required for the operational conditions was 14.0 MWth with an efficiency of 413.3 kJ/mol SO_2 and a conversion of 0.375. The effluent moles of sulfur dioxide were 33.8 mol/s, and the nominal pressure drop in the reactor bed was 0.18 bar.

The power demand of the boiling in the process was 9 MWth, and including the single-phase heat transfer, the power required for heating was 10 MWth. For the reaction the power required was 12 MWth, this left a maximum heat recuperation of 5.5 MWth. While the efficiency of the process with these inputs was within the target range of 450 kJ/mol SO_2 the large amount of recuperable heat shows the likelihood of the process becoming even more efficient.

4.2 Test Cases of Entire Model

With the establishment of successful independent operational capabilities of the bayonet reactor model, it was then coupled to a full system model. The full system model was not intended to act as a flowsheet simulation of the entire process, but instead, serve as a method of verification for the bayonet reactor model in an ideal system based on previous flowsheet simulations. As covered in the methodology section, the electrolysis was modeled by finding the ideal system energy requirements, and not based on real-world experience with electrolyzers. It is expected that the bayonet reactor model will be used in tandem with electrolysis models that reflect actual design constraints and operational abilities in the future. Additionally, the supplemental electrical power demand for the operational system was taken from previous flowsheet modeling to establish an expectation for the demands of the full system. Like the electrolysis, it is expected that future work

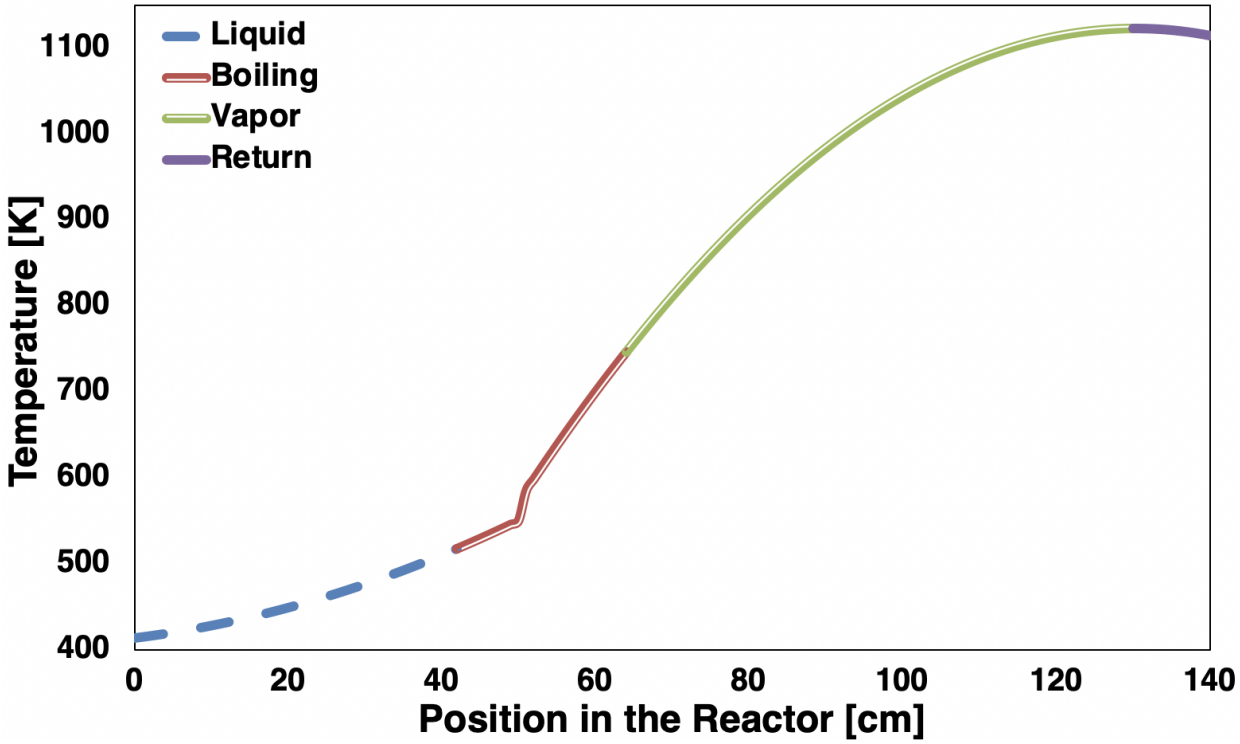

Figure 33: Bayonet decomposition model temperature profile at 15 bar, 100 mol/s, 89.1 wt% sulfuric acid, with temperature maximum of 1123 K.

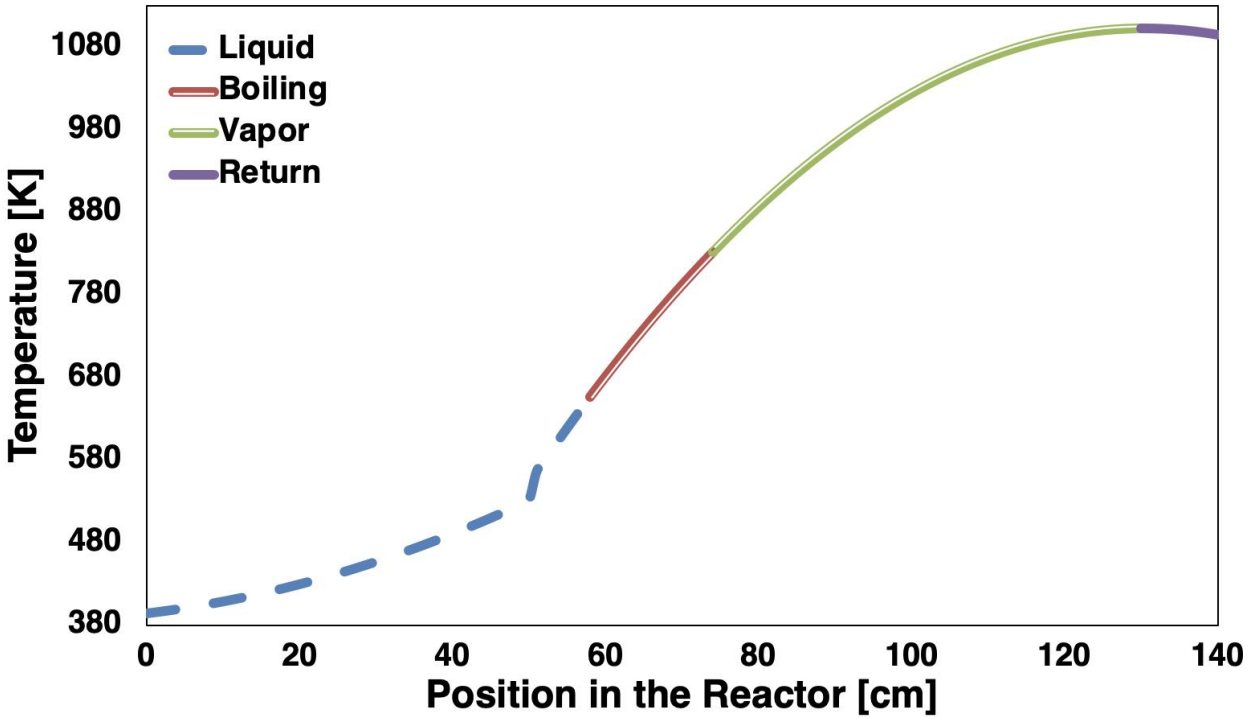

Figure 34: Bayonet decomposition model temperature profile at 86 bar, 200 mol/s, 81.7 wt% sulfuric acid, with temperature maximum of 1103 K.

will incorporate models of a fully operational system that reflect the real-world operational abilities of the supplementary equipment needed for the successful operation of the hybrid sulfur cycle.

Table 11 shows the behavior and trends of the entire modeled hybrid sulfur cycle. The weight fraction of the mixture into the bayonet was 0.8 wt fraction sulfuric acid. The total thermal demand was the thermal demand of the bayonet reactor added to the electrolysis demand and the supplementary demand with a 0.33 efficiency for the MWe for a Rankine cycle. The makeup water was the amount of water required to keep the system at a steady state, 0.8 wt fraction sulfuric acid in the incoming mixture to the bayonet reactor, and to ensure there was enough water in the electrolyzer for the reaction to proceed to the full extent. The energy to pump the makeup water was included in the supplementary electrical power. The makeup water could have been negative as well, depending on both the desired steady-state mixture and the extent of reaction in the bayonet reactor. A negative result for the makeup water would require boiling off water in the incoming mixture.

The general trends of the whole model agree with previous work. With the increase of pressure in the bayonet reactor the reactor sees better efficiency and lower energy demand in both the bayonet and the overall system. This was the case at every temperature step; however, the increase in temperature saw better efficiency overall. The electrolysis demand, hydrogen produced, and supplementary water were all proportional to the conversion of sulfur trioxide and the amount of sulfur dioxide produced. While the results demonstrated an ideal operation of a hybrid sulfur cycle with an ideal electrolyzer, a realistic model of an electrolyzer should be implemented with the bayonet reactor to gauge the feasibility of the results.

Table 11: Whole model results for bayonet reactor with ideal electrolysis.

	Temperature K	Total Thermal Demand MWth	Bayonet Demand MWth	Bayonet Efficiency kJ/mol SO_2	Electrolysis Demand MWe	Product Hydrogen kg/s	Makeup Water kg/s
86 Bar	**1173**	125.2	6.8	323.8	39.0	0.043	0.36
	1123	106.8	6.7	390.5	33.0	0.035	0.30
	1100	98.3	6.7	429.9	30.2	0.032	0.26
	1050	80.4	6.3	531.9	24.4	0.024	0.20
76 Bar	**1173**	128.2	7.3	339.1	39.9	0.044	0.37
	1123	109.4	7.1	390.7	33.8	0.036	0.31
	1100	100.7	6.9	428.4	31.0	0.032	0.27
	1050	82.5	6.5	531.6	25.1	0.025	0.21
66 Bar	**1173**	131.3	7.5	335.9	40.9	0.045	0.39
	1123	112.5	7.2	393.6	34.7	0.037	0.32
	1100	103.6	7.1	423.0	31.9	0.033	0.28
	1050	84.9	6.7	525.3	25.8	0.026	0.21
56 Bar	**1173**	135.0	7.7	335.5	42.0	0.046	0.40
	1123	116.0	7.5	392.6	35.8	0.038	0.33
	1100	107.0	7.3	422.5	32.9	0.035	0.30
	1050	87.8	6.7	517.3	26.7	0.027	0.22
46 Bar	**1173**	139.4	8.0	338.0	43.4	0.048	0.41
	1123	120.4	7.9	396.0	37.1	0.040	0.34
	1100	111.1	7.6	423.0	34.2	0.036	0.31
	1050	91.4	7.2	513.4	27.8	0.028	0.24
36 Bar	**1173**	144.9	8.4	339.0	45.0	0.050	0.43
	1123	126.7	8.1	387.9	38.8	0.042	0.36
	1100	116.4	8.0	422.5	35.8	0.038	0.33
	1050	96.0	7.5	500.2	29.2	0.030	0.25

Chapter 5. Conclusions & Recommendations

The four key questions that this work set out to answer were:

1. What lessons can be learned from previous experience with advanced reactors driving chemical plants?
2. What simplifying assumptions can be made in a reduced-order model of sulfuric acid that still produces good agreement with past experiments?
3. Can the reaction and thermodynamics be coupled into a simplified model of the overall integrated energy system?
4. Does the hydrogen production process meet efficiency goals to be competitive with electrolysis?

The review of the Aktau NPP and nuclear hydrogen identified key safety features of an IES with a nuclear reactor:

1. Redundancy of thermal supply and dimensions of feedback between the chemical process and the reactor to reduce transient feedback between the process and the nuclear reactor, as well as radiation contamination.
2. Implementation of the process and reactor into a grid to address issues of scale by expanding the usage of the thermal energy supply as well as planned and unplanned outages.
3. Setting the scale and demand of the chemical process by the power availability of the reactor.

The Aktau NPP utilized a low-temperature demand process in seawater desalination, but in the case of a high thermal demand process such as hydrogen production, where an unplanned outage could result in catastrophic consequences and new dimensions of feedback, new criteria of evaluation were established:

1. A high-temperature process requires a direct supply of thermal energy, creating the need for evaluation of direct feedback and cascading effects between the high-temperature process and the nuclear reactor and their effects on the overall grid.
2. The ability to fit a high-temperature process, such as thermochemical hydrogen production, into a grid largely depends on the efficiency and thermal demand of the process.
3. The nature of the feedback between the high-temperature process and the nuclear reactor in the case of thermal energy supply and demand mismatch greatly depends on the chemical equilibria within the various processes.

The work done modeling the thermal decomposition of sulfuric acid was based on providing a method for future work to incorporate the Hybrid Sulfur cycle in an IES grid model and address these criteria. While key assumptions and design criteria for a flexible model were identified for use within an IES grid for evaluation of steady state and transients.

While using the established assumptions and design criteria this work was able to replicate and agree with previous modeling work that showed the ability of the hybrid sulfur cycle to produce hydrogen with an efficiency competitive with current electrolysis methods. The model incorporated the temperature and pressure dependency on the decomposition of sulfuric acid. As well as the effects temperature, pressure, and weight fraction sulfuric acid had on the efficiency of the bayonet reactor.

The temperature profile used in the model was able to produce results that agreed with previous work, however, a linear temperature profile produced similar overall results as the modeled temperature profile and could serve as useful to use with simplified overall grid evaluation. Therefore, based on the type of IES or grid evaluation, the temperature profile of the sulfuric acid-water mixture could be altered to fit the desired temperature range or heating fluid and still produce bayonet reactor energy demand and efficiency results that agree with expected results of sulfuric acid decomposition. This agnostic method of modeling meant the bayonet model was a model with the ability to be coupled with any IES with any heating fluid and provide results that could be used in IES grid evaluation.

For the results of the bayonet reactor, high pressures at high temperatures were the most efficient and had the lowest energy demand when compared to low-pressure systems with high or low pressures. This also was consistent with previous work. Increasing pressure lowered

conversion rates but resulted in an overall more efficient process, provided the temperature was high enough. The high pressure resulted in decreased total power demand regardless of temperature. An increase in pressure lowered the ratio of the pressure drop in the reactor bed as well, increasing the potential for a more efficient process.

The weight fraction of sulfuric acid in the incoming mixture also played a large part in the efficiency of the process. While the model of the bayonet reactor tended to show higher efficiency results when compared to previous work, the range of operation, 0.63-0.89 weight fraction sulfuric acid, did agree with previous work. The trend of the model's efficiency results above 0.89 weight fraction was lower than found in previous modeling. However, the operational range of the reactor demonstrated the ability to provide steady-state results for a bayonet reactor capable of coupling to electrolysis models and even models of nuclear reactors.

The target of less than 450 kJ/mol SO_2 maximum efficiency in the bayonet reactor was to ensure its competitiveness with electrolysis. Under ideal conditions, the maximum hydrogen produced with a 100 mol/s flow rate into the bayonet reactor, which is still at target efficiency, could produce up to 1500 metric tons of hydrogen gas per year. The minimum hydrogen produced, which was inefficient, could produce as much as 730 metric tons of hydrogen per year. While the amount of hydrogen production modeled is smaller compared to real-world electrolysis plants, the model showed that small to medium-scale hydrogen production with the hybrid sulfur cycle in an IES can be an efficient and attractive alternative to electrolysis, especially considering the scalability of thermochemical cycles. The scalability of thermochemical cycles has the potential to produce large amounts of hydrogen with comparable or better efficiency.

The agnostic nature of the bayonet model design fit previous work and showed promise as a method to provide a holistic, steady-state energy demand for an IES with the hybrid sulfur cycle. For future work involving transients, this method of modeling the chemistry and thermodynamics of the bayonet reactor showed promise for implementation into a full-scale grid analysis. For higher fidelity models the specific design and full-scale dimensions of the bayonet reactor are crucial, and while other work has established efficient designs of a bayonet reactor, the nature of any possible transient and accident scenarios within an IES with both hydrogen production and a nuclear reactor could be captured with the current method of modeling. Additionally, other sulfur-based cycles, such as the Sulfur Iodine cycle, could incorporate the methodology of this thesis for the model of sulfuric acid decomposition within the Sulfur Iodine cycle.

High temperatures and high pressures are the most efficient for the decomposition of sulfuric acid. This is due to the effect pressure has on raising the boiling point of the mixture, reducing the overall energy required for vaporization. The effects of pressure and temperature show the balance between efficiency and scale that can be addressed by the bayonet reactor, where even with the comparatively poorer conversion results of the chemical reaction at high pressures, the efficiency is still below the target of 450 kJ/mol SO_2 by reducing the power requirements for heating and boiling.

In general, the assumptions used to model sulfuric acid decomposition within a bayonet reactor overestimated the energy required per mole of sulfur dioxide produce when compared to previous work. However, the results of the reduced order model still had good agreement, and still showed the Hybrid Sulfur cycle to have efficiency results competitive with water electrolysis. Additionally, the range of operation based on temperature, pressure, and weight fraction sulfuric acid agreed with past research on the bayonet reactor.

While the real-world application of a thermochemical cycle coupled to an advanced reactor is likely still in the future. The results of this work and other work have shown that the use of the Hybrid Sulfur cycle, and others, is still promising. The use of an advanced reactor and the implementation of a hydrogen production process could give large-scale nuclear hydrogen a significant impact on the reduction of carbon emissions in a hydrogen-powered world. By using the methodology outlined in this thesis, the impacts of an advanced reactor-powered IES can be targeted for high temperature chemical operations.

References

1. Barnert, H., V. Krett, and J. Kupitz, *Nuclear energy for heat applications: Co-generating electricity and heat is a promising application.* IAEA: Topical Reports, 1991.
2. Leurent, M., et al., *Driving forces and obstacles to nuclear cogeneration in Europe: Lessons learnt from Finland.* Energy Policy, 2017. **107**.
3. Muralev, E.D., et al., *Experience Gained in the Operation and Maintenance of the Nuclear Desalination Plant in Aktau, Kazakhstan.* IAEA-SM-347, 1997.
4. Weinburg, J. and A. Ophir, *Experience Gained in the Ashdod Plant and Other Dual Purpose Desalination Plants Using Multi-Effect Distillation with Aluminium Tubes.* IAEA-SM-347, 1997.
5. Baranov, J.S., *Operating Experience of Desalination Units in Schevchenko.* Desalination, 1983. **45**: p. 167-174.
6. Suman, S., *Hybrid nuclear-renewable energy systems: A review.* Journal of Cleaner Production, 2018. **181**: p. 166-177.
7. Brown, N.R. and S.T. Revankar, *An Endothermic Chemical Process Facility Coupled to a High Temperature Reactor. Part II: Transient Simulation of Accident Scenarios Within the Chemical Plant.* Nuclear Engineering and Design, 2012. **246**: p. 266-276.
8. Gorensek, M.B. and W.A. Summers, *Hybrid sulfur flowsheets using PEM electrolysis and a bayonet decomposition reactor.* International Journal of Hydrogen Energy, 2009. **34**.
9. Norman, J.H., et al., *Thermoochemical Water-Splitting Cycle, Bench-Scale Investigations, and Process Engineering*. 1982, General Atomic.
10. Fillo, J.A., et al., *Hydrogen Production From Fusion Reactors Coupled with High Temperature Electrolysis*, in *BNL-24625*. 1978, Brookhaven National Lab: Upton, NY (USA).
11. *Hydrogen Scaling up. A Sustainable Pathway for the Global Energy Transition*. 2017, Hydrogen Council.
12. Muradov, N.Z. and T.N. Veziroglu, *From Hydrocarbon to Hydrogen-Carbon to Hydrogen Economy.* International Journal of Hydrogen Energy, 2005. **30**: p. 225-237.
13. *The hydrogen economy: opportunities, costs, barriers, and R&D needs.* 2004, National Academy of Engineering: Washington, DC.
14. *Annual Energy Outlook 2008*. 2008, U.S. Department of Energy, Energy Information Administration.
15. Yalcin, S., *A Review of Nuclear Hydrogen Production.* Internation Journal of Hydrogen Energy, 1989. **14**: p. 551-561.
16. Dincer, I. and C. Zamfirescu, *Sustainable Hydrogen Production*, Elsevier, Editor. 2017: Amsterdam, NL.
17. Holladay, J.D., et al., *An Overview of Hydrogen Production Technologies.* Catalysis Today, 2008. **139**: p. 244-260.
18. Seifritz, W., *Proposal for a Possible Use of Fusion Power for Hydrogen Production Within This Century.* International Journal of Hydrogen Energy, 1981. **6**: p. 331-338.
19. Spath, P.L. and M.K. Mann, *Life Cycle Assessment of Hydrogen Production via Natural Gas Steam Reforming*. 2001, National Renewable Energy Laboratory: Golden, CO.

20. Staffel, I., et al., *The Role of Hydrogen and Fuel Cells in the Global Energy System.* Energy Environ. Sci., 2018. **12**: p. 463-491.
21. Zink, J., *Trends Favors Nuclear-Hydrogen Economy.* Power Eng., 2003.
22. Brown, N.R. and S.T. Revankar, *An endothermic chemical process facility coupled to a high temperature reactor. Part II: Transient simulation of accident scenarios within the chemical plant.* Nuclear Engineering and Design, 2011. **246**: p. 266-276.
23. Fortum Power, H.O., *Application for a Decision-in-Principle Concerning the Construction of a Nuclear Power Plant Unit - Loviisa 3.* 2009.
24. Safa, H., *Heat recovery from nuclear power plants.* Electrical Power and Energy Systems, 2012. **42**.
25. Jaskólski, M., *Modelling long-term technological transition of Polish power system using MARKAL: Emission trade impact.* Energy Policy, 2016. **97**.
26. Kummu, M., et al., *The world's road to water scarcity: shortage and stress in the 20th century and pathways towards sustainability.* Scientific Reports, 2016. **6**.
27. Penfield, S., et al., *Use of Nuclear Reactor for Seawater Desalination*, in *IAEA-TECDOC-574*. 1990, International Atomic Energy Agency: Vienna.
28. Masra, B.M., *Optimization of the Coupling of Nuclear Reactors and Desalination Systems*. 2005, International Atomic Energy Agency.
29. Hammad, F.H., *Technology Transfer in Nuclear Desalination.* IAEA-SM-347, 1997. **18**: p. 429-448.
30. Helmer, R., *Water Demand and Supply.* IAEA-SM-347, 1997.
31. Schiffer, M., *Perspectives and challenges for desalination in the 21st century.* Desalination, 2004. **165**.
32. Kutbi, I.I., Z.A. Sabri, and A.A. Hussein, *Selection for Desalination Processes for Dual-Purpose Nuclear Plants.* Desalination, 1986. **58**.
33. IAEA, *Potential for Nuclear Desalination as a Source of Low Cost Potable Water in North Africa.* IAEA-TECDOC-917, 1996.
34. Muralev, E.D., *Experience in the Application of Nuclear Energy for Desalination and Industrial use in Kazakstan.* IAEA-TECDOC-1056, 1998: p. 361-368.
35. IAEA, *Thermodynamic and Economic Evaluation of Co-production Plants for Electricity and Potable Water.* IAEA-TECDOC-942, 1997.
36. Juhn, P.E., *IAEA Activities on the Nuclear Desalination of Sea Water.* IAEA-SM-347, 1997.
37. Barak, A., et al., *Nuclear desalination: Experience, needs, and prospects.* IAEA Bulletin, 1990.
38. Weinberg, J. and A. Ophir, *Experience Gained in the Ashod Plant and other Dual Purpose Desalination Plants Using Multi-Effect Distillation with Aluminum Tubes.* IAEA-SM-347, 1997. **41**: p. 379-390.
39. Abdel Hamid, S.B., et al., *Options identification programme for demonstration of nuclear desalination*. 1996, International Atomic Energy Agency: Austria.
40. Goto, T., et al., *Operating Experience Gained with Nuclear Desalination Plants by Japanese Electric Companies.* IAEA-SM-347, 1997: p. 367-378.
41. *Status of design concepts of nuclear desalination plants*. 2002, International Atomic Energy Agency: Vienna, Austria.
42. Al-Mutaz, I.S., *Coupling of a nuclear reactor to hybrid RO-MSF desalination plants.* Desalination, 2003. **157**.

43. Khan, S.U.-D. and S.U.-D. Khan, *Karachi Nuclear Power Plant (KANUPP): As a case study for techno-economic assessment of nuclear power coupled with water desalination.* Energy, 2017. **127**: p. 372-380.
44. Barak, A., et al., *Nuclear Desalination: Experience, needs, and prospects, a review of demonstration plants and recent studies*. 1990, International Atomic Energy Agency. p. 43-48.
45. Newton, D., J. Connery, and P. Wells, *U.S. EXPERIENCE IN THE DECOMMISSIONING OF THE BN-350 FAST BREEDER REACTOR IN KAZAKHSTAN.* Office of International Nuclear Safety & Co-operation, Department of Energy, 2002.
46. Staats, E.B., *Can The U.S. Breeder Reactor Development Program Be Accelerated By Using Foreign Technology?* 1976, Comptroller General of the United States: Report to the Joint Economic Committee Congress of the United States.
47. Novikov, E.P., et al., *Nuclear Industrial Desalination Plant with Fast Neutron Reactor at Shevchenko.* Desalination, 1969. **6**: p. 349-367.
48. *The future of hydrogen; Seizing today's opportunities*. 2019, International Energy Agency: Japan.
49. *Today's Hydrogen Production Industry*. 2003, US DOE: Office of Fossil Energy.
50. Herzog, H., *CO2 Sequestration.* Proceedings of Greenhouse Gas Reduction Programs and Technologies Symposium, 2002.
51. Stevens, S. and J. Gale, *Geologic CO2 Sequestration.* Oil & Gas J., 2000. **98**: p. 40-44.
52. Audus, H., O. Kaarstad, and M. Kowal, *Decarbonization of Fossil Fuels: Hydrogen as an Energy Carrier.* Proceedings of the 11th World Hydrogen Energy Conference, 1996.
53. Grimes, C.A., O.K. Varghese, and S. Ranjan, *Water and Hydrogen: The Solar Generation of Water by Water Photoelectrolysis*. 2008, Springer: New York, NY.
54. Guerra, O.J., et al. *Cost-Competitive Electrolysis-Based Hydrogen Under Current U.S. Electric Utility Rates*. in *AIChE Annual Meeting*. 2018. Pittsburg, PA.
55. *High pressure electrolysers: 10-60 Nm3/h*. Norsk Hydro Electrolysers AS.
56. *Product Development - the shape of things to come*. Norsk Hydro Electrolysers AS.
57. Steinberg, M., *Fossil Fuel Decarbonization Technology for Mitigating Global Warming.* Int. J. of Hydrogen Energy, 1999. **24**.
58. T-Raissi, A., *Water Splitting: Thermochemical. Encyclopedia of Inorganic and Bioinorganic Chemistry*, L. John Wiley & Sons, Editor. 2012.
59. Schuster, J.R., *Status of Thermochemical Water-Splitting Development at General Atomics*, in *Gen. Atom. GA Report*. 1977, General Atomics.
60. Brown, L.C., et al., *High Efficiency Generation of Hydrogen Fuels Using Nuclear Power.* General Atomics Report GA-A23510, 2000: p. 1-18.
61. Brown, N.R. and S.T. Revankar, *A Review of Catalytic Sulfur (VI) Decomposition Experiments.* International Journal of Hydrogen Energy, 2012. **37**: p. 2685-2698.
62. Parma, E., et al., *Modeling the Sulfuric Acid Decomposition Section for Hydrogen Production.* 2010: p. 1-7.
63. Brown, L.C., et al., *High Efficiency Generation of Hydrogen Fuels Using Nuclear Power*. 2003, U.S. Department of Energy.
64. Gorensek, M.B. and T.B. Edwards, *Energy Efficiency Limits for a Recuperative Bayonet Sulfuric Acid Decomposition Reactor for Sulfur Cycle Thermochemical Hydrogen Production.* Ind. Eng. Chem. Res., 2009. **48**.

65. Gorensek, M.B. and W.A. Summers, *Nuclear Hydrogen Production Handbook*. 2011: Taylor & Francis Group, LLC.
66. *Editorial On the right track.* Nature Energy, 2019. **4**.
67. Bhosale, R.R., et al., *A decade of ceria based solar thermochemical H2O/CO2 splitting cycle.* Int. J. Hydrogen Energy, 2019. **44**: p. 34-60.
68. Brown, L.C., et al., *Nuclear production of hydrogen using Thermochemical water-splitting cycles*, in *International Congress on Advanced Nuclear Power Plants*. 2002: Hollywood, FL.
69. Norman, J.H., S.R. Mysels, and D. Williamson, *Studies of the sulfur-iodine thermochemical water-splitting cycle.* International Journal of Hydrogen Energy, 1982. **7**: p. 545-556.
70. Brecher, L.E. and C.K. Wu, *Electrolytic decomposition of water*, W.E. Corps, Editor. 1975.
71. *International nuclear energy research initiative. 2006 Annual Report*. 2007, Department of Energy: Washington, D.C.
72. Parma, E.J., et al., *Modeling the Sulfuric Acid Decomposition Section for Hydrogen Production.* Int Topical Mtg on Safety and Technol of Nucl Hydrogen Prodn, Control.Mgmt, 2007: p. 154-160.
73. Schwartz, D., et al., *A Kinetic Study of the Decomposition of Spent Sulfuric Acids at High Temperature.* Industrial & Engineering Chemical Research, 2000. **39**: p. 2183-2189.
74. Coetzee, M.D., *The Chemical Reactor for the Decomposition of Sulphuric Acid for the Hybrid Sulfur Process.* 2008: p. 1-186.
75. Bell, C. and Contributors, *Thermo: Chemical properties component of Chemical Engineering Design Library (ChEDL)* 2016-2023.
76. Bell, C., Y.R. Cortes-Pena, and Contributors, *Chemicals: Chemical properties component of Chemical Engineering Design Library (ChEDL)*. 2016-2023.
77. Que, H., Y. Song, and C.C. Chen, *Thermodynamic Modeling of the Sulfuric Acid-Water-Sulfur Trioxide System with the Symmetric Electrolyte NRTL Model.* Journal of Chemical & Engineering Data, 2011. **56**: p. 963-977.
78. Nilges, J. and J. Schrage, *Vapor-liquid equilibrium of the system H2SO4-SO3. Part II Thermodynamic description with regard to the formation of H2S2O7.* Fluid Phase Equilibria, 1991. **68**: p. 247-261.

Vita

After graduating high school in Montana, CT Callaway joined the Marine Corps where he served for five years as an Arabic linguist in California, Texas, and Georgia. He returned to Montana for his undergraduate studies where he received his B.S. in Chemical Engineering from Montana State University. He then decided to pursue a M.S. in Nuclear Engineering from The University of Tennessee in Knoxville, where he developed his interests in nuclear hydrogen and other nuclear-driven thermal processes. After finishing his M.S. degree, he will begin his career with BWXT.